



Substructure Condition Evaluation of the Willow Valley Creek Bridge Using Geophysical Logging Methods

PUBLICATION NO. FHWA-HRT-23-080

OCTOBER 2023



U.S. Department of Transportation
Federal Highway Administration

Research, Development, and Technology
Turner-Fairbank Highway Research Center
6300 Georgetown Pike
McLean, VA 22101-2296

FOREWORD

Foundation reuse is increasingly being considered in bridge replacement and rehabilitation efforts to save money, reduce carbon emissions, and decrease construction time; however, the viability of reuse requires verifying the integrity, durability, and geotechnical and structural capacities of the existing foundations. The research presented in this report, carried out in partnership with the Federal Highway Administration's Central Federal Lands Highway Division, examined the use of geophysical wireline logging methods and seismic imaging to evaluate and confirm the reuse of the existing substructures of the Willow Valley Creek Bridge carrying Lake Mary Road in Arizona. The methods described in this report could also be useful for other investigations such as posthazard assessment. The results of this study benefit Federal, State, and local transportation agencies, design consultants, contractors, and researchers engaged in bridge-related work.

Jean A. Nehme, Ph.D., P.E.
Director, Office of Infrastructure
Research and Development

Notice

This document is disseminated under the sponsorship of the U.S. Department of Transportation (USDOT) in the interest of information exchange. The U.S. Government assumes no liability for the use of the information contained in this document.

The U.S. Government does not endorse products or manufacturers. Trademarks or manufacturers' names appear in this report only because they are considered essential to the objective of the document.

Quality Assurance Statement

The Federal Highway Administration (FHWA) provides high-quality information to serve Government, industry, and the public in a manner that promotes public understanding. Standards and policies are used to ensure and maximize the quality, objectivity, utility, and integrity of its information. FHWA periodically reviews quality issues and adjusts its programs and processes to ensure continuous quality improvement.

TECHNICAL REPORT DOCUMENTATION PAGE

1. Report No. FHWA-HRT-23-080	2. Government Accession No.:	3. Recipient's Catalog No.	
4. Title and Subtitle Substructure Condition Evaluation of the Willow Valley Creek Bridge Using Geophysical Logging Methods		5. Report Date October 2023	
		6. Performing Organization Code	
7. Authors F. Jalinoos (ORCID: 0000-0001-8330-7603), A. K. Agrawal (ORCID: 0000-0001-6660-2299), E. Hoomaan (ORCID: 0000-0001-9089-9838), R. E. Crowder (ORCID: 0009-0006-8105-7763), and J. Descour (ORCID: 0009-0007-5289-6901.)		8. Performing Organization Report No.	
9. Performing Organization Name and Address The City College of New York 160 Convent Ave. New York, NY 10031		10. Work Unit No. (TRAIS)	
		11. Contract or Grant No. DTFH61-14-D-00010-T-14001	
12. Sponsoring Agency Name and Address Office of Research, Development, and Technology Federal Highway Administration 6300 Georgetown Pike McLean, VA 22101-2296		13. Type of Report and Period Covered Final Report; September 2014–February 2018.	
		14. Sponsoring Agency Code: HRDI-30	
15. Supplementary Notes The contracting officer's representative was Frank Jalinoos (ORCID: 0000-0001-8330-7603).			
16. Abstract A project to widen the Willow Valley Creek Bridge carrying Lake Mary Road in Arizona planned to add 5-ft (1.5-m) shoulders along each side. The rehabilitation plan also emphasized reusing the existing stone masonry piers and abutments and providing a steel girder superstructure that retains the same “look” as the existing bridge and blends well within the forest environment of the project site. The research presented in this report—carried out in partnership with the Federal Highway Administration’s Central Federal Lands Highway Division—examines geophysical logging methods used for evaluating the structural integrity and durability of existing substructures, including the foundations. The researchers performed an indepth geophysical wireline logging investigation and seismic imaging through coreholes drilled from the bridge deck into the substructures and into the bedrock. The field testing results present an indepth condition evaluation of the stone masonry wall foundations around the coreholes.			
17. Key Words Wireline logging, geophysical investigation, nondestructive evaluation, foundation reuse, structural integrity		18. Distribution Statement No restrictions. This document is available to the public through the National Technical Information Service, Springfield, VA 22161. https://www.ntis.gov	
19. Security Classif. (of this report) Unclassified	20. Security Classif. (of this page) Unclassified	21. No of Pages 100	22. Price N/A

SI* (MODERN METRIC) CONVERSION FACTORS

APPROXIMATE CONVERSIONS TO SI UNITS

Symbol	When You Know	Multiply By	To Find	Symbol
LENGTH				
in	inches	25.4	millimeters	mm
ft	feet	0.305	meters	m
yd	yards	0.914	meters	m
mi	miles	1.61	kilometers	km
AREA				
in ²	square inches	645.2	square millimeters	mm ²
ft ²	square feet	0.093	square meters	m ²
yd ²	square yard	0.836	square meters	m ²
ac	acres	0.405	hectares	ha
mi ²	square miles	2.59	square kilometers	km ²
VOLUME				
fl oz	fluid ounces	29.57	milliliters	mL
gal	gallons	3.785	liters	L
ft ³	cubic feet	0.028	cubic meters	m ³
yd ³	cubic yards	0.765	cubic meters	m ³
NOTE: volumes greater than 1,000 L shall be shown in m ³				
MASS				
oz	ounces	28.35	grams	g
lb	pounds	0.454	kilograms	kg
T	short tons (2,000 lb)	0.907	megagrams (or "metric ton")	Mg (or "t")
TEMPERATURE (exact degrees)				
°F	Fahrenheit	5 (F-32)/9 or (F-32)/1.8	Celsius	°C
ILLUMINATION				
fc	foot-candles	10.76	lux	lx
fl	foot-Lamberts	3.426	candela/m ²	cd/m ²
FORCE and PRESSURE or STRESS				
lbf	poundforce	4.45	newtons	N
lbf/in ²	poundforce per square inch	6.89	kilopascals	kPa
APPROXIMATE CONVERSIONS FROM SI UNITS				
Symbol	When You Know	Multiply By	To Find	Symbol
LENGTH				
mm	millimeters	0.039	inches	in
m	meters	3.28	feet	ft
m	meters	1.09	yards	yd
km	kilometers	0.621	miles	mi
AREA				
mm ²	square millimeters	0.0016	square inches	in ²
m ²	square meters	10.764	square feet	ft ²
m ²	square meters	1.195	square yards	yd ²
ha	hectares	2.47	acres	ac
km ²	square kilometers	0.386	square miles	mi ²
VOLUME				
mL	milliliters	0.034	fluid ounces	fl oz
L	liters	0.264	gallons	gal
m ³	cubic meters	35.314	cubic feet	ft ³
m ³	cubic meters	1.307	cubic yards	yd ³
MASS				
g	grams	0.035	ounces	oz
kg	kilograms	2.202	pounds	lb
Mg (or "t")	megagrams (or "metric ton")	1.103	short tons (2,000 lb)	T
TEMPERATURE (exact degrees)				
°C	Celsius	1.8C+32	Fahrenheit	°F
ILLUMINATION				
lx	lux	0.0929	foot-candles	fc
cd/m ²	candela/m ²	0.2919	foot-Lamberts	fl
FORCE and PRESSURE or STRESS				
N	newtons	2.225	poundforce	lbf
kPa	kilopascals	0.145	poundforce per square inch	lbf/in ²

*SI is the symbol for International System of Units. Appropriate rounding should be made to comply with Section 4 of ASTM E380.
(Revised March 2003)

TABLE OF CONTENTS

CHAPTER 1. WILLOW VALLEY CREEK BRIDGE PROJECT.....	1
Existing Willow Valley Creek Bridge	1
Rehabilitation Plan	6
CHAPTER 2. COREHOLE LOGGING INVESTIGATION.....	7
Introduction.....	7
Objectives of Geophysical Investigation	8
Pier and Abutment Materials	9
Geophysical Logging Methods Used	9
CHAPTER 3. MEASUREMENT THEORY.....	13
Acoustic Televiwer (ATV) Logging Tool	13
Optical Televiwer (OTV) Logging Tool.....	14
Natural Gamma Logging Tool.....	14
Gamma-Gamma Density (DEN) Logging Tool.....	15
Full Waveform Sonic (FWS) Logging Tool.....	16
Electric Logging (ELOG) Tool	18
Caliper Tool.....	20
Unusual Conditions and Problems.....	20
CHAPTER 4. LOG PROCESSING STEPS.....	23
Geophysical Log Processing.....	23
Elastic Moduli and Rock Hardness	27
CHAPTER 5. FINDINGS AND RESULTS.....	29
Calipers Logging	29
Image Log Logging	29
Observations Over the Concrete Pads in Holes B1, B2, B7, and B8.....	30
Observations From the Stone Masonry Construction.....	34
Observations From the Bedrock	38
Physical Parameter Summaries.....	43
Gamma and Electric Logs.....	53
CHAPTER 6. SEISMIC TESTING AND IMAGING.....	55
Downhole Seismic Testing.....	55
Example Downhole Survey Result	58
Seismic Imaging	59
CHAPTER 7. CONCLUSIONS.....	63
APPENDIX. GEOPHYSICS LOGGING RESULTS.....	65
ACKNOWLEDGEMENT.....	91
REFERENCES.....	93

LIST OF FIGURES

Figure 1. Photo. Elevation view of Willow Valley Creek Bridge.	2
Figure 2. Drawing. Plan and profile for Willow Valley Creek Bridge (FHWA 2015).	3
Figure 3. Drawing. Plan view of the bridge with pier and abutment details.	4
Figure 4. Photo. The general condition of pier 1 of the Willow Valley Creek Bridge.	5
Figure 5. Illustration. Coreholes in the Willow Valley Creek Bridge.	8
Figure 6. Illustration. Acoustic televiewer tool (ATV).	13
Figure 7. Illustration. Optical televiewer tool (OTV).	14
Figure 8. Illustration. Compensated dual-detector density tool.	16
Figure 9. Illustration. Full waveform sonic (FWS) tool.	17
Figure 10. Illustration. Normal (left) and modified (right) resistivity array tools.	19
Figure 11. Illustration. Correlation example between the gamma electric logs and the gamma density logs collected on Abut1-RT-B8.	25
Figure 12. Illustration. Geophysical summary showing properly depth-correlated logs for the Abut1-RT-B8.	26
Figure 13. Equations. Elastic physical properties equations.	27
Figure 14. Illustration. Caliper logs from the newer foundation side (a to d) and from the older foundation side (e to h).	29
Figure 15. Illustration. Image logs across the concrete pad in Pier1-RT-B1 showing no apparent cracks or fractures.	31
Figure 16. Illustration. Image logs across the concrete pad in Pier2-RT-B2 showing no apparent cracks or fractures.	32
Figure 17. Illustration. Image logs across the concrete pad in Abut2-RT-B7 showing no apparent cracks or fractures.	33
Figure 18. Illustration. Image logs across the concrete pad in Abut1-RT-B8 showing no apparent cracks or fractures.	34
Figure 19. Illustration. Image logs across stone masonry in Pier2-RT-B2.	35
Figure 20. Illustration. OBI images of the stone masonry in the old foundation (B3–B6) showing the various amount of enlargement of the mortar around clasts.	36
Figure 21. Illustration. Detailed OBI image in Abut1-LT-B5. The two near-vertical enlarged joints have a strike of N41E (MN).	37
Figure 22. Illustration. Optical televiewer image (right) and stereographic projections and tadpole (left) of Pier2-LT-B4 over the bedrock interval.	38
Figure 23. Illustration. Image logs for Pier1-RT-B1 and Pier2-RT-B2 in the bedrock.	39
Figure 24. Illustration. OBI images in old foundation (B3–B6) over the bedrock interval.	39
Figure 25. Illustration. Image logs for old foundation Abut2-RT-B7 and Abut1-RT-B8 in the bedrock.	40
Figure 26. Illustration. The large near-vertical enlargements in Abut1-LT-B5 are striking N41E (MN).	40
Figure 27. Illustration. Tadpole summary plot of the bedrock feature picks in B1–B4 and B6–B8.	41
Figure 28. Illustration. Schmidt plots of the feature picks in the bedrock in B1, B3, B6, and B8.	42
Figure 29. Illustration. Schmidt plots for the feature picks in B2, B4, B7, and for all the holes combined.	42

Figure 30a. Illustration. Pier1-RT-B1 physical parameter summary.....	44
Figure 30b. Illustration. Pier1-RT-B1 physical properties (elastic moduli) logs.	45
Figure 31. Illustration. Pier2-RT-B2 physical parameter summary.	46
Figure 32. Illustration. Abut2-RT-B7 physical parameter summary.....	47
Figure 33. Illustration. Abut1-RT-B8 physical parameter summary.....	48
Figure 34. Illustration. Pier1-LT-B3 physical parameter summary.....	49
Figure 35. Illustration. Pier2-LT-B4 physical parameter summary.....	50
Figure 36. Illustration. Abut1-LT-B5 physical parameter summary.	51
Figure 37. Illustration. Abut2-LT-B6 physical parameter summary.	52
Figure 38. Photo. Source with the attached handle being applied at the rock surface.....	55
Figure 39. Photo. Source driving assembly, source signal monitor, and seismograph.....	56
Figure 40. Photo. Twelve-hydrophone line in B-1, folded to shrink offset between hydrophones to 3.3 ft (1 m).....	56
Figure 41. Photo. Folded hydrophone line suspended in corehole Pier1-LT-B1.	57
Figure 42. Illustration. Typical downhole seismic field records after cross-correlation (Abut2, source position 06).....	57
Figure 43. Illustration. Configuration of sources (dots), hydrophones (diamonds), and accelerometers (triangles) used for seismic survey of Abut1.	58
Figure 44. Illustration. Downhole seismic records from seven source positions and hydrophone positions in Abut1, corehole B8.....	59
Figure 45. Illustration. Tomogram combined with the volumetric contour image of velocity distribution reconstructed along Abut1 from measured wave travel times (Jalinoos 2015).....	60
Figure 46. Illustration. Reflectogram migrated image of Abut1 superimposed on volumetric velocity model (Jalinoos 2015).....	61
Figure 47. Illustration. Density log of Abut1-LT-B5.	66
Figure 48. Illustration. Sonic log of Abut1-LT-B5.....	67
Figure 49. Illustration. Optical images of Abut1-LT-B5.....	68
Figure 50. Illustration. Density log of Abut2-LT-B6.	69
Figure 51. Illustration. Optical images of Abut2-LT-B6.....	70
Figure 52. Illustration. Sonic log of Abut2-LT-B6.....	71
Figure 53. Illustration. Density log of Pier1-LT-B3.	72
Figure 54. Illustration. Optical images of Pier1-LT-B3.	73
Figure 55. Illustration. Sonic log of Pier1-LT-B3.	74
Figure 56. Illustration. Density log of Pier2-LT-B4.	75
Figure 57. Illustration. Optical images of Pier2-LT-B4.	76
Figure 58. Illustration. Sonic log of Pier2-LT-B4.	77
Figure 59. Illustration. Density log of Pier1-RT-B1.....	78
Figure 60. Illustration. Optical images of Pier1-RT-B1.	79
Figure 61. Illustration. Sonic log of Pier1-RT-B1.	80
Figure 62. Illustration. Density log of Pier2-RT-B2.....	81
Figure 63. Illustration. Sonic log of Pier2-RT-B2.	82
Figure 64. Illustration. Optical images of Pier2-RT-B2.	83
Figure 65. Illustration. Density log of Abut2-RT-B7.	84
Figure 66. Illustration. Sonic log of Abut2-RT-B7.....	85
Figure 67. Illustration. Optical images of Abut2-RT-B7.....	86

Figure 68. Illustration. Density log of Abut1-RT-B8.	87
Figure 69. Illustration. Sonic log of Abut1-RT-B8.....	88
Figure 70. Illustration. Optical images of Abut1-RT-B8.....	89

LIST OF TABLES

Table 1. Types of geophysical logs used at the Willow Valley Creek Bridge (1 ft = 0.3 m).....	9
Table 2. Summary of geophysical logs.....	10
Table 3. Intervals where sonic data could be obtained because of field conditions.	21
Table 4. USGS image classification scheme.	30

LIST OF ABBREVIATIONS AND ACRONYMS¹

2D	two dimensional
3D	three dimensional
AASHTO	American Association of State Highway and Transportation Officials
ABI	acoustic borehole imager
Abut	abutment
ADT	average daily traffic
API	application programming interface
ARI	acoustic reflectance index
ASR	alkali-silica reaction
ATV	acoustic televiewer
Azi	azimuth
BRD	bed resolution density
CSL	crosshole sonic logging
cps	counts per second
DEN	gamma density logging
DEF	delayed ettringite formation
ELOG	electric logging
FL	fluid level
FWS	full waveform sonic
FHWA	Federal Highway Administration
LSD	long-spaced density
LT	left
MN	magnetic north
NM	north magnetic
OBI	optical borehole imager
OTV	optical televiewer
PVC	polyvinyl chloride
P wave	compressional wave
RT	right
Rx	receiver
SON	sonic waveform
SP	spontaneous potential
SPR	single point resistance
SSD	short-spaced density
Sst wave	Stoneley wave
S wave	shear wave
TT	transit time
Tx	transmitter
UCS	uniaxial compressive strength
USGS	U.S. Geological Survey
VDL	variable density

¹Note: For the convenience of the audience, in some instances, we have repeated the spelled-out version of an abbreviation or an acronym.

CHAPTER 1. WILLOW VALLEY CREEK BRIDGE PROJECT

The Willow Valley Creek (Lake Mary Road) Bridge is a three-span, 104-ft (32-m)-long by 34-ft (10-m)-wide bridge, with a cast-in-place deck supported by steel rolled girders located on the low-volume Lake Mary Road in Coconino County, AZ. The bridge is located 40 mi (64 km) southeast of Flagstaff, AZ, on I-17 and 50 mi (80 km) north of Payson, AZ. The route also provides access to Lake Mary, Mormon Lake, and the recreational lands of the Coconino National Forest. The coordinates of the existing bridge are longitude 111° 21' 38.6" W and latitude 34° 38' 11.8" N. The current average daily traffic (ADT) of the project is 1,288, and the projected ADT is 2,110. Commercial trucks and logging trucks use the road regularly.

The bridge was originally constructed in 1934 and widened in 1968. In 2014, the Federal Highway Administration's (FHWA) Central Federal Lands Highway Division planned to widen the deck and replace the existing superstructure that was supported by mass-gravity masonry substructure units. Because of the satisfactory condition of piers and abutments, the agency decided to reuse the foundation of this bridge. However, the viability of the reuse decision depended on the resolution of a number of issues, including verification of geotechnical and structural capacities of the existing abutment and pier foundation to support current load requirements for the new structure, verification of pier and abutment widths adequate for the proposed wider structure, and verification of integrity and durability of existing foundations (Agrawal et al. 2018). The most vital concern for the feasibility of foundation reuse was to verify the load-bearing resistance and the long-term viability of the existing foundation for supporting the design loads.

To evaluate the integrity of the masonry substructure of the bridge, we used a number of nondestructive evaluation (NDE) and geophysical methods. This report summarizes the results from the wireline logging methods used to evaluate the structural integrity and durability of a stone masonry foundation.

EXISTING WILLOW VALLEY CREEK BRIDGE

The Willow Valley Creek Bridge is a 104-ft (31.7-m)-long, three-span structure that was originally constructed in 1934 and widened in 1968. Figure 1 shows an elevation view of the bridge. The existing bridge consists of two traffic lanes with a clear opening of 31 ft 6 1/4 inch (9.61 m) curb-to-curb and a 34 ft 1 3/4 inch (10.4 m) out-to-out width. The original bridge plans and the original widening project and as-built plans of the widening project are available for this bridge. Figure 2 shows drawings of the plan and an elevation view of the bridge. Figure 3 shows a plan with cross-sectional details of piers. Three spans of the bridge are 27 ft (8.3 m), 50 ft (15.2 m), and 27 ft (8.3 m) long with a 35-ft (10.7-m)-long suspended span in the middle of span 2. The superstructure is composed of seven steel rolled beams, with a cast-in-place concrete deck. The superstructure is continuous along the bridge length, except for interruptions at the suspended span, which is attached by pin and hanger type connections at the girders and expansion joints through the concrete slab.

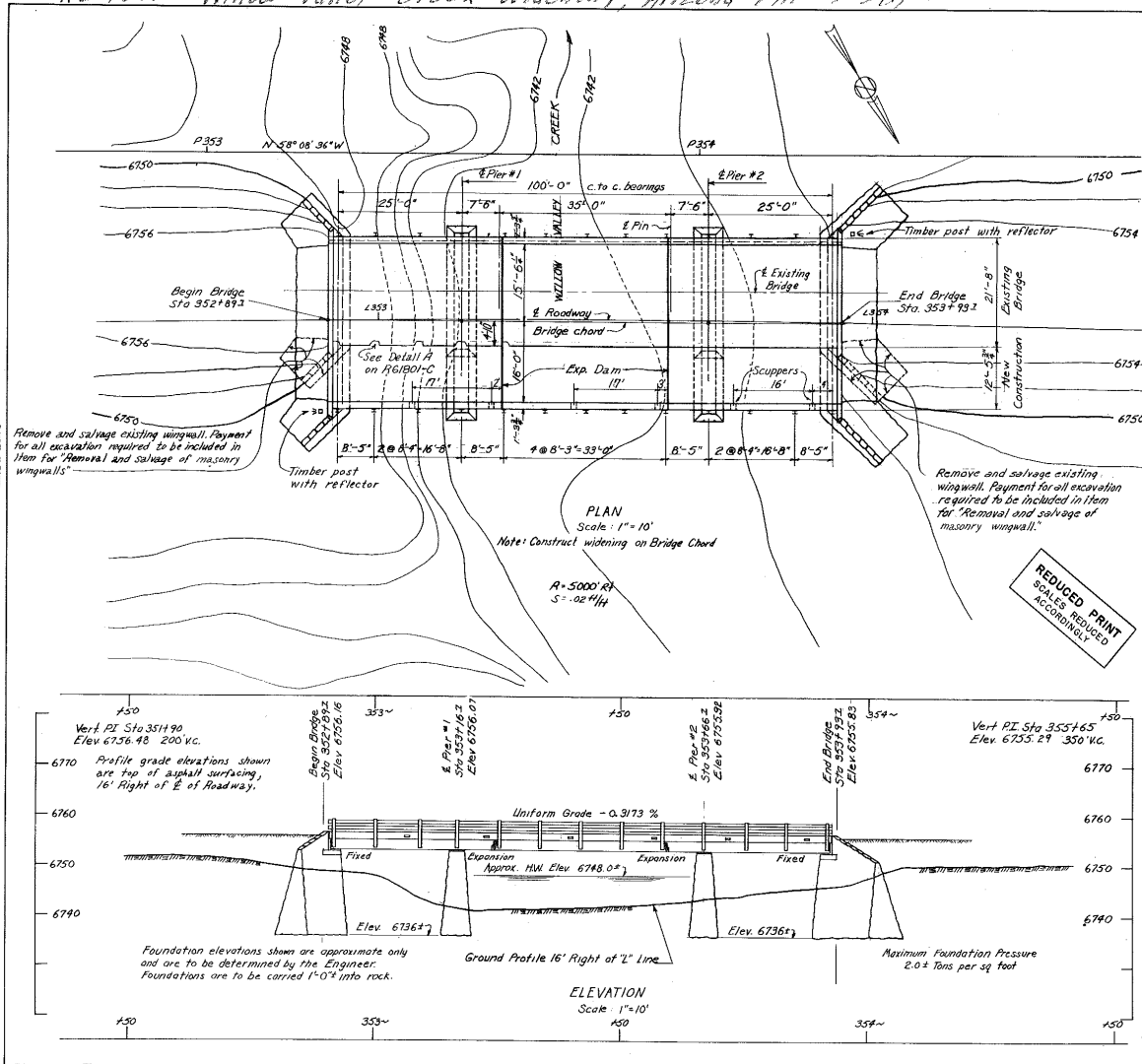


Source: FHWA.

Figure 1. Photo. Elevation view of Willow Valley Creek Bridge.

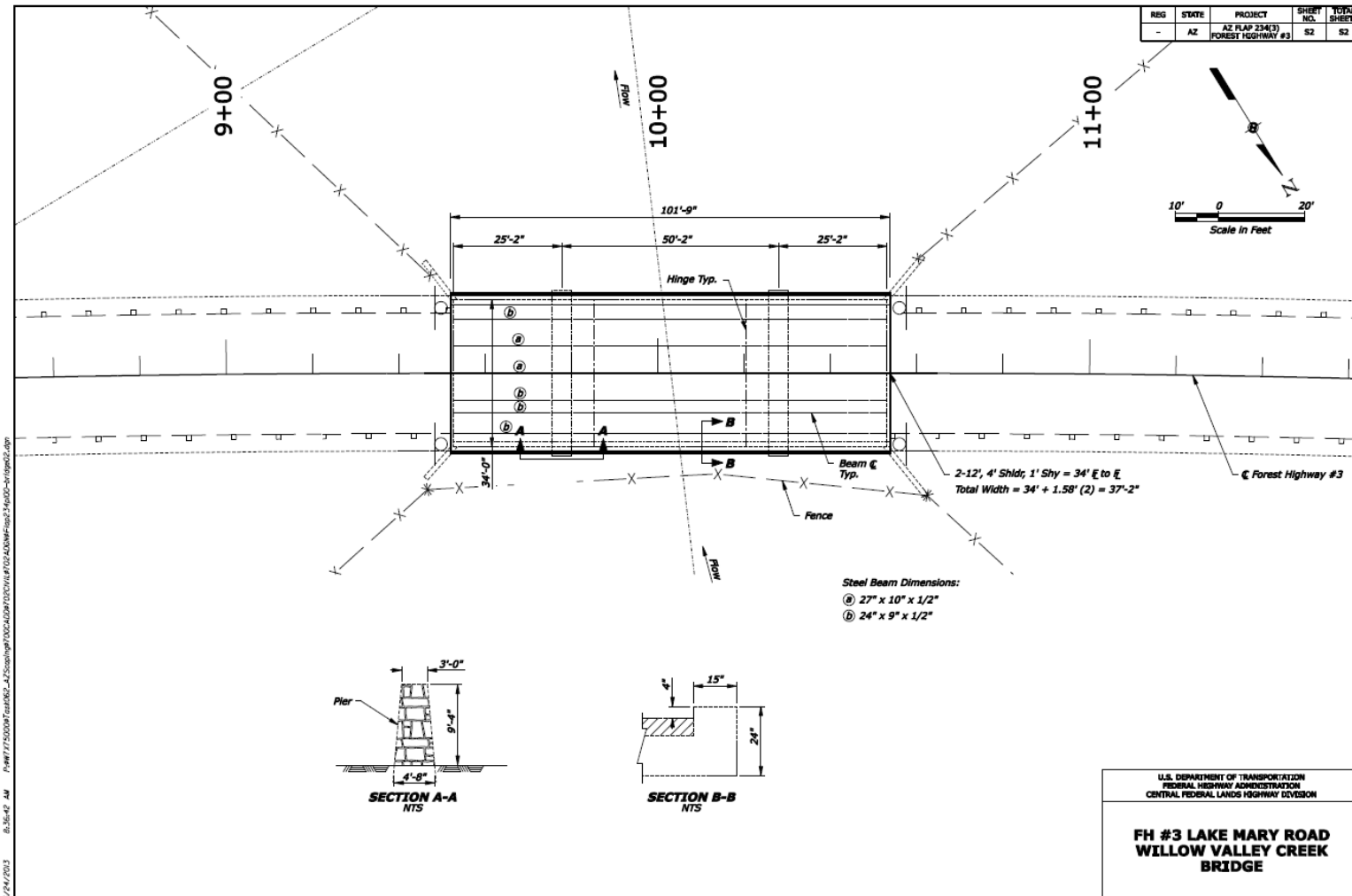
Bridge piers are gravity-type walls constructed of mortared rubble limestone masonry with bases keyed into bedrock. The abutments are also gravity-type walls with 8–12-ft (2.4–3.6-m)-long wingwalls flaring out from the abutments at 45 degrees. Elevations on the design plans indicate approximately 4 ft (1.2 m) of soil above bedrock at the pier locations and approximately 15 ft (4.6 m) of soil above bedrock at the abutments. The total heights of the piers, at the boring locations, range from 16.7 to 19.1 ft (5.1 to 5.8 m) for pier 1 and from 14 to 14.5 ft (4.3 to 4.4 m) for pier 2. The total heights of the abutments range from 19.9 to 24 ft (6.1 to 7.3 m) for abutment 1 and from 13.7 to 14.1 ft (4.2 to 4.3 m) for abutment 2. Due to local scour and soil/rock deposits, the actual embedded lengths of each pier and abutment may vary significantly along the lengths.

RG 1801 Willow Valley Creek Widening, Arizona FAP 3-3(B)



Source: FHWA.

Figure 2. Drawing. Plan and profile for Willow Valley Creek Bridge (FHWA 2015).

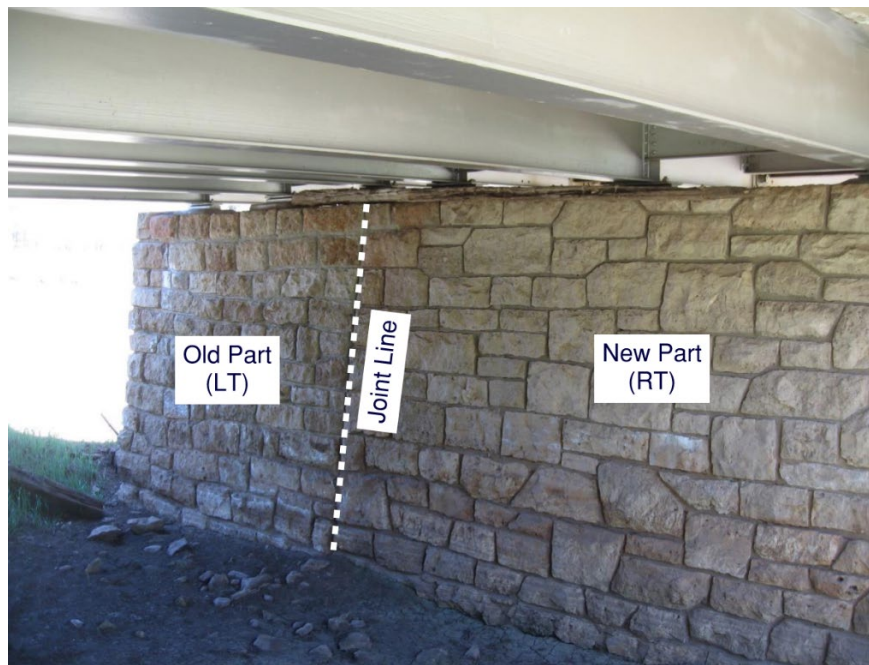


Source: FHWA.

Figure 3. Drawing. Plan view of the bridge with pier and abutment details.

The widening project in 1968 extended the pier and abutment widths with similar construction using mortared rubble masonry. However, as-built drawings (figure 2) show that concrete bases were constructed at the bottom of the walls below the rubble masonry sections. This construction method resulted in all four piers and abutments having very distinct “old” and “new” sections, with visible differences in the condition of the masonry in the two sections. A very distinct vertical joint line also separates the two sections on each pier and abutment, with (typically) a clear vertical crack or partial discontinuity at this joint line. Concrete-bearing seats are inset within the top of the abutment and pier masonry walls.

The 2014 bridge inspection reports noted that the bridge deck condition rating was in fair condition, with hairline transverse cracking and spalls with exposed rebar at the suspended slab joint locations. The overall girder was rated as poor, with isolated corrosion. The abutment and pier were rated overall to be in satisfactory condition, with isolated cracks noted in mortar joints. Figure 4 shows the general condition of pier 1. The inspection reports also indicated that water had reached the steel girders. A detailed hydraulic analysis of the bridge indicated that the bridge abutment and pier were socketed at a 1 ft (0.3 m) minimum into the bedrock, and the bridge was not scour critical.



Source: FHWA.
LT = left; RT = right.

Figure 4. Photo. The general condition of pier 1 of the Willow Valley Creek Bridge.

For the existing structure, the engineers estimated the maximum vertical reactions at the bearing seats were to be approximately 156 kips (694 kilonewtons (kN)) per abutment and 425 kips (1,890 kN) per pier unit. This loading assumed the live loading specified for the widening portion of the bridge as a basis, according to the American Association of State Highway and Transportation Officials’ (AASHTO) HS20 (AASHTO 2020). The anticipated maximum loads for the new superstructure, assuming the current HL93 design vehicle and proposed typical

section configuration, were estimated to be approximately 125 kips (556 kN) for the abutments and 470 kips (2,091 kN) per pier unit (AASHTO 2020). Hence, the new structure will impose smaller abutment loads but slightly higher pier loads.

REHABILITATION PLAN

The high elevation of the roadway and rolling terrain makes Lake Mary Road very popular with bicyclists and runners, and several bicycling events are held each year. The main objective of the rehabilitation was to widen the paved shoulders and the bridge to add 5 ft (1.5 m) shoulders along each side to make the entire corridor available for multimodal use, creating an opportunity for the route to become a world-class training/event course. The rehabilitation plan also emphasized retaining the existing stone masonry piers and abutments and providing a steel girder superstructure that retains the same look as the existing bridge to blend well within the forest environment of the project site.

The proposed replacement bridge superstructure will be a three-span structure, approximately 107 ft (33 m) long. The superstructure will be continuous and with slightly longer end spans than the existing configuration. The longer end spans will allow drop-in endwalls to be placed behind the existing abutments and improve the span ratio to better balance the design and reduce uplift from the live load at the abutments.

CHAPTER 2. COREHOLE LOGGING INVESTIGATION

INTRODUCTION

In borehole logging, probes that can measure physical properties are lowered into the borehole or the corehole. Geophysical logs are defined as a series of measurements made along the axis of a borehole. These data are generally recorded in digital format and are made at evenly spaced depth intervals—commonly from 0.2 to 0.1 ft (0.06 to 0.03 m). Two numbers represent each data point: depth and measured data value.

A number of different geophysical measurements can be made in boreholes. These measurements can be divided into general classes of data representing borehole or formation properties, such as borehole diameter or formation resistivity.¹ Although each geophysical measurement is interpreted according to the specific physical principles involved, all sets of geophysical logs have three fundamental attributes that contribute to the analysis of formation properties in a way that is unique to this class of measurement:

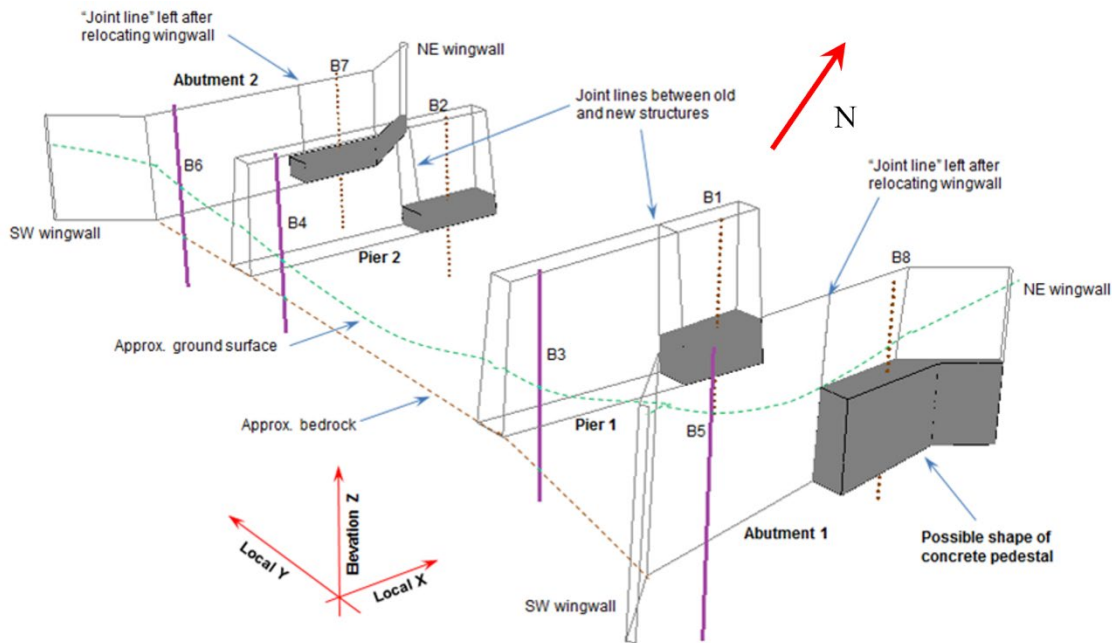
- Geophysical logs contain a continuous depth scale associated with a continuous series of measurements, each made in the same way with the same equipment. The dataset has no missing or misplaced intervals, and none of the data are affected by handling, desiccation, or desegregation, as are cuttings or core samples.
- Geophysical logging equipment is designed so that more than one geophysical measurement typically can be made in the same borehole. These measurements are based on different physical principles such as nuclear, electrical, or acoustic, and therefore, are analyzed by using independent (in the statistical and mathematical sense) interpretational equations.
- The availability of multiple, independent measurements enables complicated interdependencies between formation properties—such as electrical conductivity, mineral content, and degree of water saturation—to be uncoupled.

Different types of logs—such as calipers logs and acoustic televiewer logs—are typically collected to take advantage of their synergistic nature since physical properties are interrelated. For the Willow Valley Creek Bridge project, the structural integrity was investigated by evaluating the existing foundation elements using 10 HQ coreholes—eight 2.5-inch (63.5-mm) diameter cores, and two 3.78-inch (96-mm) diameter open holes. Two borings that were made at each foundation element (abutments and piers) advanced from the bridge deck (at locations where gaps between the girders exist), and two borings were made on the abutments through 15 ft (4.6 m) of fill. Eight coreholes through the existing piers and abutment foundations and one boring through the abutment fill were logged with borehole geophysics. However, the results of

¹In wireline geophysical logging, formation refers to the geological formation around a borehole drilled into the ground. In this report, formation refers to a civil human-made structure (masonry, concrete, etc.) around drilled coreholes. Therefore, in this context, the terms borehole and corehole are used interchangeably.

boring through abutment fill are not discussed because this report’s focus is on the evaluation of the integrity of substructure elements.

As shown in figure 5, the engineers drilled the coreholes to investigate the older (1934) foundations (borehole (B)5, B3, B4, and B6) on the left side of the bridge (looking north) and the newer (1968) foundations (B8, B1, B2, and B7) on the right side in the fall of 2014. For all figures in this report, the term left (LT) denotes the older foundation, and right (RT) denotes the newer foundation. A borehole geophysical logging consultant collected the geophysical logs in October 2014. Post field data collection, the consultant also provided data processing and interpreted the image features and elastic moduli.



Source: FHWA.
NE = northeast; SW = southwest.

Figure 5. Illustration. Coreholes in the Willow Valley Creek Bridge.

OBJECTIVES OF GEOPHYSICAL INVESTIGATION

The goal of the borehole geophysical logging work was to use borehole image logging tools to visualize the condition of the inside walls of the drill holes to detect fractures, cracks, and deficits in the stone masonry and concrete construction. Additionally, the bedrock structure was investigated for the same types of features plus bedding, foliation, voids, vugs, breccia, conglomerate, and other texture/feature variations. Relative rock hardness can be obtained from the acoustic reflectance log generated from an acoustic televiewer (ATV). The magnetometer in the orientation sensors can be used to locate magnetic material in the human-made structure, and the orientation sensor package provides the path of the drill holes. Borehole density, sonic, and electric logs can be used to measure physical parameters in the borehole wall. Formation density can be used to calculate porosity and can be combined with sonic data to calculate elastic moduli. Formation compressional velocity can be used to calculate porosity, and when combined with shear velocity and density data, it can be used to calculate elastic moduli, including

Poisson’s ratio and Young’s modulus. Formation resistivity is also a unique physical parameter that can be used to identify lithology and, for some applications, corrosivity.

PIER AND ABUTMENT MATERIALS

As described previously, the engineers drilled eight coreholes into abutments and piers for this bridge. Three material zones were penetrated by these holes:

1. Concrete: conventional aggregate concrete poured as a pad on the right side of the bridge (coreholes B1, B2, B7, and B8). These pads were apparently constructed in 1968. The holes drilled on the left side of the bridge (B3–B6) that penetrated the 1936 foundations did not penetrate any concrete.
2. Stone masonry: limestone block veneer around a core filled with mortar and rubble/large aggregate clasts. Coreholes B3–B6 showed the mortar cement to have deteriorated and become friable and washed out during drilling. These holes would not hold water within the stone masonry portion of the holes. B1, B2, B7, and B8 held fluid up to near the top of the piers and abutments.
3. Bedrock: kaibab limestone and calcareous shale sediments.

GEOPHYSICAL LOGGING METHODS USED

The research team logged each of the eight coreholes using the logging tools listed in table 1. The following acronyms are used for logging tools:

- ABI: acoustic borehole imager.
- OBI: optical borehole imager.
- ELOG: electric logging.
- DEN: gamma density logging.
- SON: full waveform sonic (FWS) logging.

Table 1. Types of geophysical logs used at the Willow Valley Creek Bridge (1 ft = 0.3 m).

Hole ID	Drill Depth (ft)	OBI	ABI	ELOG	SON	DEN
Pier1-RT-B1	30.9	Yes	Yes	Yes	Yes	Yes
Pier2-RT-B2	28.0	Yes	Yes	Yes	Yes	Yes
Pier1-LT-B3	31.0	Yes	—		Yes	Yes
Pier2-LT-B4	30.0	Yes			Yes	Yes
Abut1-LT-B5	36.0	Yes			Yes	Yes
Abut2-LT-B6	28.0	Yes			Yes	Yes
Abut2-RT-B7	28.0	Yes	Yes	Yes	Yes	Yes
Abut1-RT-B8	33.2	Yes	Yes	Yes	Yes	Yes

—No data.

Abut = abutment; ID = identification.

Table 2 provides a listing of various wireline logging technologies, their uses, and probe detail notes.

Table 2. Summary of geophysical logs.

Logging Technology	Measured Parameters	Probe Details
Optical televiewer (OTV)	Digitally images the inside of corehole wall using optical camera. Records an oriented 360°unwrapped and 3D image of the corehole wall or a “digital core.”	Ran in air-filled coreholes. (For water-filled holes, clear water is required.)
Acoustic televiewer (ATV)	Oriented images inside of the fluid filled corehole using acoustic transducer. Provides similar imagery as ATV.	Ran in water filled coreholes. (ATV also works in muddy (unclear) water.)
Density log (DEN)	Compensated density measures density values as a function of depth.	Focused density, BRD, SSD, and LSD: 125 mCi Cs-137 source. Ran with natural gamma and one-arm caliper.
Caliper logs (mechanical and acoustic)	Measure the corehole diameter and any change due to voids or washout zones in soil or bedrock.	Ran with DEN log.
Gamma log	Measures the amount of gamma radiation produced mainly by isotopes of potassium, thorium, and uranium. Can identify differing concrete mix or concrete deterioration.	Ran with DEN log.
SON—Full waveform sonic (FWS) log	Measures compressional (P), shear (S) Stoneley, and tube wave arrivals and amplitude. Along with density logs, determines elastic properties logs: shear, bulk, Young’s moduli and Poisson ratio as a function of depth.	FWS tool: One Tx, three Rx; 15 kHz monopole; 2 ft (0.6 m), 2.6 ft (0.8 m), and 3.3 ft (1.0 m) Tx-Rx spacings.
ELOG	Determines electrical resistivity of material at different radius of investigation as well as single point resistance (SPR) and spontaneous potential (SP). Can identify areas of high conductivity in concrete and possibly rebar corrosion.	SP, SPR, 16-inch (0.4-m) short-normal and 64-inch (1.6-m) long-normal resistivity. Run with natural gamma log.
Electromagnetic induction logs	Measure electromagnetic conductivity. Can measure areas of high conductivity and presence of steel.	Not collected at Willow Valley Creek Bridge.
Thermal neutron log	Measures the amount of hydrogen atoms in a formation for determination of porosity or presence of moisture.	Not collected at Willow Valley Creek Bridge.

3D = three-dimensional; BRD = bed resolution density; LSD = long-spaced density; Rx = receiver; SON = sonic waveform; SSD = short-spaced density; Tx = transmitter.

The following list describes some specific engineering applications of geophysical logging for condition evaluation of human-made structures:

- **Crack Mapping:** Optical televiewer (OTV), ATV, and mechanical/acoustic caliper logs are used for mapping cracks, in-place condition, or imaging voids. The OTV/ATV can detect microcracks and determine their orientation. The OTV/ATV logs can also image voids with their depth computed by mechanical/acoustic caliper logs.
- **Physical (Elastic) Properties:** A combination of FWS sonic and compensated density logs are used to generate elastic moduli logs (Young, shear, and bulk moduli and Poisson ratio) continuously as a function of depth (typically 1–2 inches (2.5–5.0 cm)).
- **Material Properties:**
 - Natural gamma and spectral gamma are used to assess different concrete mixes and properties. In concrete, the ^{40}K gamma counts mostly originate from the Portland cement. In some cases, gamma counts can be due to aggregate if crushed granite or trap rock were used, but this occurrence is not common. Elevated ^{40}K gamma counts can also infer potential (but not positively identify) concrete deterioration due to alkali–silica reaction (ASR) or delayed ettringite formation (DEF). Petrographic analysis of cored samples can be used for final verification of suspected zones.
 - Thermal neutron logs are used to detect the presence of moisture, which is important for assessing the potential for corrosion or other concrete deterioration.
- **Corrosion (Durability):** The resistivity, electromagnetic induction, and spontaneous potential logs are used to evaluate potential for rebar corrosion.
- **Construction Defects:** Checks for defects are used to detect voids and defective construction zones—such as soil intrusion, bulging, necking, honeycombing, cold joints, and poor quality concrete.
 - FWS and crosshole sonic logging (CSL) logs—FWS potentially detect defects using the reflection of compressional wave in the sonic record or changes in tube wave characteristics. FWS is a more advanced form of single-hole sonic logging. The use of CSL in this application is well established (Wightman et al. 2004).
 - Four-pi gamma–gamma density log—detects defects about 3–4 inches (7.6–10 cm) from the corehole wall.
 - Downhole seismic and ultraseismic vertical profiling—downhole seismic uses a seismic source on top of the foundation and a hydrophone (or geophone) string in the corehole. Ultraseismic uses seismic source on top of the foundation and a line of accelerometers attached directly to the structure (Wightman et al. 2004).
 - Cross-corehole tomography—requires two or more coreholes for two dimensional volumetric imaging between them.

- Borehole radar—detects reflection of radar data from defects and voids in stone masonry elements. In heavily reinforced concrete, borehole radar data can be unusable due to strong reflection from steel masking the defect signals.

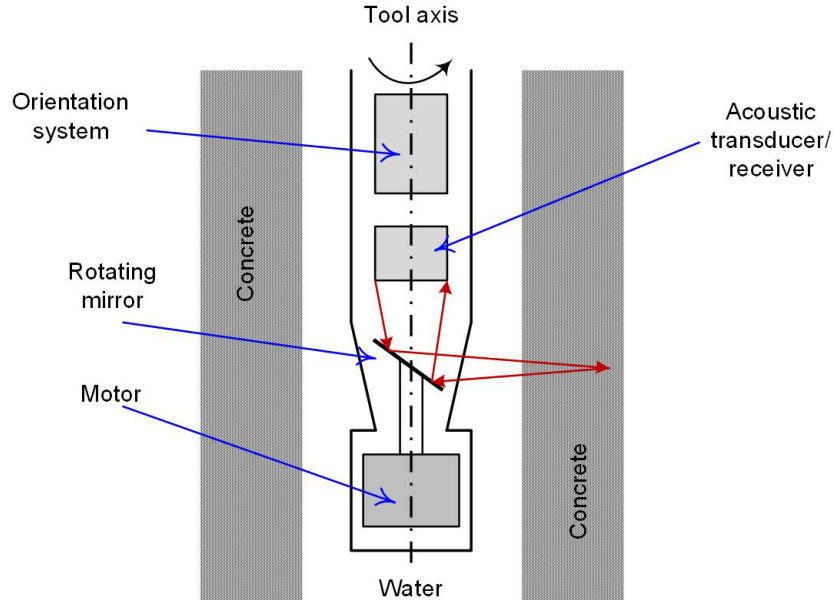
At the Willow Valley Creek Bridge, the coreholes were extended through the foundation wall element into the underlying rock formation. The engineers used the rock properties from corehole logs along with soil properties from a borehole drilled close to the foundation to evaluate geotechnical integrity at the site. Thus, wireline logging is a key technology for evaluating structural and geotechnical integrity of the substructure elements in this application.

CHAPTER 3. MEASUREMENT THEORY

ACOUSTIC TELEVIEWER (ATV) LOGGING TOOL

ATV (or acoustic borehole imager (ABI)) is an ultrasonic borehole wall-scanning tool that can be collected in the fluid-filled section of a borehole. The ATV records a magnetically oriented, 360-degree acoustic image of the borehole wall (Zemanek et al. 1969). The tool measures both the amplitude of the reflected ultrasonic waveforms and the two-way travel times. This ATV allows a very accurate borehole shape to be determined (acoustic caliper). The amplitude can be averaged to determine an acoustic reflectance index (ARI) that is proportional to rock strength. Interactive software allows the fractures to be oriented and other features to be measured. This software also allows three-dimensional (3D) cylindrical projections of the image to be made. The probe includes a three-axis magnetometer and a three-axis accelerometer orientation sensor that enables a borehole path survey to be made simultaneously. The three-axis magnetometer can also be processed as a total magnetic field log.

In this project, an ATV tool was used to collect an ultrasonic image of the inside of the corehole. The data were collected every 2.5 degrees around the borehole (144 samples/revolutions) and every 0.1 inches (0.23 cm) vertically. As shown in figure 6, in the ATV head, a mirror rotates, and the ultrasonic transducer is both the transmitter (Tx) and the Rx. The image is oriented with a three-axis magnetometer and three-axis accelerometer sensor package. Figure 6 shows the two-way travel time and amplitude of the reflected signal.



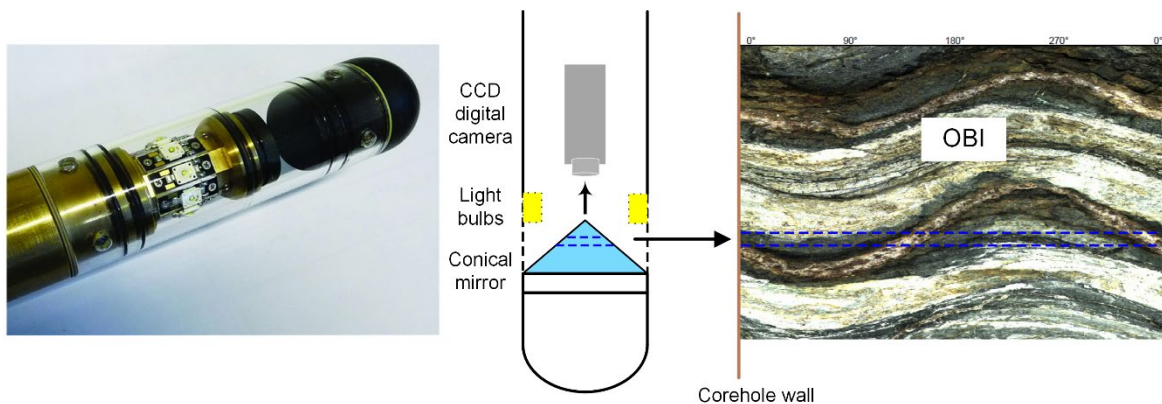
Source: FHWA.

Figure 6. Illustration. Acoustic televiewer tool (ATV).

OPTICAL TELEVIEWER (OTV) LOGGING TOOL

An OTV (or optical borehole imager (OBI)) provides an oriented, 360-degree color optical image of the inside of the borehole (Williams and Lane 1998). This image is oriented to magnetic north (MN) and is presented in a two-dimensional (2D) image. Interactive software allows the fracture orientations and other features to be measured. This software also allows 3D cylindrical projections of the image to be made. The tool includes a three-axis inclinometer and two accelerometers, which allow a borehole deviation path survey to be made simultaneously. The optical borehole images can only be collected in the dry or clear fluid section of a borehole.

Figure 7 shows a composite OBI: a photograph of the OBI shown on the left, a schematic of the OBI tool shown in the middle, and an example of a sinusoidal “unwrapped” image shown on the right. For the Willow Valley Creek Bridge project, an OBI tool was used in the coreholes to create an image that was sampled vertically every 3 inches (0.3 cm) and horizontally for every 1 degree.



© 2022 Mount Sopris Instruments, Inc.
CCD = charge-coupled device.

Figure 7. Illustration. Optical televiewer tool (OTV).

NATURAL GAMMA LOGGING TOOL

The natural gamma log (also known as gamma or gamma ray log) provides a measurement recorded in counts per second (cps) that is proportional to the natural radioactivity of the formation. The actual counts depend on the detector size and efficiency, but they are often normalized in application programming interface (API) units. The depth of investigation for the gamma log is typically 10–12 inches (25.4–30.48 cm), and the log measurement can be collected in a wet or dry hole and through casing. This log is one of the most common and basic types of logging measurements, and it was run to conduct lithologic identification, to make a stratigraphic correlation, to identify any radioactive mineralization, and to determine clay content.

The gamma-emitting radioisotopes that naturally occur in geologic materials are potassium⁴⁰ and the nuclides in the uranium²³⁸ and thorium²³² decay series. Potassium⁴⁰ occurs with all potassium minerals, including potassium feldspars. Uranium²³⁸ is typically associated with dark shale and uranium mineralization. Thorium²³² is typically associated with biotite, sphene, zircon, and other

heavy minerals. The usual interpretation of the gamma log is that measured counts are proportional to the quantity of clay minerals present. Usually, gamma logs show an inverse linear correlation between gamma counts and the average grain size (higher counts indicate smaller grain size, lower counts indicate larger grain size). Limestone typically has low gamma log values, and shale has higher gamma values.

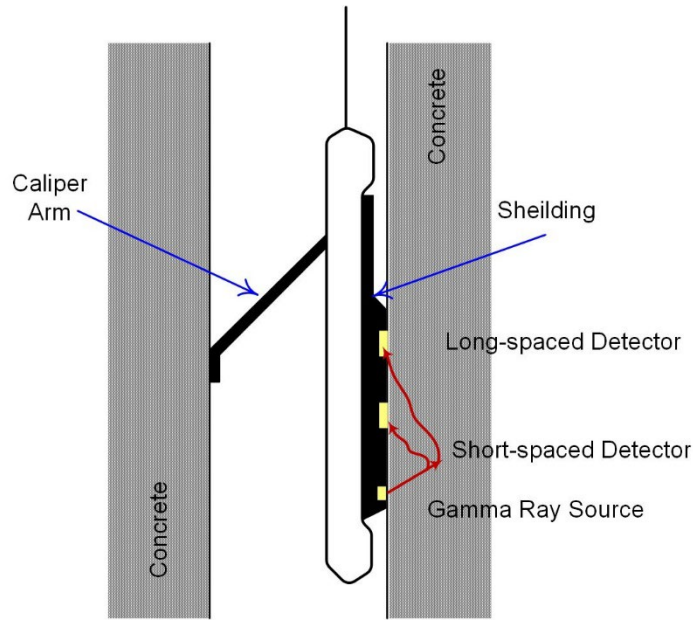
In concrete, the ^{40}K gamma counts originate mostly from the portland cement. The gamma counts can also come from the aggregate if crushed granite or trap rock is used. The ^{40}K radiation cannot be used to positively detect concrete deterioration—such as ASR or DEF. However, both processes involve elevated alkali levels in the cement, so the ^{40}K can be used to indicate the potential for their occurrence.

Gamma logs are usually combined with other measurements on different logging tools, and they serve as a common depth correlation log between different logging tools. The volume of investigation of the natural gamma measurement is a function of the detector size and the density of the material surrounding the tool. For this environment, the radius of investigation should be 10–12 inches (25.4–30.48 cm). At the Willow Valley Creek Bridge site, gamma logs were collected on two combination logging probes: ELOG and the density.

GAMMA-GAMMA DENSITY (DEN) LOGGING TOOL

The principle behind density logging is the detection of Compton-scattered gamma rays that originate from a small radioactive source housed in the probe (Keys 1990). The intensity of the radiation scattered back to the detectors is primarily a function of the bulk density of the media in which the gamma rays are introduced and scattered. A compensated dual-detector density tool provides a quantitative measurement of the formation density compensated for the effects of the borehole.

As shown in figure 8, the tool uses a cesium radioactive source with two or more detectors, and it is decentralized with a one-arm caliper. The tool is shielded and focused to see a directional “pie-shaped” wedge on the low side of the drill hole. This measurement is calibrated and quantified, and it is typically one of the most accurate log measurements recorded. This log is used to determine the formation density, which is related to porosity lithology and is used in the rock modulus calculations.



Source: FHWA.

Figure 8. Illustration. Compensated dual-detector density tool.

We used a sidewall density combination logging probe at the Willow Valley Creek Bridge to measure density at three different depths: a very short-spaced bed resolution density (BRD), a short-spaced density (SSD) 8 inches (20.32 cm) from the source, and a long-spaced density (LSD) 12 inches (30.48 cm) from the source. The BRD density has a very high vertical resolution but sees less than 1 inch (2.54 cm) into the formation. The SSD and LSD see deeper into the formation, and they are used to calculate a compensated density measurement. The SSD is impacted by hole rugosity more than the LSD, and the SSD is used to correct the LSD for the compensated calculation.

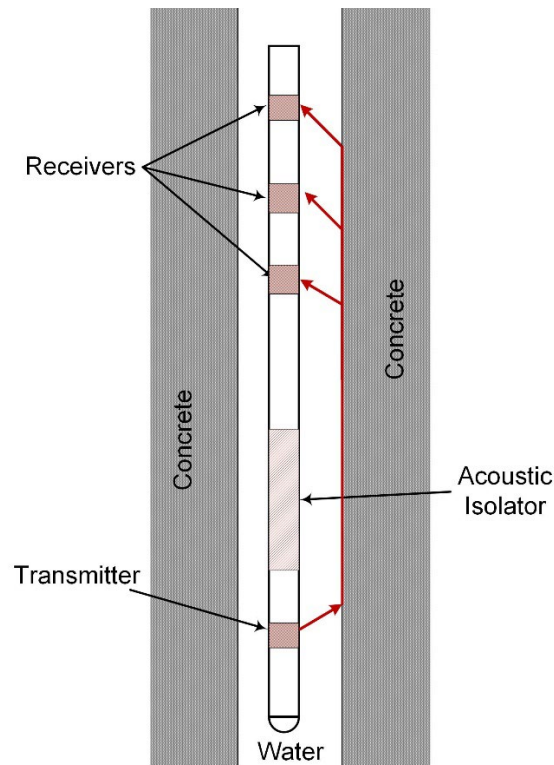
We collected density data vertically at 3 inches (7.62 cm), which also limits the vertical resolution of the tool to 3 inches (7.62 cm), even for the BRD measurement. A Cs-137 radioactive source that was rated at 125 mCi strength when manufactured was utilized. The age of the Cs-137 is unknown; however, it was acquired by the borehole geophysical logging consultant in 1982. The radioactive half-life of Cs-137 is 30.17 yr. Therefore, because this source is less than half its original strength, the count rates will be lower, especially for denser materials.

FULL WAVEFORM SONIC (FWS) LOGGING TOOL

Considerable information on the lithology and structure can be obtained by analyzing the various components of the received FWS signal. These analyses may include amplitude changes, ratios of the velocities of various components of the wave train and frequency-dependent effects (Wightman et al. 2004). The sonic waveforms (SONs) are interpreted to determine compressional (P), shear (S), and Stoneley (Sst) waves' slowness (sonic transit time (TT) or "delta-T" time) recorded in $\mu\text{s}/\text{ft}$ and amplitude. Note that sonic "slowness" is the inverse of velocity. The waveforms from one receiver (Rx) are presented in variable density (VDL) display

to highlight fractured intervals and to investigate the homogeneity of the rock mass around the drill hole.

Figure 9 shows a schematic drawing of a four-Rx sonic tool. In this project, we collected FWS logs in the fluid-filled, downward-drilled holes with a digital FWS probe using a monopole Tx and three different Rxes at 23.6 inches (0.6 m), 31.5 inches (0.8 m), and 39.4 inches (1.0 m), respectively. We used a monopole Tx frequency of approximately 15 kHz to resolve both P and S waves and collected data at a 4 $\mu\text{s}/\text{pixel}$ sample rate as well as a second longer time window (16 μs) sample rate to resolve reflected tube waves or possibly from structural boundaries. The waveforms were collected every 3 inches (7.62 cm) vertically in coreholes B1, B2, B7, and B8, and every 0.6 inches (1.52 cm) in coreholes B3–B6, which had short fluid-filled intervals.



Source: FHWA.

Figure 9. Illustration. Full waveform sonic (FWS) tool.

The probe transmits a waveform through the borehole fluid into the formation. The transmitted signal simulates P and S waves within the formation, which propagate through the formation and are then refracted back to a number of acoustic receivers (Rx1, Rx2, etc.). The difference in the first arrival times at two receivers is referred to the transit time TT or ΔT time, which is the P-wave slowness or a reciprocal of P-wave velocity.

In analyzing the data, we interpreted SONs to determine “ S_p ” or P, “ S_s ” or S, and “ S_{st} ” or Sst waves’ slowness (sonic TT or ΔT time) recorded in $\mu\text{s}/\text{ft}$ and amplitude. Note that sonic “slowness” is the inverse of velocity. The waveforms from one Rx are presented in VDL display to highlight fractured intervals and to investigate the homogeneity of the rock mass around the drill hole.

Vertical waterfall stacking of the individual waveforms creates the full waveform wavelets display, which uses the individual waveforms to represent the sinusoidal nature of sonic waves. A VDL is made from the wavelets by assigning different color bands to the waveform amplitude values. The degree of discontinuity of the rock is reflected by the deviation from parallel banding in the FWS display. A decrease in the amplitude of the Sst or tube wave is indicative of permeability. These tube waves are generally recognized as high-amplitude coherent wave trains. Because the tube wave is coupled to the formation through which it is traveling, it can perturb the formation across open fractures intersecting the borehole. This squeezing effect can generate secondary or reflected tube waves that travel both up and down from the fracture location. These reflected tube waves can diagnose the presence of open fractures and their amplitude-related qualitatively to the length and width of the fluid-filled fracture space; that is, strong reflected tube waves indicate wider, more permeable fractures located some distance from the corehole.

In geological formations, P-wave TT can be used to calculate porosity and to provide additional information regarding lithology, consolidation, and the presence of discontinuities (Keys 1990). In our project, P- and S-wave velocities were determined from the respective TTs. These velocities were combined with the compensated density measurement to calculate rock elastic moduli.

Acoustic FWS, generated by vertical waterfall stacking of individual waveforms with depth, indicate fracturing by attenuation of the waveform signal with time and by deviation from parallel banding (diffraction) in the FWS display. Other heterogeneities in the rock, such as conglomerate and breccia layers, may also scatter the waveforms; however, they do not attenuate the signal as much as permeable fractures. Open fractures significantly attenuate and lower the amplitude of the waveforms, and Sst or tube wave amplitude analysis is directly related to permeability in close proximity of the borehole.

ELECTRIC LOGGING (ELOG) TOOL

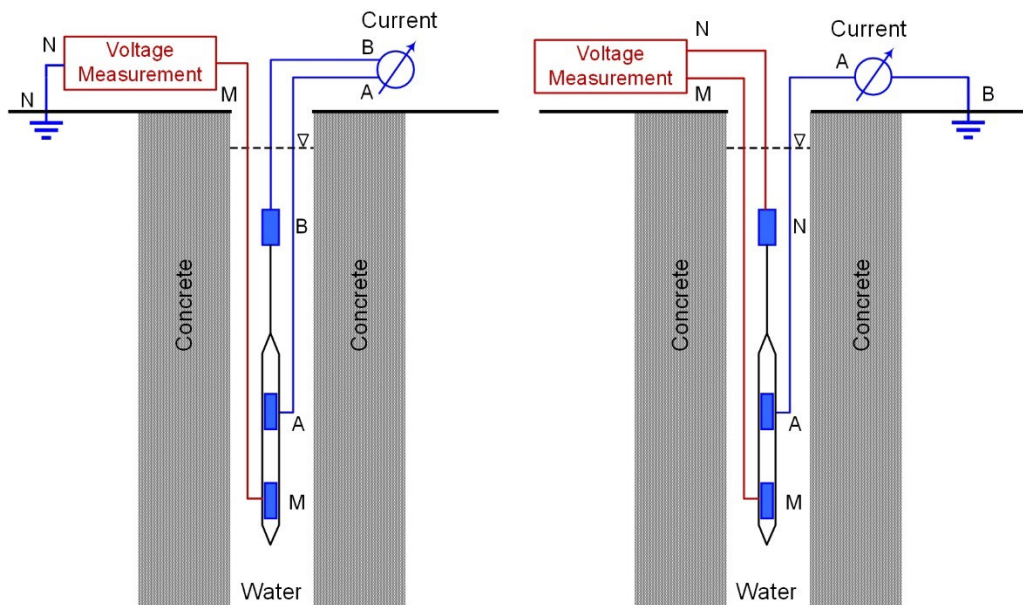
ELOG is a fundamental tool for resistivity logging to obtain important information on porosity, hydraulic conductivity, and fluid content of formations drilled in fluid-filled boreholes (Wightman et al. 2004). The ELOG tools include spontaneous potential (SP), single point resistance (SPR), and 16-ft (0.41-m) short-normal (16N) and 64-ft (1.6-m) long-normal resistivity (64N). These logs can only be collected in the fluid-filled, open-hole section of the borehole or through a polyvinyl chloride (PVC) screen, although the percentage of open screen may affect the log response.

The SP log responds to changes in the natural or self-potential in the formation. Three factors contribute to these changes:

1. The electrochemical component from the differences in the borehole fluid and formation of water quality.
2. The electromechanical component, including membrane effects of fluid moving into or out of the formation (streaming potential).
3. The redox or the oxidation-reduction of sulfide.

The degree to which these factors contribute to the total SP log cannot be quantified. The SP log is qualitative and dynamic, and it changes with time. In dry holes recently filled with water, a streaming potential may be significant in the SP.

Resistivity is a quantitative physical property of the formation. Normal resistivity arrays are one method of measuring this physical property (figure 10). New tools working on single conductor logging cable utilize a 25-ft (7.62-m)-long insulated bridle with the surface electrode replaced with an electrode at the top of the bridle. They utilize four electrodes: two current electrodes (A and B) and two potential (M and N) electrodes. The AM spacing determines the depth of investigation. Long-normal (64N) resistivity looks deeper into the formation than the short-normal (16N) array. The resistivity is controlled by borehole and formation water quality, saturation, rock fabric (grain size, grain shape, etc.), porosity, and mineralization. High resistivity is anticipated in low porosity, cemented, partially to nonsaturated, and nonmineralized formations. Lower resistivity in soil or rock may indicate more conductive water quality, increased porosity, increased conductive mineralization, or clay content. Limestone is usually more resistive than shale. Concrete and mortar may be resistive, depending on saturation and additives. Electrical (Wenner array) resistivity measurements have been used in the past to characterize the corrosive environment in reinforced concrete structures (Wightman et al. 2004).



Source: FHWA.

Figure 10. Illustration. Normal (left) and modified (right) resistivity array tools.

SPR measures the resistance between two electrodes in a manner similar to a voltage ohmmeter. Unlike the normal resistivity, SPR measurements are qualitative and change with the borehole fluid and contact resistance around the electrodes. SPR provides a higher vertical resolution qualitative log related to resistivity and follows the normal resistivity measurements. The volume of investigation of SP and SPR is determined by the electrode size and variations in the measurement array. Typically, the volume of investigation should be 1 ft (30.5 cm) for the tool used.

During the field evaluation at the Willow Valley Creek Bridge, we used a surface electrode in place of an isolation bridle because of the shallow depth of the drill holes. The normal resistivity values may be in error near the fluid level when the cable armor is out of fluid. The SP and SPR logs should be valid to near fluid level. A 0.05-ft (1.52-cm)-vertical sample was used for this probe.

CALIPER TOOL

Caliper logs measure hole diameter and can be mechanical or acoustic. Mechanical calipers range from one-arm calipers used to help decenter combination probes, such as the density, to three-arm averaging calipers, to four-arm X-Y calipers, which use two independent pairs of arms. Additionally, multiarm calipers as part of microresistivity logging tools, such as a dip meter or a formation microscanner, can be utilized. Many arm calipers for casing inspections are also available. Acoustic calipers are calculated from ultrasonic measurements, of which the most common is from ATVs. Mechanical calipers are lowered into the drill hole with the arm(s) closed. They are usually opened at the bottom of the logged interval by utilizing an electric worm gear with a compression spring release mechanism. When the arms are opened, the probe is then pulled upward at a constant speed and tension. The accuracy of a mechanical caliper depends on the number of arms utilized, the diameter of the end of the arms, arm length, hole diameter, vertical sample interval, and design.

The density combination probe at the Willow Valley Creek Bridge consisted of a one-arm caliper. This caliper was used to decenter the density probe. The caliper's arm length allowed measure enlargements out to at least 15 inches (38 cm) to be conducted. However, this caliper was unable to sense small-scale diameter variations in the core holes. Additionally, this caliper measurement was sampled at a 3-inch (7.62-cm)-vertical sample rate, which further minimized its sensitivity. Minimum, maximum, and average acoustic calipers were calculated from the ATV data, and the 2D travel time image was calibrated as a radius image in inches instead of microseconds. Acoustic calipers can have a smaller dynamic range of operation but a much higher vertical sample rate and accuracy than other calipers. The ATV on this project was sampled 144 times horizontally around the hole and at 0.1 inch (0.23 cm) vertically. The radius image provides a detailed shape of the coreholes.

UNUSUAL CONDITIONS AND PROBLEMS

The Willow Valley Creek Bridge is located in an arid location over a seasonal dry creek, and nearly all the stone masonry is located above ground level. Consequently, the coreholes were largely dry upon completion and then had to be filled for the acoustic and ELOG tools. Coreholes B3–B6 did not hold fluid above 20 ft (6 m) in depth, and this portion of the holes could not be logged with the acoustic and resistivity measurements. Furthermore, a significant portion of the material penetrated by all the holes was not saturated enough to obtain valid sonic log data.

Optical televiewers can only be obtained in dry holes or clear fluid. The presence of turbid fluid and mud on some of the drill coreholes coated the lens and degraded the image. B8 had turbid fluid below 19 ft (5.8 m), which impacted the quality of the OBI image. B5 could not be logged to total depth due to fill that was probably from mortar washing out of the pier. ATVs can only be

obtained in the fluid-filled portions of the coreholes and were not run in the short fluid-filled section of holes B3–B6.

Electric logs can only be obtained in the fluid-filled portions of the coreholes. Furthermore, normal resistivity measurements are four electrode arrays, and one of the electrodes is the cable armor. Most normal resistivity logging utilizes an approximately 25 ft (7.6 m) bridle, which means that valid normal resistivity measurements cannot be used within 25 ft (7.6 m) of the fluid level. A separate mud electrode can be used on the surface; however, this process still requires the cable armor to be insulated from 6 to 20 ft (1.8 to 6 m) from the probe when the armor comes out of fluid. Due to the shallow depth of these holes, the short–normal resistivity values may be valid up to 6 ft (1.8 m) below the fluid level. The long–normal resistivity logs will probably not be valid in any of these holes. The SP and SPR logs should be valid to near fluid level; however, both are qualitative logs.

Some of the coreholes could not be completely filled (primarily the coreholes drilled to investigate the older (1934) foundations (B5, B3, B4, and B6) on the west side of the bridge). This issue prevented 100-percent coverage with the ABI, ELOGs, and Sonic tools. Furthermore, the reduction from 100-percent saturation to almost 95-percent saturation reduces the compressional (P) sonic velocity by 50 percent. Since a monopole sonic Tx was used, the tool cannot resolve compressional or shear (S) velocities less than the velocity of the borehole fluid (5,000 ft/s or 1,524 m/s). Therefore, valid sonic data could not be collected to fluid level and, in most cases, could not be collected above 20 ft (6 m) below the top of the hole because the formation was not completely saturated. Table 3 shows the intervals where sonic data could be obtained.

Table 3. Intervals where sonic data could be obtained because of field conditions.

Hole ID	Drill Depth (ft)	SON	Filled FL (ft)	Top of Saturation (ft)	Valid Sonic Interval (ft)
Pier1-RT-B1	30.9	Yes	4	10	15–31
Pier2-RT-B2	28.0	Yes	5	9.6	9.6–27.8 (intermittent)
Pier1-LT-B3	31.0	Yes	15	21.8	26.6–27.7
Pier2-LT-B4	30.0	Yes	13	21.1	25.5–28
Abut1-LT-B5	36.0	Yes	14	22.7	27.5–32
Abut2-LT-B6	28.0	Yes	12.4	22	22–27.9
Abut2-RT-B7	28.0	Yes	6.4	23	23–27.7
Abut1-RT-B8	33.2	Yes	4	23	23–32.8

FL = fluid level.

CHAPTER 4. LOG PROCESSING STEPS

GEOPHYSICAL LOG PROCESSING

Geophysical log processing included the following steps:

- Import the raw data into a borehole well logging software, and format the data from each tool.
- Observe any data errors and overall data quality. When available, check repeated data to ensure they repeat and use the best quality data.

The following steps are specific to image logs:

- Import, format, and orient image to the high side or MN.
- Correlate depth with mechanical calipers and other image logs.
- Correct both amplitude and travel time images for magnetic effects if oriented to MN.
- Filter and centralize TT image.
- Calculate fluid velocity.
- Calculate radius image and minimum, maximum, and average acoustic calipers.
- Normalize the amplitude image:
 - Static normalization (used to help visualize low amplitude features).
 - High-pass normalization (used to minimize vertical banding).
- Insert blank structure logs, and pick and classify planar features oriented to MN relative to the hole axis.
- Correct feature picks for hole deviation and convert to a tadpole plot.

The following steps are specific to sonic logs:

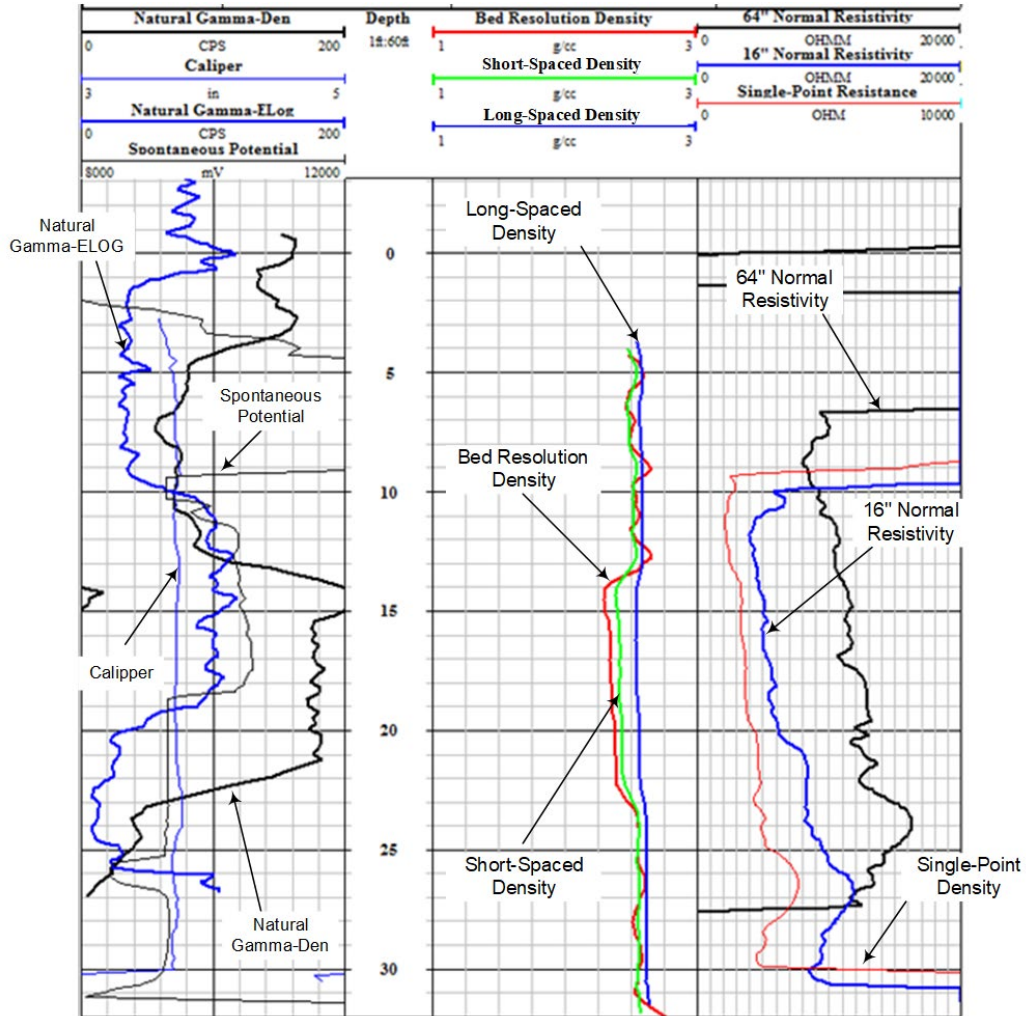
- Import SONS and format.
- Correct waveform baseline offset using spreadsheet and log acquisition and processing software applications.
- Filter the waveforms to remove the high-frequency noise.
- Stack the waveforms.

- Pick the first arriving P wave (TT in microseconds) on the waveforms and, where possible, the S wave (TT).
- Conduct a velocity semblance analysis.
- Calculate TT (delta-T time in microseconds/feet) for the P wave between Rx1 and Rx2 TT picks.
- Utilize TT pick from above to choose velocity semblance VDL for P- and S-wave slowness.
- Convert P- and S-wave slowness (microsecond/feet) to velocity (feet/seconds).

The following steps are specific to DEN and ELOG:

- Import and format the individual logs.
- Determine where data are valid.
- Convert density from grams per cubic centimeters to pounds per cubic feet.
- Correlate depth with the gamma logs for these tools (note that the caliper from the density tool is also a correlation log for image logs).

In figure 11, the individual tool files correctly depth correlate the different measurements on a given probe. However, when the two files are compared, the natural gamma log counts on the electric probe (blue curve, track 1) are higher than the natural gamma log on the density probe (black curve, track 1).



Source: FHWA.

g/cc = grams per cubic centimeters; OHM = ohms; OHMM = ohm meters.

Figure 11. Illustration. Correlation example between the gamma electric logs and the gamma density logs collected on Abut1-RT-B8.

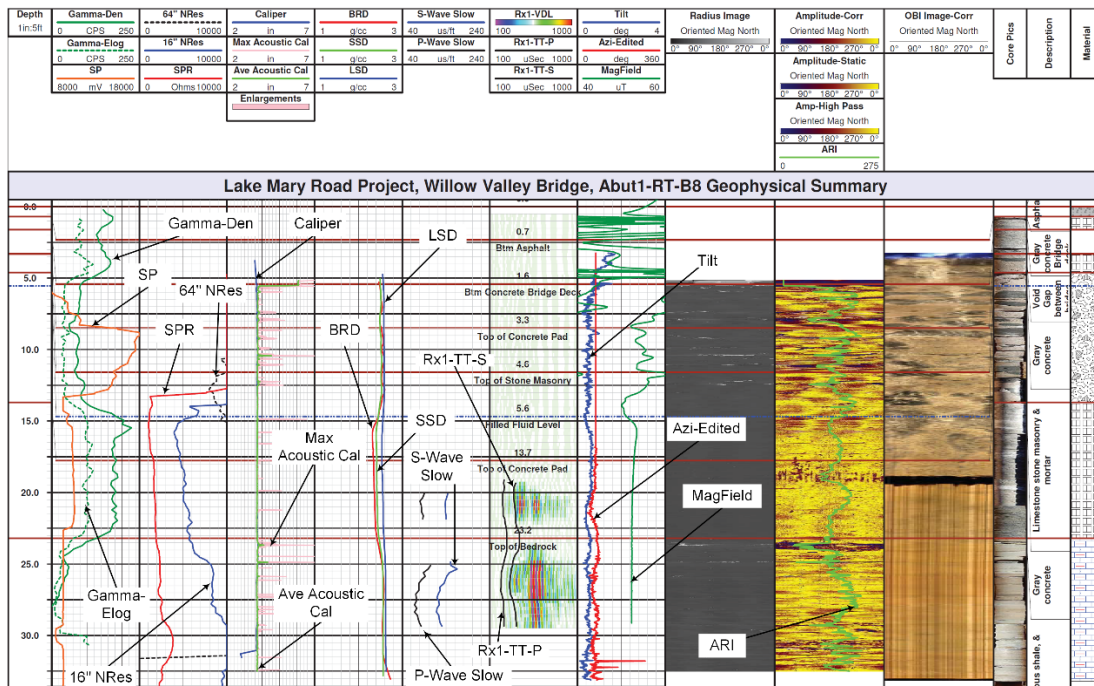
The following steps are specific to core photos and lithology data:

- Crop and edit core box photos and import them into borehole well logging software.
- Import lithology and other information into a borehole well logging software.
- Depth correlate logs to the core depths.

The following steps are specific to summary logs:

- Generate a geophysical summary log by combining relevant logs.
- Generate a physical summary log by combining relevant logs.
- Determine the average density and velocity for the respective material types.

The two gamma logs are plotted in figure 12 at the same scale. However, the gamma collected with the ELOG probe has lower cps values because it has a smaller gamma detector than the gamma on the density probe. Frequently, gamma logs are normalized in API units instead of cps. One gamma API unit is 1/200 of the full-scale value of the gamma log in a specially constructed model in Texas. Additionally, the higher gamma cps values between 15 ft (4.57 m) and 23 ft (7 m) are associated with the concrete foundation. As expected, carbonate sediments have very low cps values. Elastic moduli were only calculated in Pier1-RT-B1 due to limited velocity information. They are calculated with the formulas described in the next section.



Source: FHWA.

Ave = average; Azi = azimuth; MagField = magnetic field; NRes = normal resistivity.

Figure 12. Illustration. Geophysical summary showing properly depth-correlated logs for the Abut1-RT-B8.

ELASTIC MODULI AND ROCK HARDNESS

Initially, we calculated the normalized rock hardness log from the amplitude portion of the ATV data, and it is included in the log summary and physical properties summary plots. Rock hardness is a function of the acoustic reflection coefficient, which is related to density and P-wave velocity. A pseudo-density was calculated using the relationship between density, P-wave velocity from the sonic, and the reflection coefficient. The pseudo-density log was calibrated against the gamma-gamma density log when present and against core-specific gravity values and showed a good relationship when good sonic and ATV data were available. Additionally, this approach requires the ATV probe to be well aligned with the borehole axis. This approach should allow density data to be obtained from sonic and ATV logs on future holes where gamma-gamma density logs cannot be run.

Elastic properties are derived using the equations shown in figure 13.

$$\text{Poisson's Ratio} = \frac{\text{Lateral Strain}}{\text{Longitudinal Strain}} = \nu = \frac{0.5(t_s/t_c)^2 - 1}{(t_s/t_c)^2 - 1} \quad (1)$$

$$\text{Shear Modulus} = \frac{\text{Applied Stress}}{\text{Shear Strain}} = G = (\rho_b/t_s^2)a \quad (2)$$

$$\text{Bulk Modulus} = \frac{\text{Hydrostatic Pressure}}{\text{Volumetric Strain}} = K = \rho_b(1/t_c^2 - 4/3t_s^2)a \quad (3)$$

$$\text{Young's Modulus} = \frac{\text{Applied Uniaxial Stress}}{\text{Normal Strain}} = E = 2G(1 + \nu) \quad (4)$$

Figure 13. Equations. Elastic physical properties equations.

Where:

t_s = shear TT in $\mu\text{s}/\text{ft}$ (from full waveform sonic log).

t_c = compression TT in $\mu\text{s}/\text{ft}$ (from full waveform sonic log).

ρ_b = bulk density in g/cc (from density log).

$a = 1.34 \times 10^{10}$ = constant conversion factor producing modulus in psi.

Geophysical log-derived elastic moduli are low stress/strain measurements. They are comparable to triaxial core laboratory tests. The density log provides apparent electron density that is nearly the same as bulk density for most material; however, for some materials such as barite, a Z (atomic number)/ A (molecular weight) correction must be applied.

Elastic moduli calculated under near in situ formation conditions may be significantly different than static structural or rock mechanical properties, such as uniaxial compressive strength (UCS) obtained from core specimens. UCS tests are made without confinement, and the strength of the rock is a function of its cohesive and frictional properties. P-wave velocity is dependent on the nature of the grains and the compactness of the material in the direction of wave propagation. Changes may occur in UCS due to changes in the moisture content in fine-grained sediments and the degree of cementing, but that are not evident P-wave velocities. A first estimate of UCS is approximately P-wave velocity cubed. While empirical relationships are widely applied, especially in sediments, erroneous strength estimates have been made, particularly in weaker

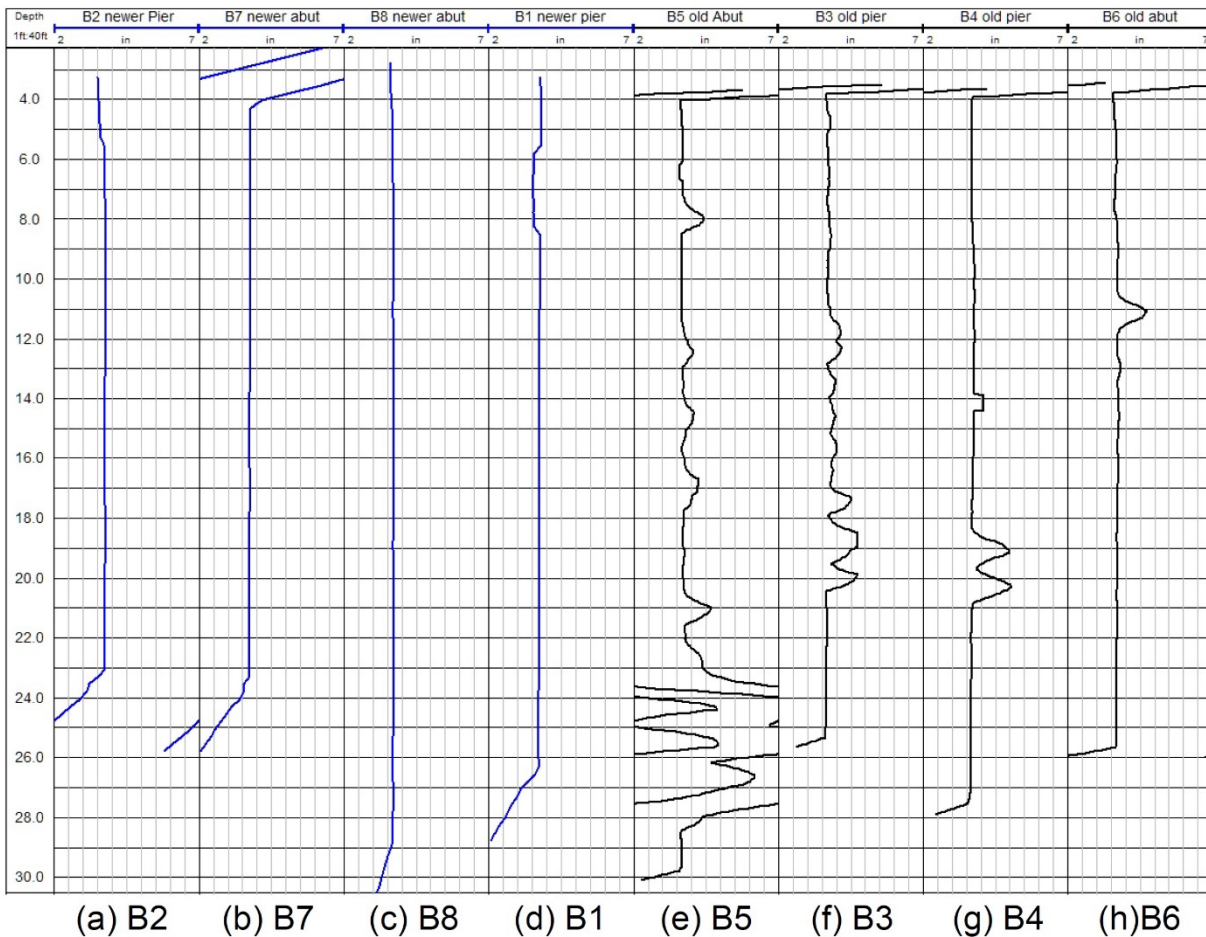
materials using an incorrect relationship. Static core measurements are used when available to determine empirical relationships used for the log-calculated UCS.

Elastic moduli, including Poisson's ratio, shear and bulk modulus, Young's modulus, and bulk compressibility, can be calculated in the fluid-filled sections of holes where density log data are available. Elastic moduli cannot be calculated in the dry portions of the boreholes above fluid level due to the lack of sonic data.

CHAPTER 5. FINDINGS AND RESULTS

CALIPERS LOGGING

We used a one-arm mechanical caliper on the density combination probe. The caliper is used to decentralize the sidewall density measurement, but it also provides the hole diameter. The caliper thus provides a gross hole condition measurement; however, it uses a long arm and provides only one point of contact. Consequently, it is not as responsive as a multiarm caliper measurement. Figure 14 shows caliper logs for newer and older sides of the bridge foundation. The caliper response indicated that coreholes B1, B2, B7, and B8 were largely in drill gauge and good condition. Coreholes B3–B6 were enlarged in the stone masonry section of the holes.



Source: FHWA.

Figure 14. Illustration. Caliper logs from the newer foundation side (a to d) and from the older foundation side (e to h).

IMAGE LOG LOGGING

The researchers used the U.S. Geological Survey (USGS) image classification scheme, shown in table 4, to classify the different features of a corehole (Keys 1990).

Table 4. USGS image classification scheme.

Classification	Feature	Color
0	Healed fracture/bedding plane	Gray
1	Partial fracture	Turquoise
2	Complete fracture	Blue
3	Open fracture	Red
4	Wide fracture/multiple fractures	Pink
5	Washout/wide fracture zone	Bright green

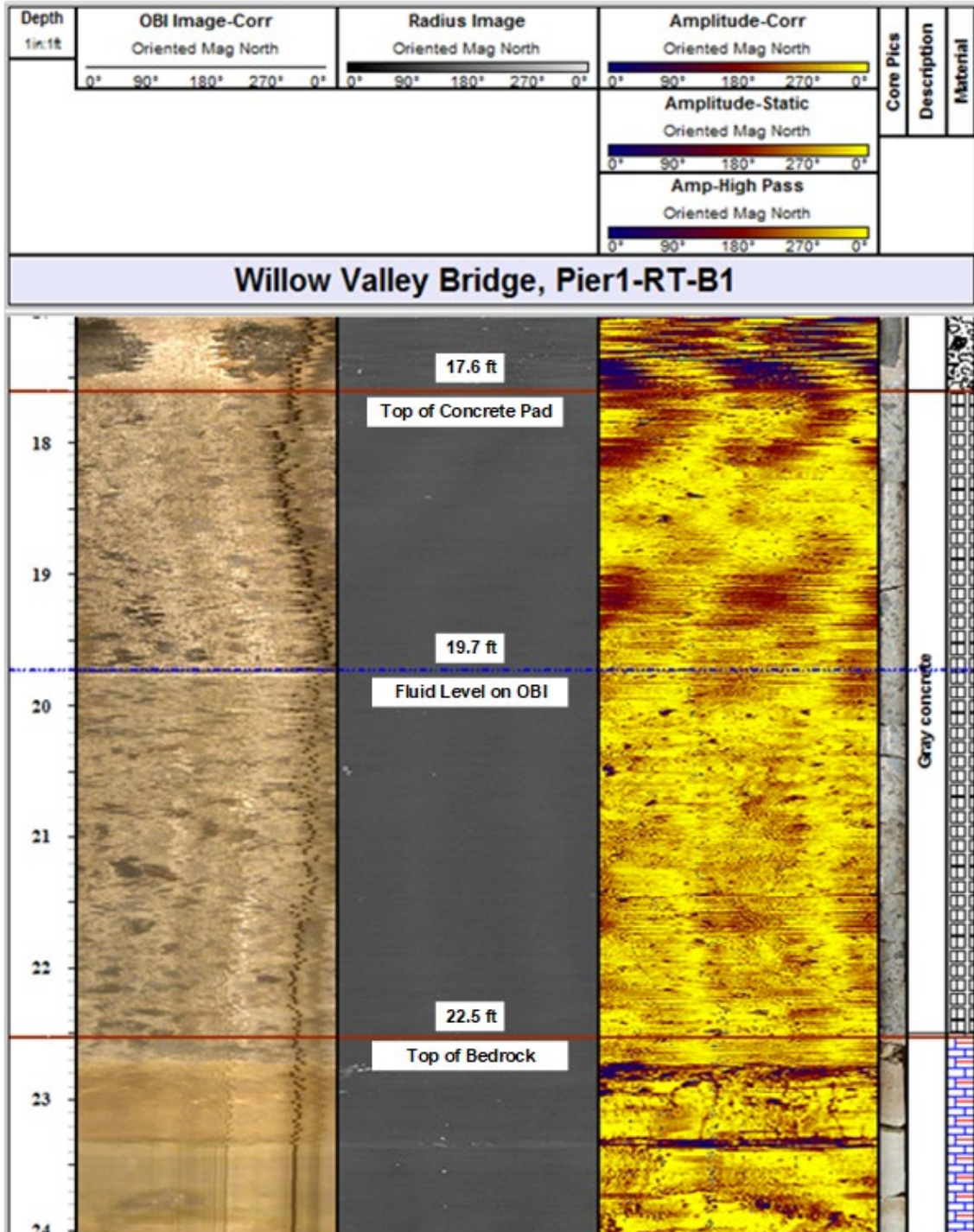
USGS initially developed this scheme to evaluate the potential for groundwater movement based on image logs. The scheme was based on the idea that the larger fracture zones would be more permeable than single or partially open fractures. USGS subsequently determined that fracture interconnection is more important for evaluating permeability than the fracture frequency or enlargement at the borehole wall.

However, this classification scheme is not appropriate for evaluating image logs in human-made structures, including concrete and stone masonry for a variety of reasons, considering that the human-made structure is largely located above ground level and is dry and not saturated. In addition, picking fractures in small diameter drill holes penetrating conglomerates and breccia clasts is always problematic because, frequently, the tool is looking at the edges of individual clasts and not bedding or fracture planes. This problem is aggravated when looking at the stone masonry mortar/rubble fill in the center of these structures. In this case, the concern is as much about near-vertical features as planar features as well as any type of enlargement or weakness. Therefore, planar feature picking should be limited to bedrock formations. This classification is based on all three images when possible (i.e., optical, travel time, or radius image and amplitude image).

During the analysis of image logs, it was possible to pick several near-vertical features near the bottom of the stone masonry in B5 that happen to lie in the same vertical plane. Significant enlargement around the clasts in the 1936 stone masonry in holes B3–B6 was also noted. Most of this enlargement appeared as if the mortar had become friable and washed out during drilling.

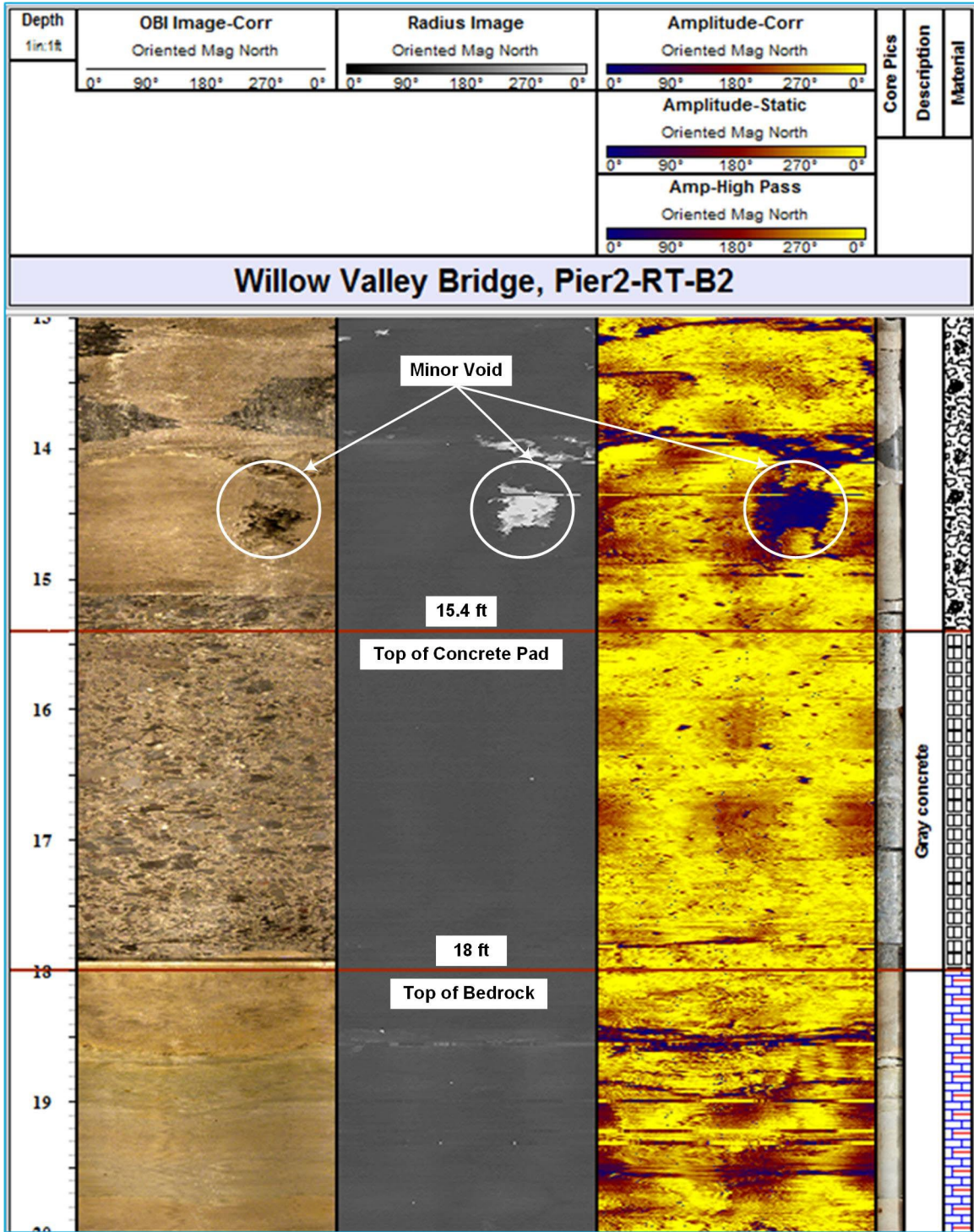
Observations Over the Concrete Pads in Holes B1, B2, B7, and B8

Concrete pads are located under the stone masonry in the new foundations in holes B1, B2, B7, and B8 on the right side of the bridge. A thinner concrete pad is also located at the top of these piers; however, the image tools did not obtain very useable images in this pad. Image logs of the concrete pad at the base are shown in figure 15 to figure 17. In figure 15, turbid water was encountered at 19 ft (5.8 m) during the OBI log. The corehole wall was coated with apparent drill cuttings/mud on the OBI image, nearly masking the concrete texture. However, this coating and the turbid fluid are transparent to the acoustic image. In figure 16, the concrete pad is several inches thicker than indicated in the core. The fluid level is located at about the middle of the pad in figure 17.



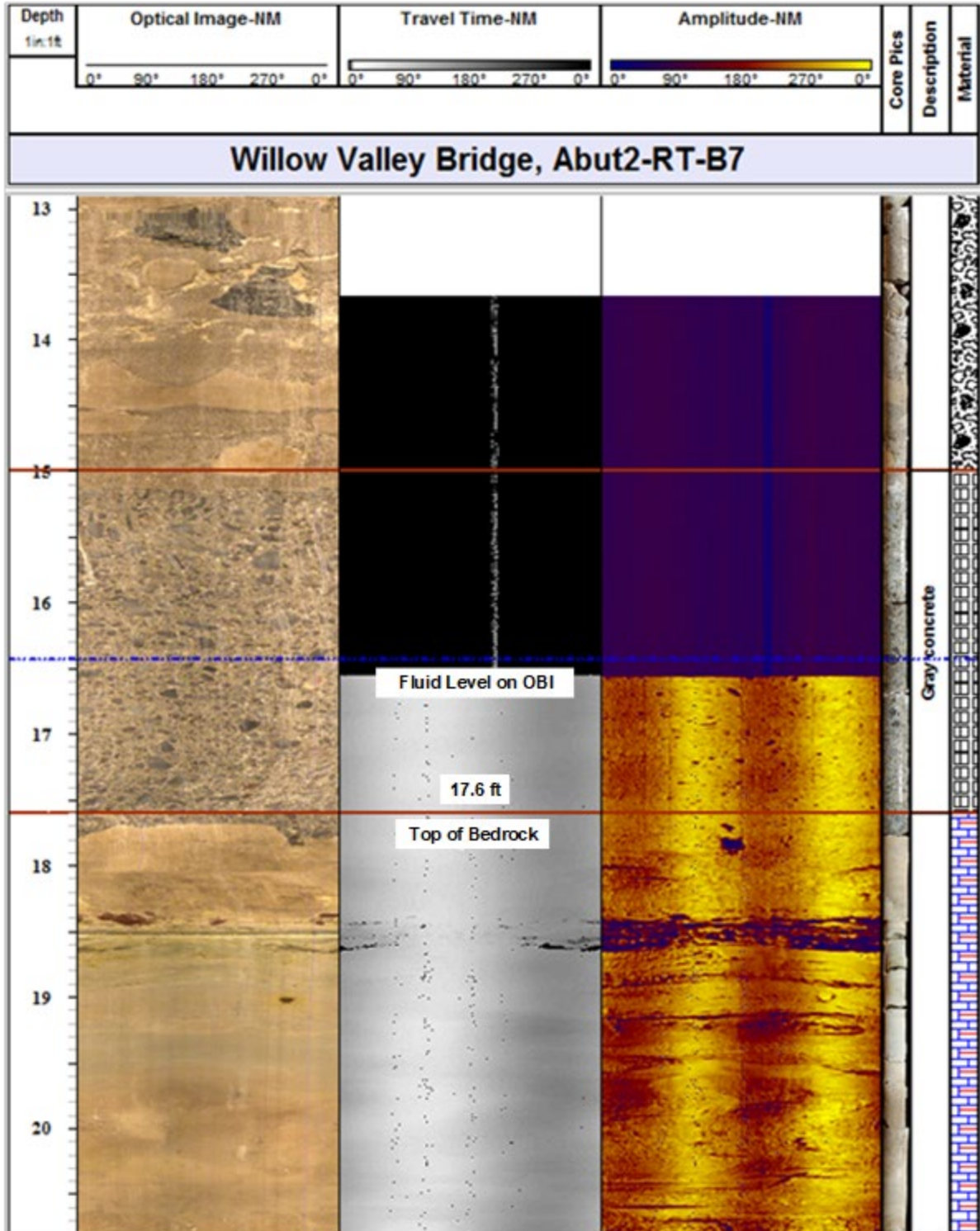
Source: FHWA.
 Corr = Corrected.

Figure 15. Illustration. Image logs across the concrete pad in Pier1-RT-B1 showing no apparent cracks or fractures.



Source: FHWA.

Figure 16. Illustration. Image logs across the concrete pad in Pier2-RT-B2 showing no apparent cracks or fractures.

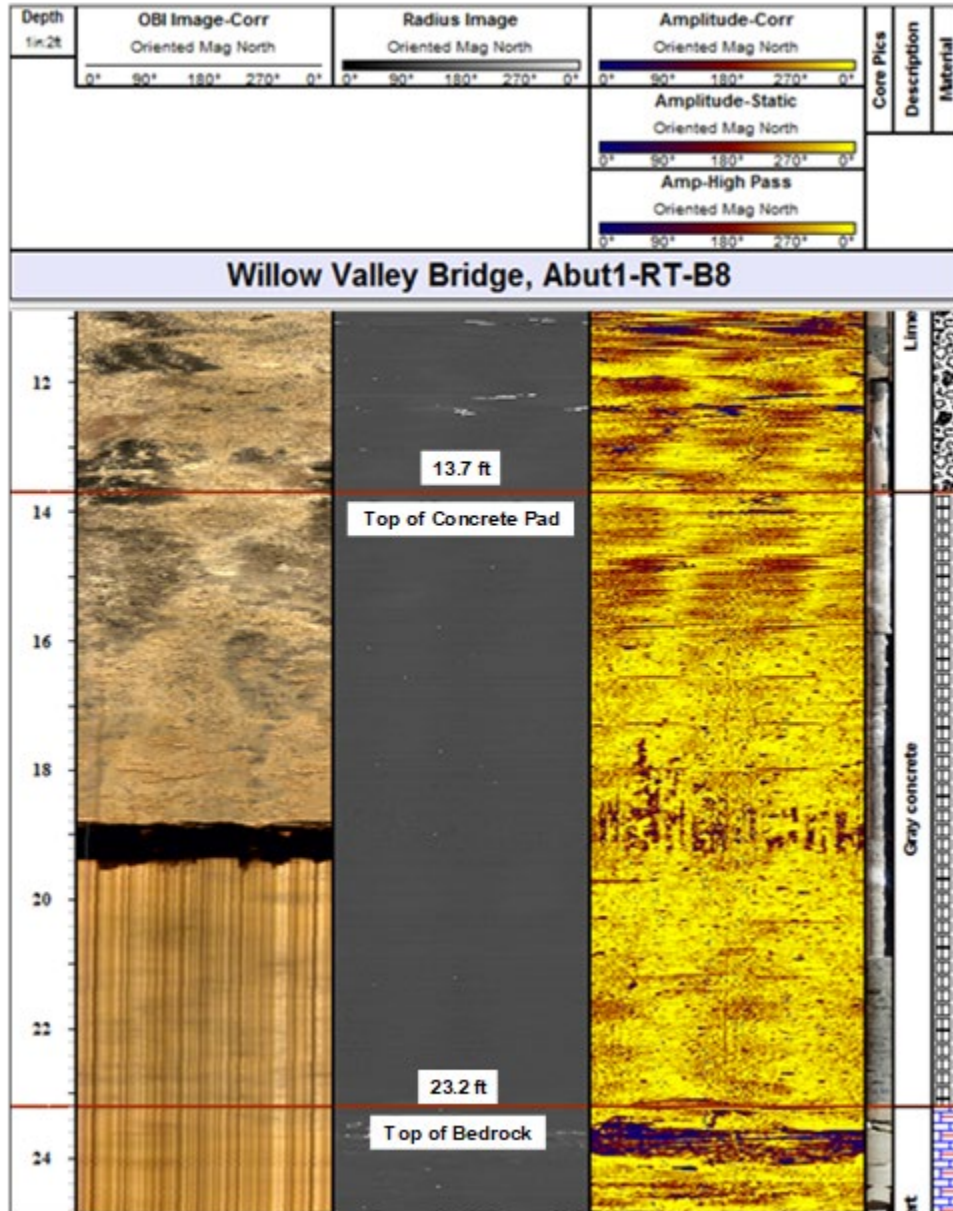


Source: FHWA.
 NM = north magnetic.

Figure 17. Illustration. Image logs across the concrete pad in Abut2-RT-B7 showing no apparent cracks or fractures.

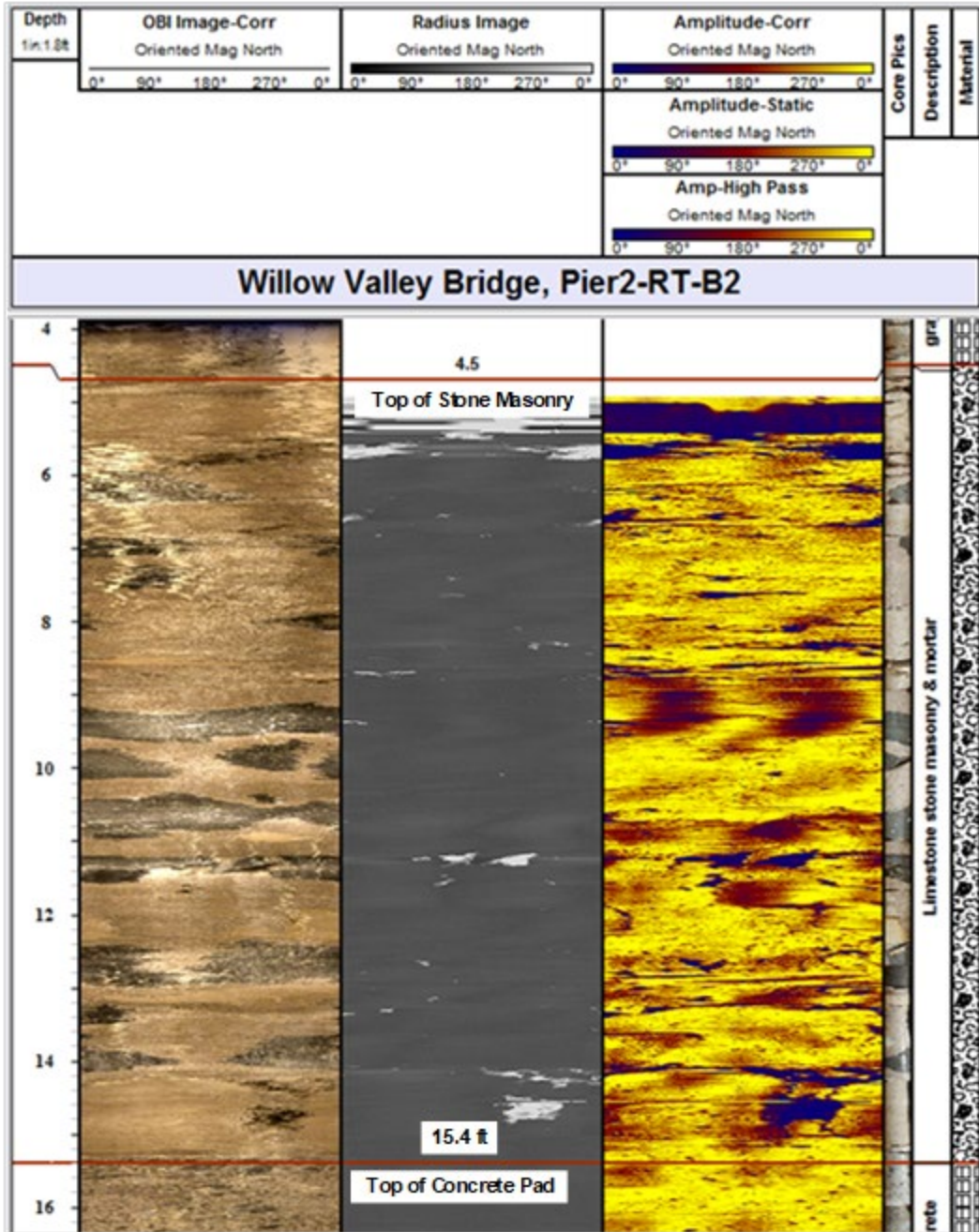
Observations From the Stone Masonry Construction

Figure 18 to figure 21 represent logs showing deterioration in stone masonry construction. The older portion of abutment 1 (where B-5 corehole is located) had the worst deterioration. In figure 19, a few minor enlargements at the edge of clasts are shown at 11 ft (3.4 m) and 14 ft–15ft (4.3 m–4.6 m) on the travel time image. However, it was possible to fill this hole to the top of the pier for the acoustic logs. In figure 20, B5 has the most deterioration. Also, two vugs are in the bedrock in B4. Fine mortar eroded around the harder rubble/clasts can also be seen in figure 21. Figure 22 shows a closeup OBI image in B4 above the bedrock.



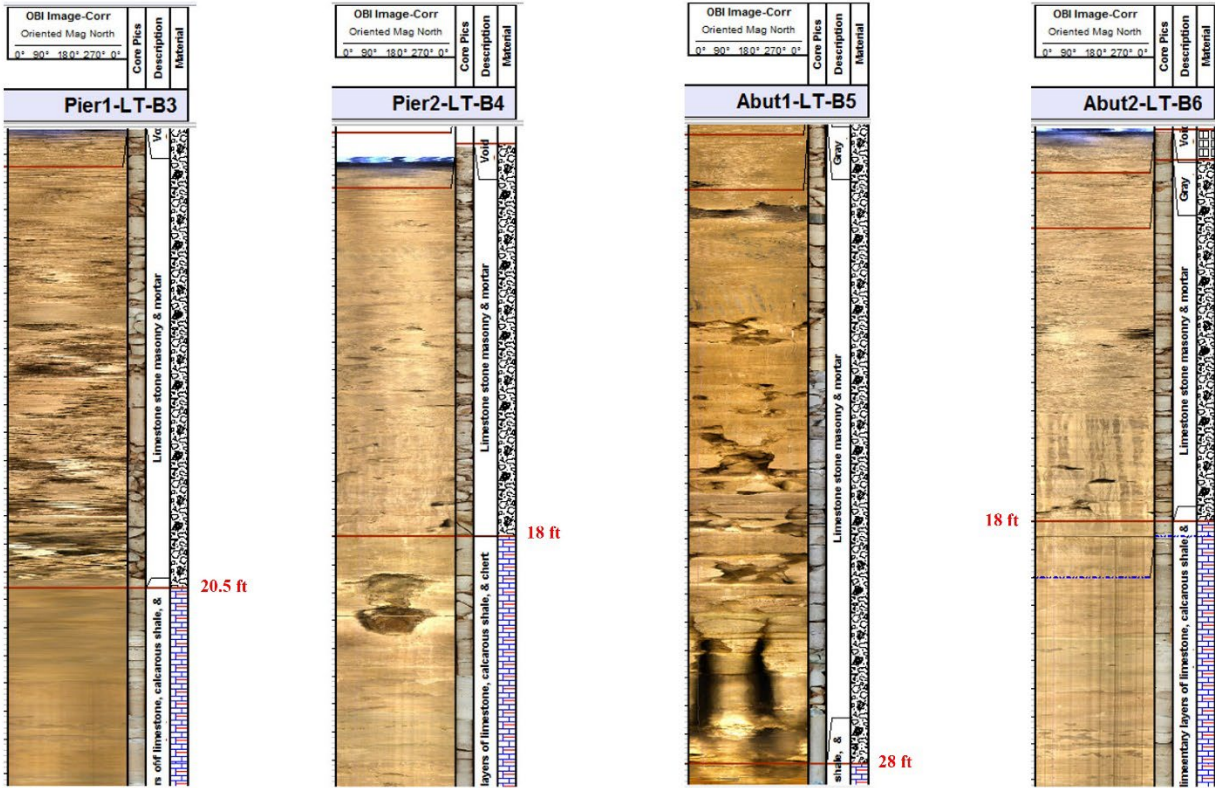
Source: FHWA.

Figure 18. Illustration. Image logs across the concrete pad in Abut1-RT-B8 showing no apparent cracks or fractures.



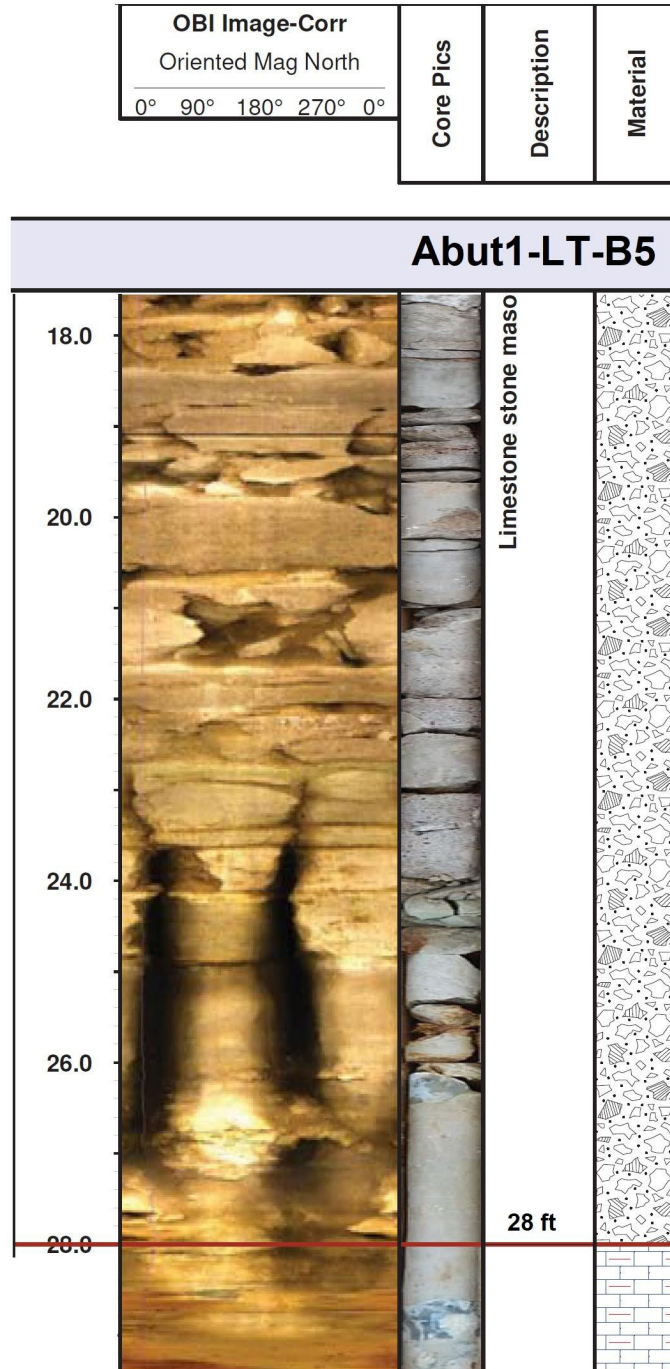
Source: FHWA.

Figure 19. Illustration. Image logs across stone masonry in Pier2-RT-B2.



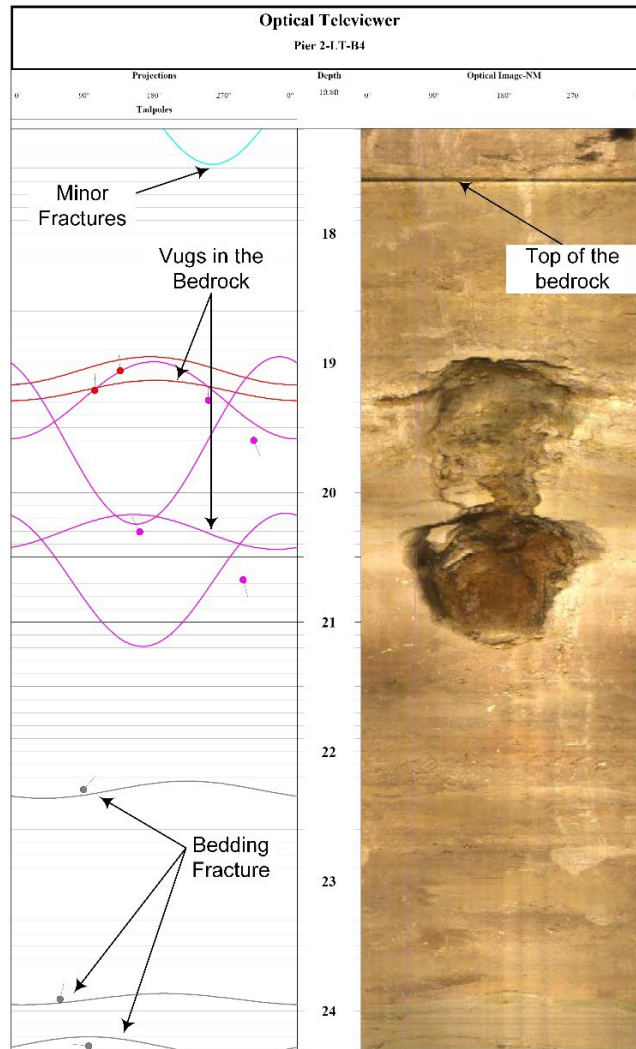
Source: FHWA.

Figure 20. Illustration. OBI images of the stone masonry in the old foundation (B3–B6) showing the various amount of enlargement of the mortar around clasts.



Source: FHWA.

Figure 21. Illustration. Detailed OBI image in Abut1-LT-B5. The two near-vertical enlarged joints have a strike of N41E (MN).

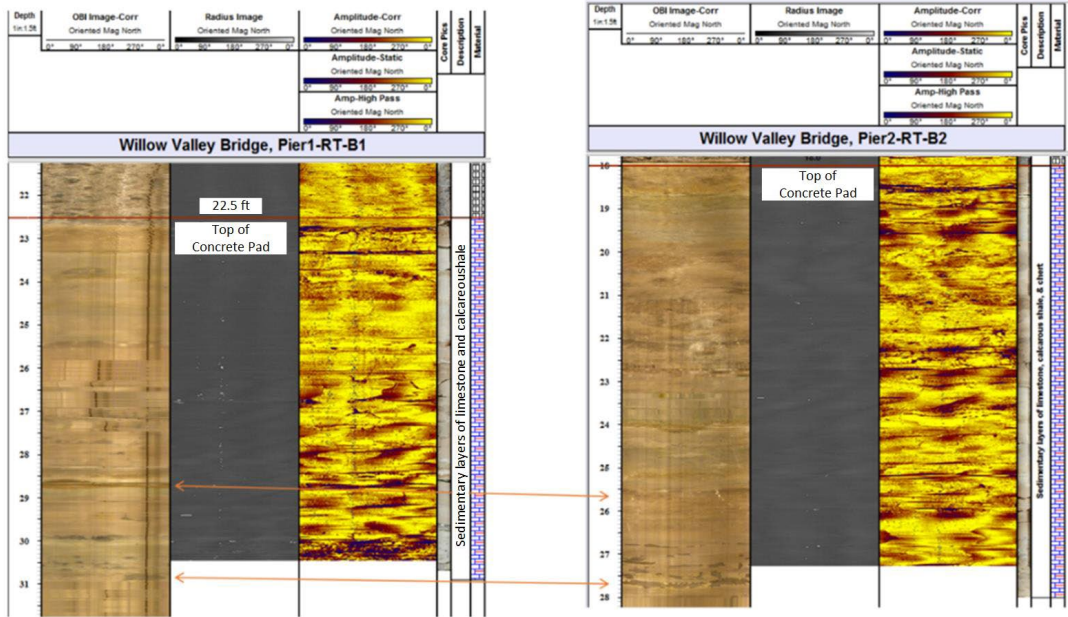


Source: FHWA.
 NM = north magnetic.

Figure 22. Illustration. Optical televiewer image (right) and stereographic projections and tadpole (left) of Pier2-LT-B4 over the bedrock interval.

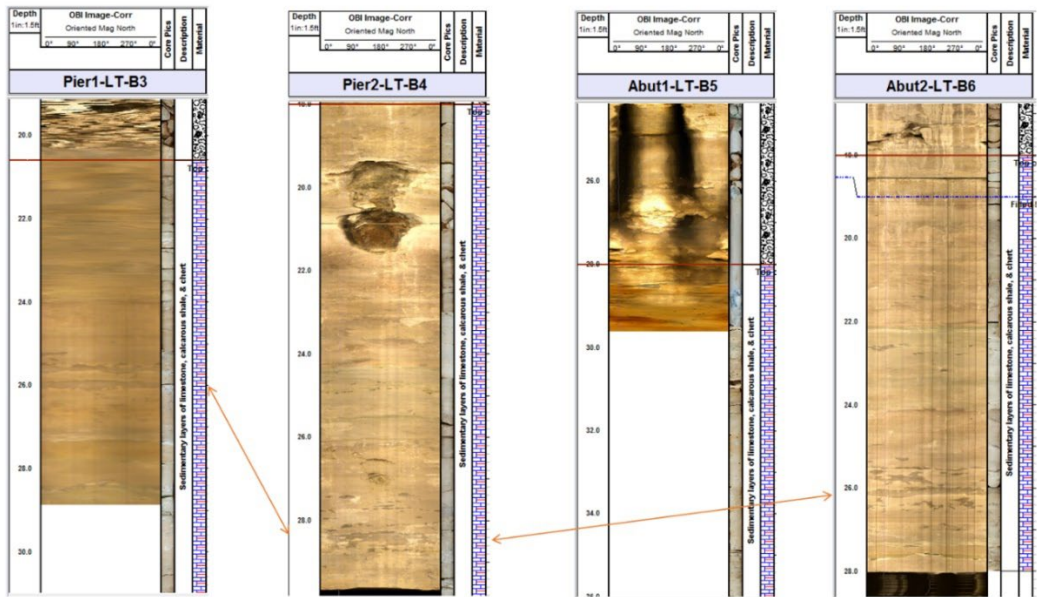
Observations From the Bedrock

Figure 23 to figure 29 show logs displaying the bedrock features. The survey data collected with the image logs shows the tilt of the coreholes is near vertical. Core breaks in the bedrock are near perpendicular to the core, which is consistent with the image log picks. In figure 23, the correlation of two features is shown with the arrows. Bedding features in B3, B4, and B6 can be correlated as shown by the arrows in figure 24. This feature is the same as seen at the bottom of B1 and B2 in figure 23. In figure 25, the poor image quality in B8 is due to turbid borehole fluid preventing any strong bedding correlation; however, the bedding features from 26 to 27 ft (7.9 to 2.1 m) in B7 appear to be the same beds correlated in figure 23 and figure 24. In figure 27, the column to the right shows all the feature picks combined in a single plot.



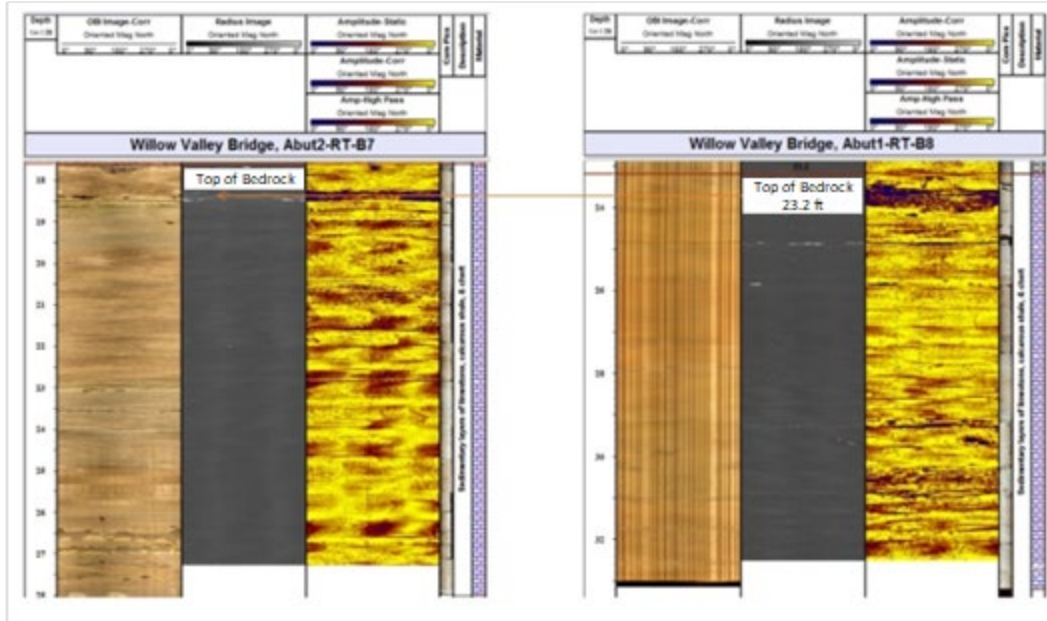
Source: FHWA.

Figure 23. Illustration. Image logs for Pier1-RT-B1 and Pier2-RT-B2 in the bedrock.



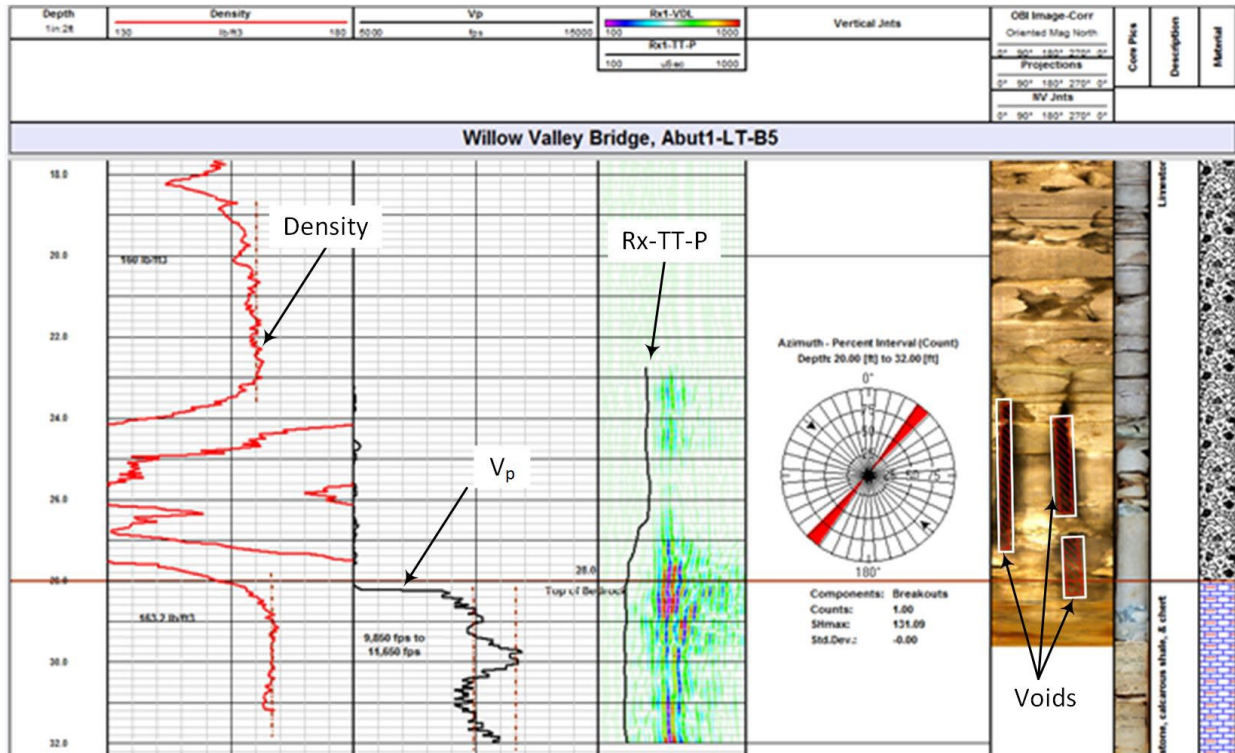
Source: FHWA.

Figure 24. Illustration. OBI images in old foundation (B3-B6) over the bedrock interval.



Source: FHWA.

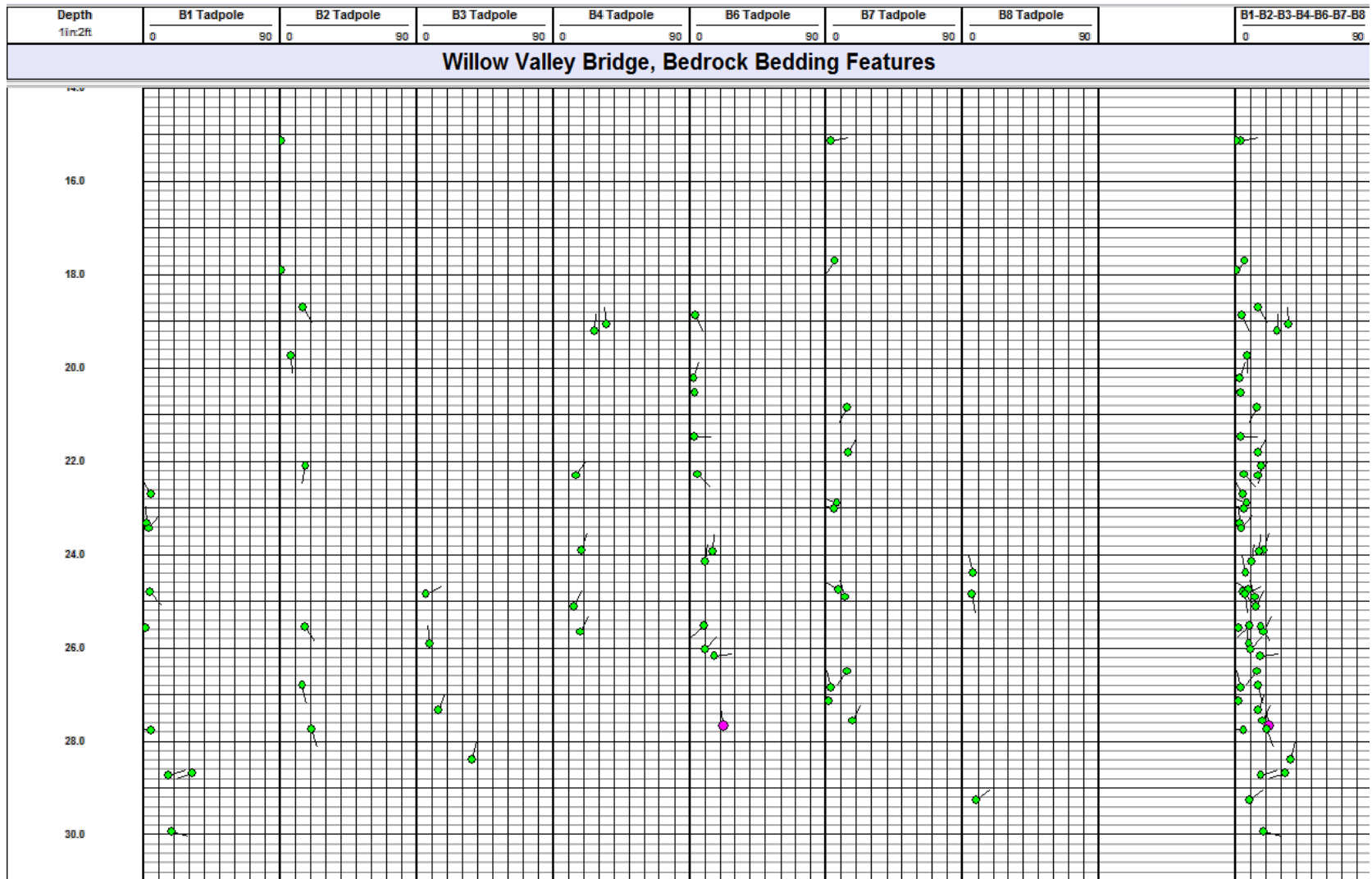
Figure 25. Illustration. Image logs for old foundation Abut2-RT-B7 and Abut1-RT-B8 in the bedrock.



Source: FHWA.

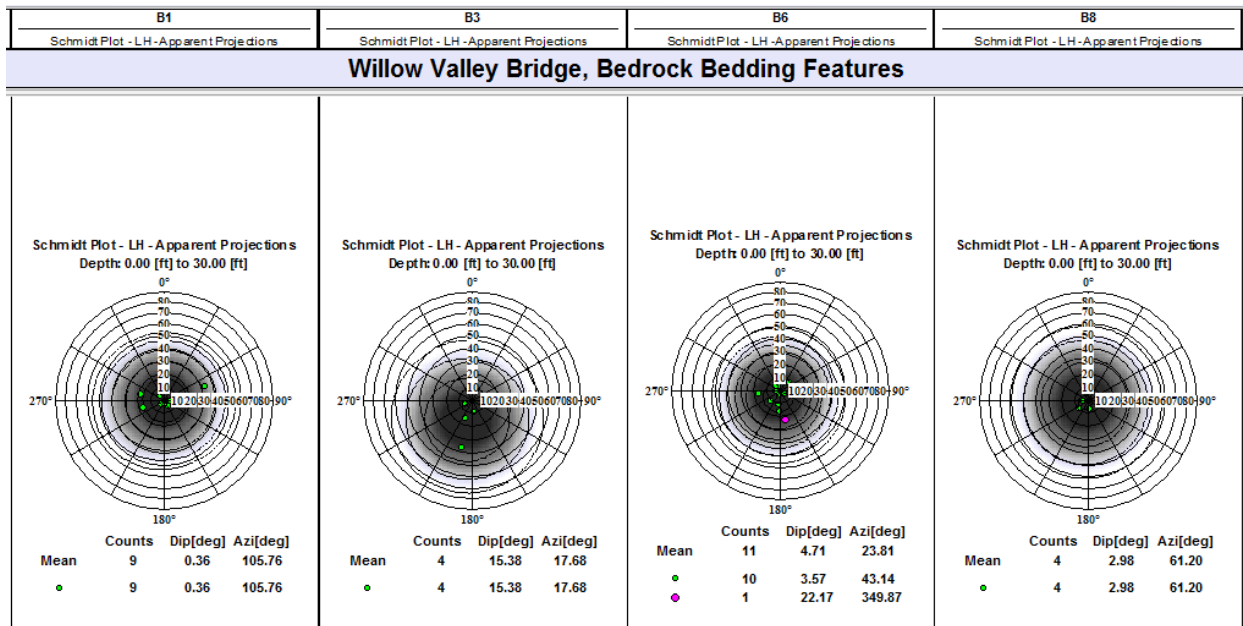
fps = feet per second; Vp = compressional velocity.

Figure 26. Illustration. The large near-vertical enlargements in Abut1-LT-B5 are striking N41E (MN).



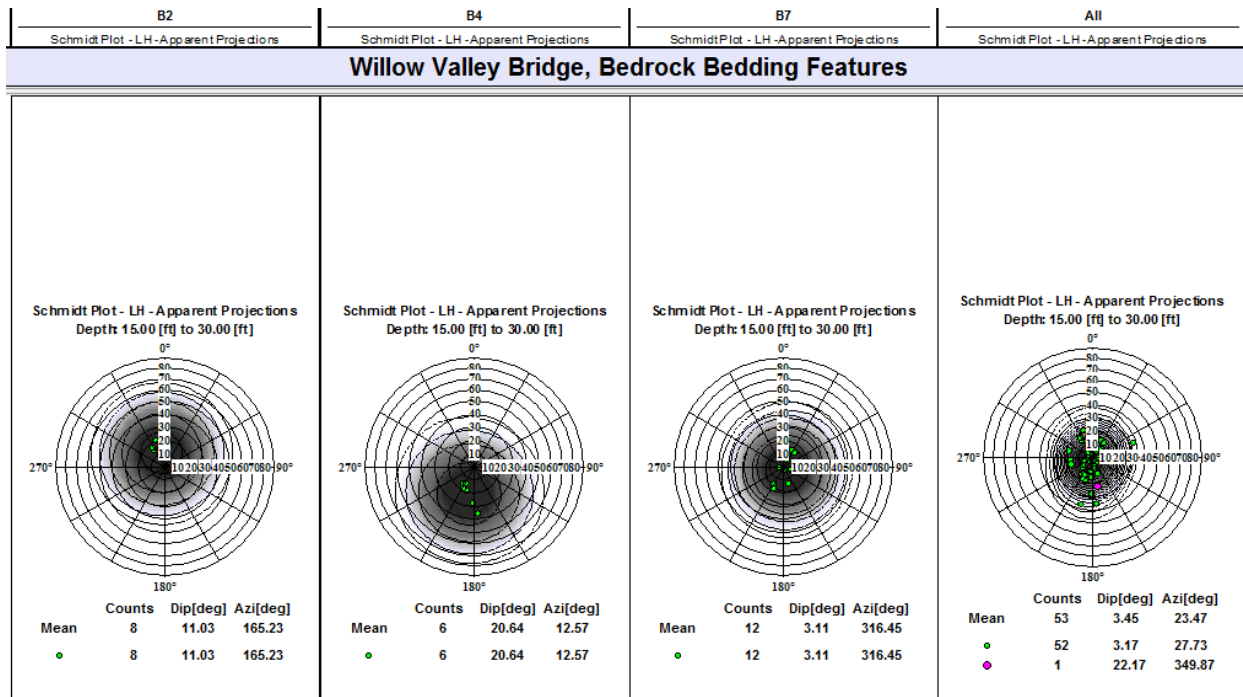
Source: FHWA.

Figure 27. Illustration. Tadpole summary plot of the bedrock feature picks in B1–B4 and B6–B8.



Source: FHWA.
LH = Lower Hemisphere.

Figure 28. Illustration. Schmidt plots of the feature picks in the bedrock in B1, B3, B6, and B8.



Source: FHWA.

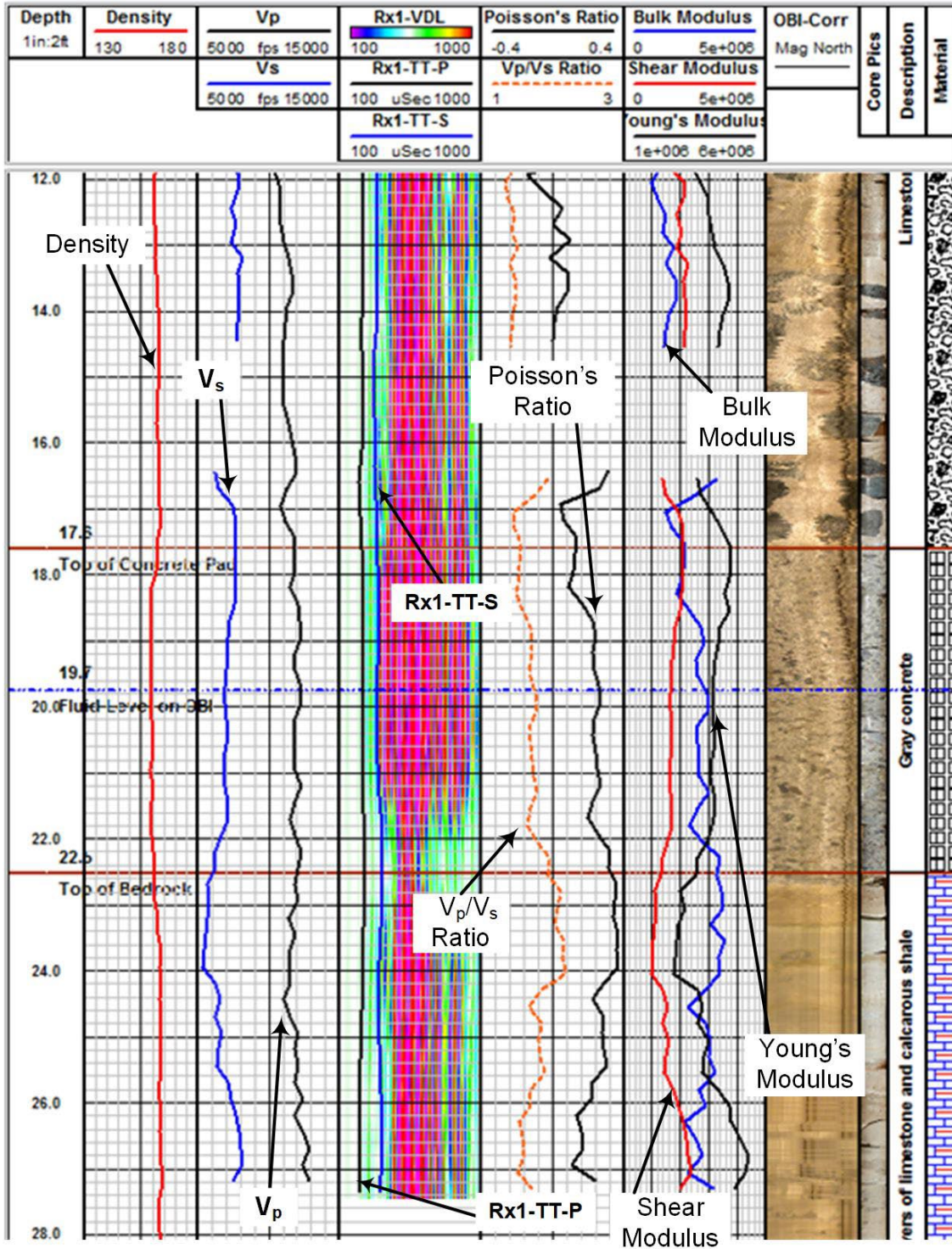
Figure 29. Illustration. Schmidt plots for the feature picks in B2, B4, B7, and for all the holes combined.

Individually, the bedding dips are widely variable, probably due to soft bed deformation when they were deposited. The average dip for all the features is 3.45 degrees toward the N23.5E. This low dip agrees favorably with the bed correlation noted on the image logs in the bedrock.

Physical Parameter Summaries

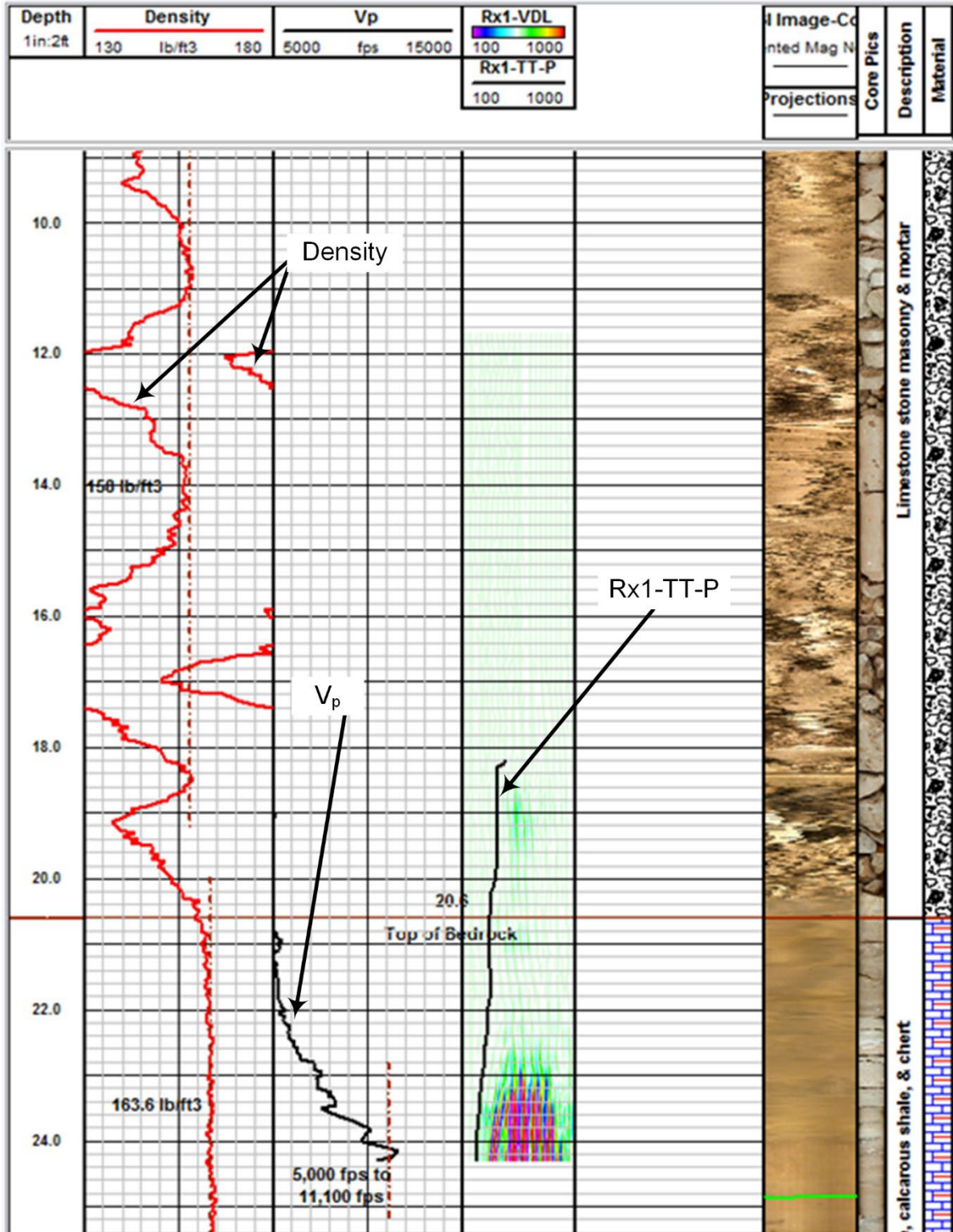
Physical parameter summaries were constructed from the LSD density and sonic data combined with the image data, core picks, and material details. Saturated material is readily apparent on the SONs. Figure 30a to figure 37 show physical property logs for different foundation elements. Figure 30a shows a composite physical property log for corehole B1 in pier 1. This figure shows a composite log of (from left to right columns) depth, density log, primary and secondary velocities logs, sonic log, radius image, ATV, optical log (OBI), and a picture of the core. The composite log shows that the pier is in good condition without any void, as also noted from the density log.

Figure 30b shows elastic moduli logs for corehole B1 in pier 1. The elastic moduli (shear, bulk, Young's moduli, and Poisson ratio) logs, shown on the right, are derived from the measured compressional and shear velocities and density logs shown on the left (refer to Figure 13 equations). Integrity assessment of the foundation element near the corehole region can be made by observing variations in elastic moduli in these logs. Very little variation in elastic moduli in figure 30b indicated the stone masonry was in good condition in the right portion of pier 1. The integrity of other parts of the stone masonry could be inferred from composite logs in figure 31 to figure 37.



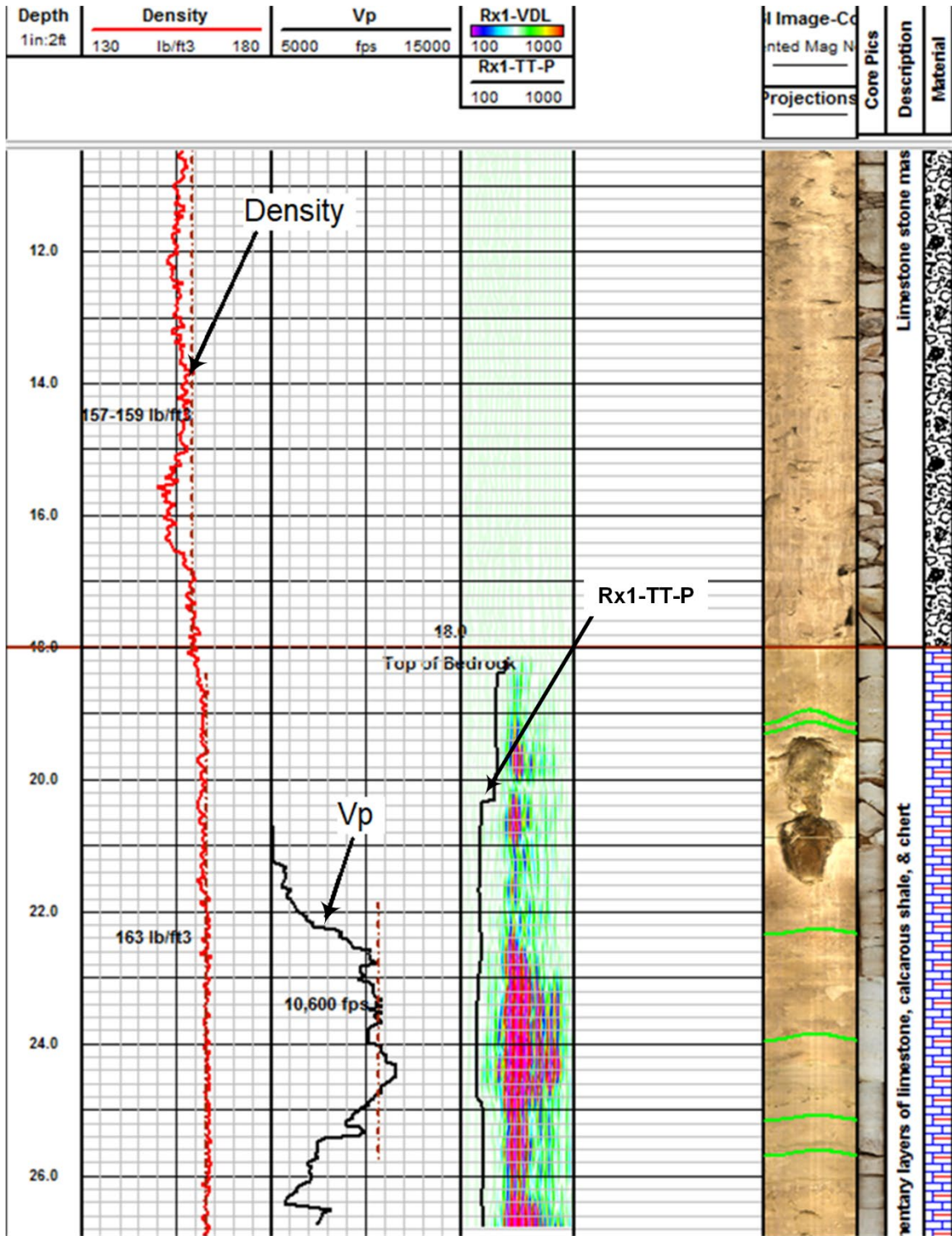
Source: FHWA.
 Vs = shear velocity.

Figure 30b. Illustration. Pier1-RT-B1 physical properties (elastic moduli) logs.



Source: FHWA.

Figure 34. Illustration. Pier1-LT-B3 physical parameter summary.



Source: FHWA.

Figure 35. Illustration. Pier2-LT-B4 physical parameter summary.

Gamma and Electric Logs

The concrete pads on bedrock in B1, B2, B7, and B8 are anomalous high gamma values. These values are probably related to the type of aggregate used but could also be attributable to another additive. The carbonate bedrock has very low gamma values, as expected. The limestone masonry has low gamma values; limestone is typically very low gamma, and the mortar does not have any naturally radioactive materials in it.

CHAPTER 6. SEISMIC TESTING AND IMAGING

DOWNHOLE SEISMIC TESTING

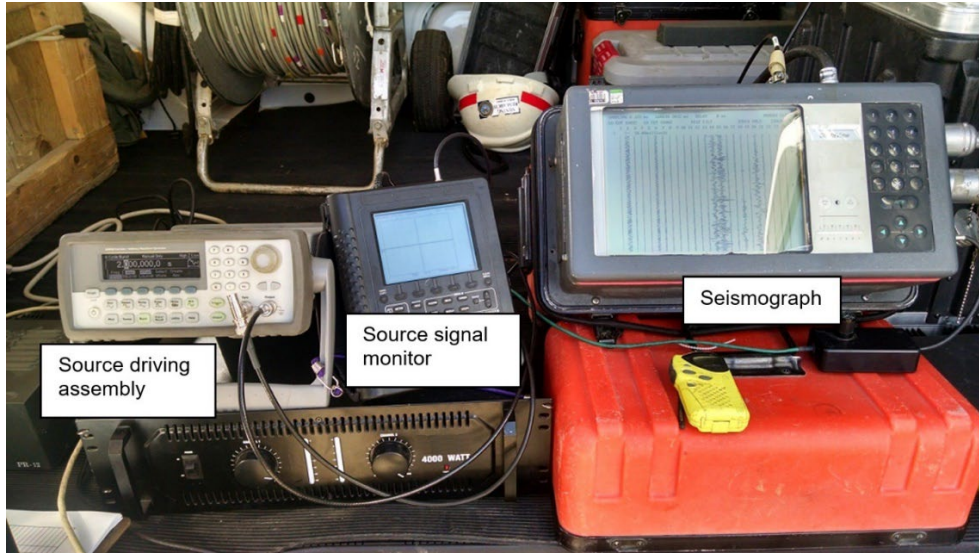
Initially, we conducted downhole seismic testing using a magnetostrictive source applied at the surface of masonry foundation and a hydrophone string that was lowered down the coreholes. At each source point, the tip of the source was pressed manually against a sufficiently flat spot on the surface of a limestone block at a foundation masonry wall, and then the source was powered to send seismic waves into the foundation structure (figure 38).



© 2022 C-Thru Ground, Inc.

Figure 38. Photo. Source with the attached handle being applied at the rock surface.

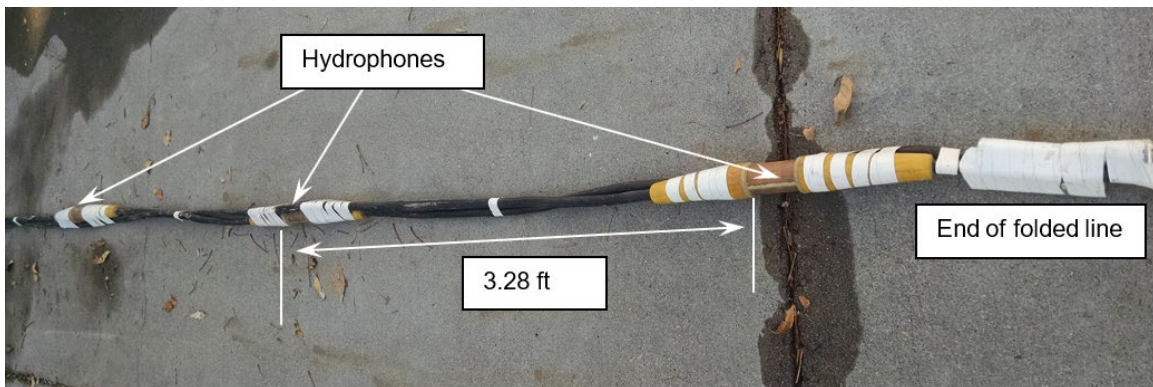
The source was driven by a 2-s swept frequency (pilot) signal ranging from 100 to 3,000 Hz and delivered via cable from the source driving assembly (figure 39). At each source point, the source emitted vibrations (seismic waves) into the foundation wall that were generally perpendicular to the sidewall of the surveyed structure (abutment or pier). Such source action produced predominantly boundary waves traveling sideways down the structure extent.



© 2022 C-Thru Ground, Inc.

Figure 39. Photo. Source driving assembly, source signal monitor, and seismograph.

We folded a string of 12 hydrophones at 6.56 ft (2 m) center to center spacing (figure 40 and figure 41) to form a linear array of hydrophones at 3.28 ft (1 m) centers, enabling a simultaneous installation of up to 8 hydrophones in coreholes that were a maximum of 30 ft (9.1 m) deep. This setting required conducting four rounds of shots through all selected source points and moving hydrophones up by 0.82 ft (0.25 m) between consecutive rounds to get the desired distribution of hydrophone records in each corehole.



© 2022 C-Thru Ground, Inc.

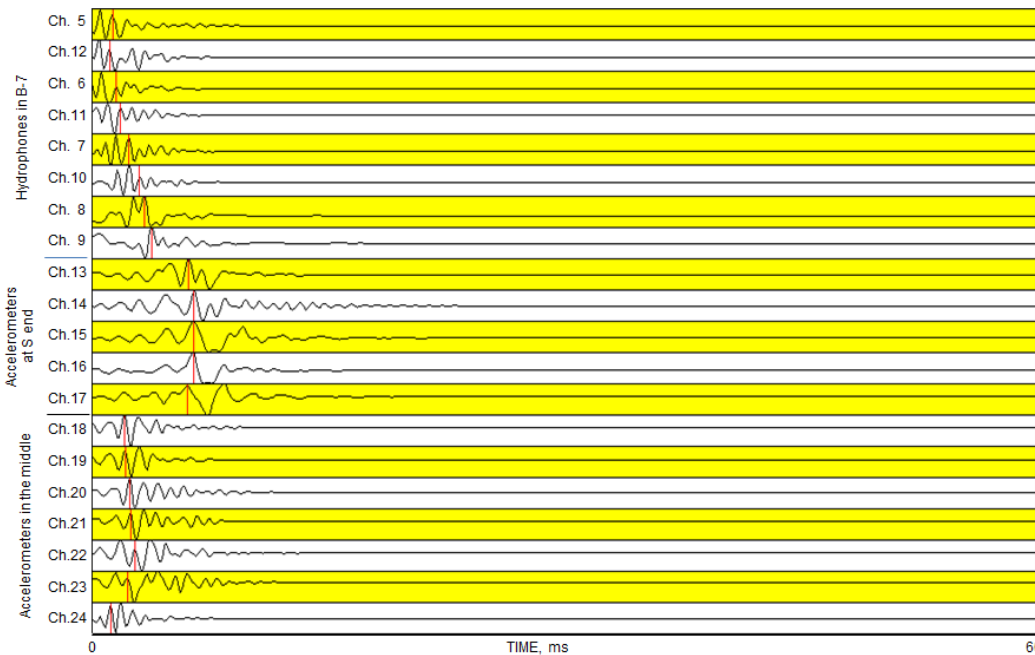
Figure 40. Photo. Twelve-hydrophone line in B-1, folded to shrink offset between hydrophones to 3.3 ft (1 m).



© 2022 C-Thru Ground, Inc.

Figure 41. Photo. Folded hydrophone line suspended in corehole Pier1-LT-B1.

For each source activation (by a manual trigger), the pilot signal and the waves detected by all Rxes were sent via long cables to the seismograph (figure 39). The software installed on the seismograph board performed a cross-correlation with the pilot signal for all detected wave signals, generating records equivalent to an impact source, as shown in figure 42. In this figure, arrival times for direct waves are marked with vertical red lines. Driving the source with a swept frequency signal significantly increased the total energy output, efficiency, and repeatability of the source. It also allowed for surveying without detectable contamination, even in a noisy environment (one traffic lane over the bridge remained open during the survey).

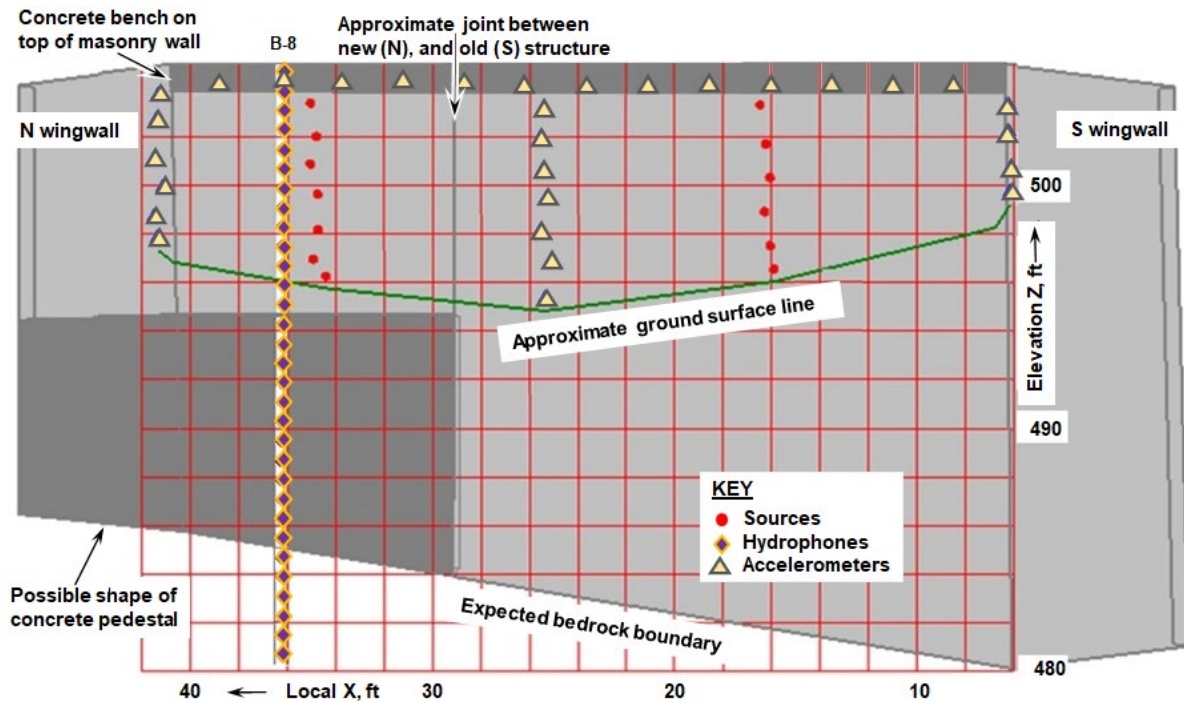


Source: FHWA.
Ch = channel.

Figure 42. Illustration. Typical downhole seismic field records after cross-correlation (Abut2, source position 06).

EXAMPLE DOWNHOLE SURVEY RESULT

An example of the downhole seismic from abutment 1 is shown in figure 43. In general, 2 approximately vertical lines of source points (dots in figure 43) were selected on a sidewall of each foundation unit, and the accelerometers (triangles) were arranged in sets of 11 stations, plus 1 common station used as a reference for all records per each foundation unit. The line of eight hydrophones (diamonds in figure 43) was lowered into the coreholes drilled from the bridge deck into the surveyed foundation unit and down into the bedrock.

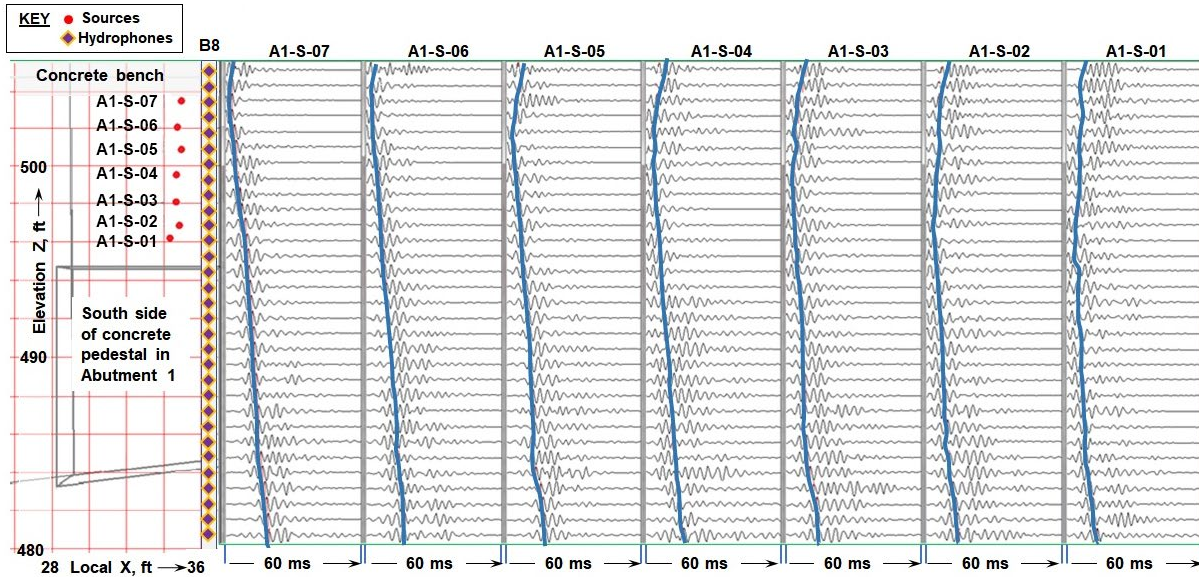


Source: FHWA.

Figure 43. Illustration. Configuration of sources (dots), hydrophones (diamonds), and accelerometers (triangles) used for seismic survey of Abut1.

The survey for each foundation unit was designed to obtain seismic records for a line of hydrophones in the corehole at 0.82 ft (0.25 m) centers resulting in up to 30 recording points per each source point. This objective was accomplished by running four rounds of source activations (shots) through selected source points while lifting the line of hydrophones by that distance between rounds.

To improve the review of scattered hydrophone records, the hydrophone traces for individual foundation units were rearranged to follow the depth sequence for respective coreholes (figure 44). The vertical lines in all seven seismic records follow changes in wave travel times from sources to hydrophones due to distance and the structural changes. Depths for consecutive source locations show uniform wave velocity in the concrete pedestal (approximately 7,000 ft/s or 2,134 m/s) and traces of waves reflected from the top and the contact between concrete and bedrock.



Source: FHWA.

Figure 44. Illustration. Downhole seismic records from seven source positions and hydrophone positions in Abutment 1, corehole B8.

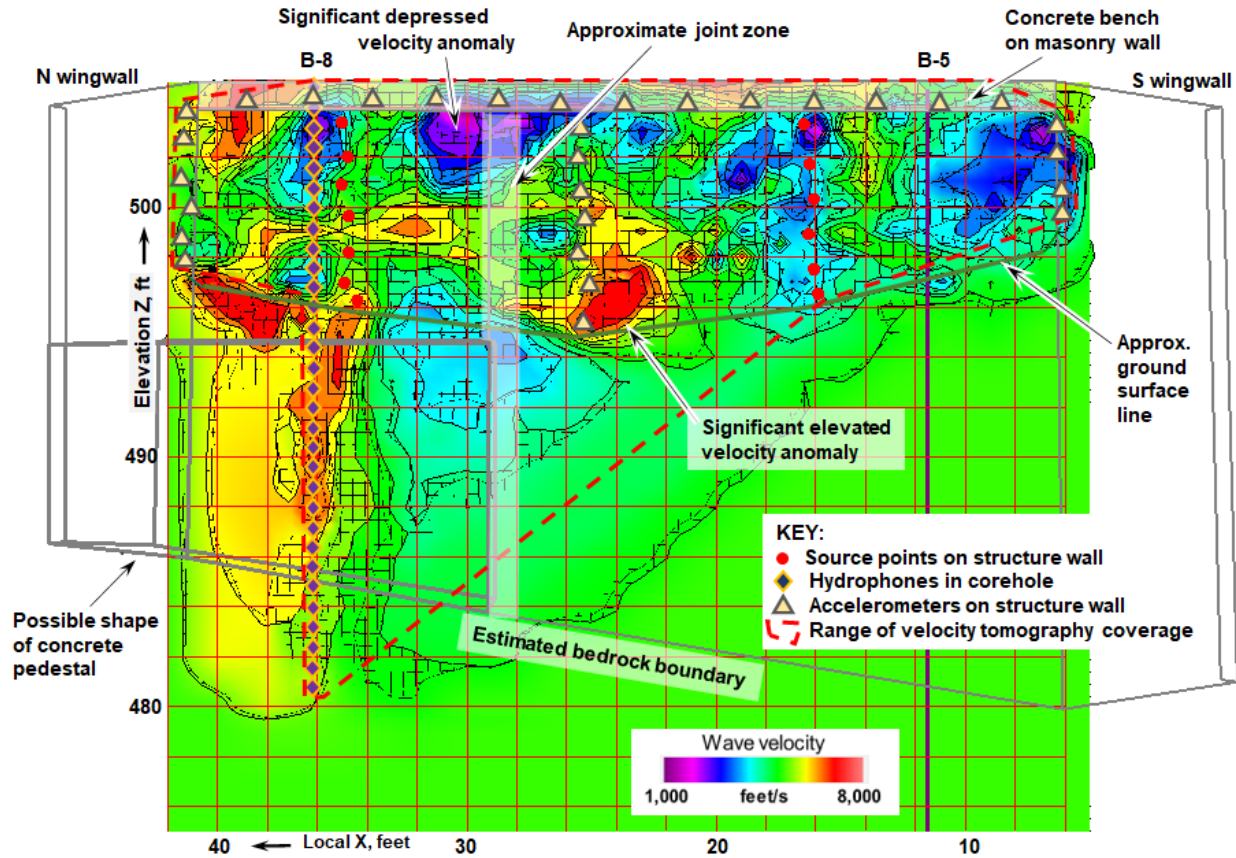
In general, the recorded seismic signals were consistent, and the quality of acquired data was good. A preliminary assessment of the average velocity for the direct seismic waves was performed by plotting travel times for each seismic trace versus distance between respective source-Rx pairs. The average velocity of the direct seismic waves for Abutment 1 was around 4,900 ft/s (1,500 m/s).

SEISMIC IMAGING

Since a pair of coreholes were drilled in each stone masonry wall foundation, the original intent was to perform crosshole tomography between each corehole pair. The tomographic surveys would have provided volumetric imaging of the foundation wall. However, the coreholes could not all retain the water necessary for conducting such tomographic surveys because of the presence of voids in some foundation walls. Therefore, for similar future surveys, facilitating the water retention issue—such as the use of corehole socks and/or bottom plugs—should be a priority.

Instead of performing crosshole tomography, as indicated in figure 43, we conducted surface-to-hole travel-time tomography by deploying seismic sources and few three-component accelerometers attached to the surface of the wall foundation and hydrophone string lowered down the corehole. Figure 45 shows an example velocity tomogram that indicates the distribution of acoustic velocity in the wall, with low velocities indicating possible anomalies. In this figure, the most significant velocity reduction appears distributed in horizontally elongated spots, predominantly at the 5 ft (1.5 m) zone along the top of the abutment wall (including the concrete bench). Elevated anomalies were observed closer to the ground surface line, and another zone appears to be aligned with the borehole over the height of the pedestal. In general, the incremental values of the boundary wave velocity are proportional to the local elastic

properties (shear/rigidity modulus) in the structure, and these values are generally higher in more competent portions and lower in weaker zones.

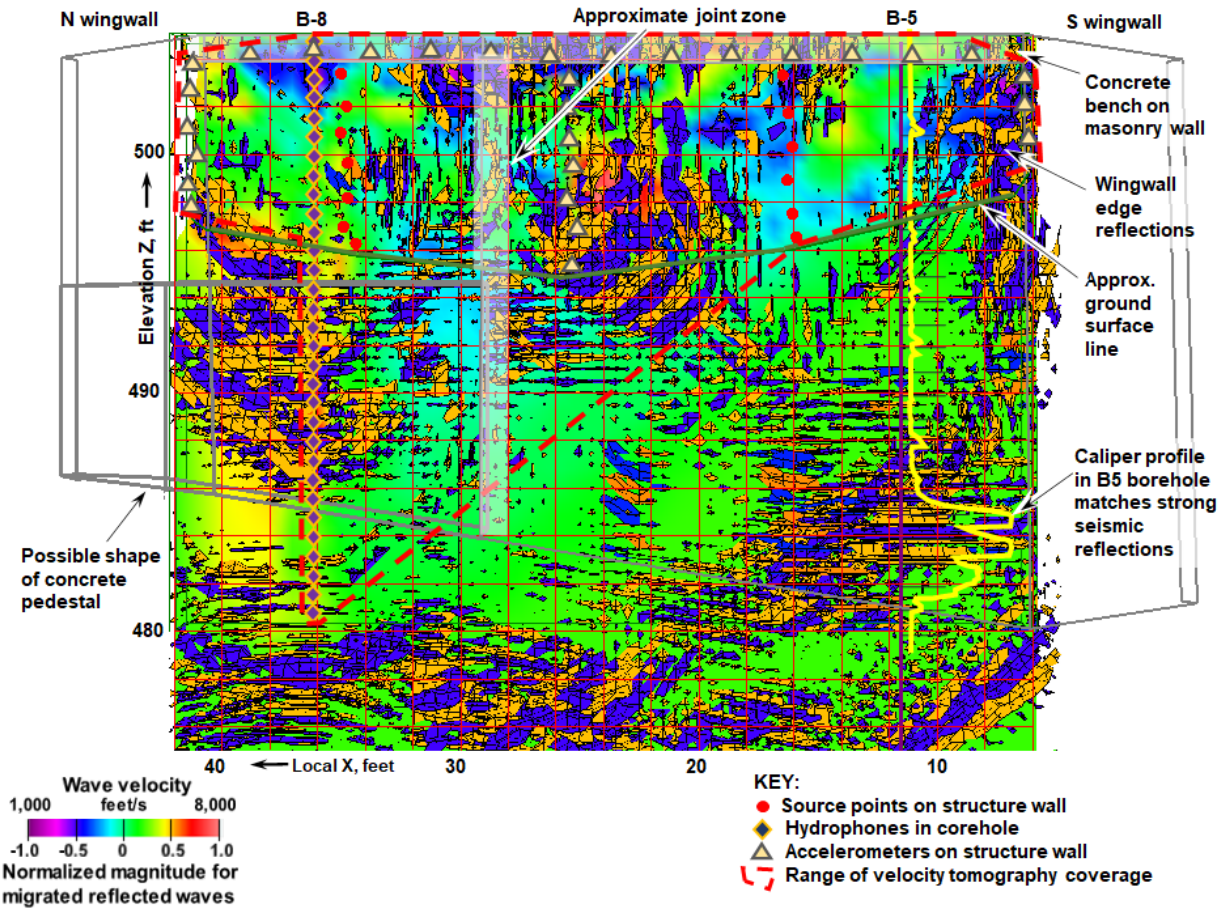


Source: FHWA.

Figure 45. Illustration. Tomogram combined with the volumetric contour image of velocity distribution reconstructed along Abut1 from measured wave travel times (Jalinos 2015).

The velocity tomogram survey coverage area is limited to the approximate triangular-shaped line in figure 45. The survey coverage is obtained using time of flight data from many source and receiver combinations. However, the voids observed in the figure 36 televiewer plot (near bedrock from corehole B5), were located outside the perimeter of the survey coverage. To get information outside the crosshole coverage area, we used the volumetric reflector tracing method to migrate reflected wavelets to their reflection points using the velocity model in figure 45 (Ashida and Sassa 1993).

Figure 46 indicates “reflectogram” images constructed through migration of reflected seismic waveforms to their reflection points superimposed on the velocity model in Figure 45. Because it uses reflected arrivals, the reflectogram has full wall coverage. The migrated waveforms correlated well with the known abutment wall boundaries and with the interpreted location of voids in the wall foundation (indicated by the yellow caliper line). A strong reflective anomaly correlates with the elevated velocity related to the pedestal. Furthermore, an S-shaped dipping zone below the depth of 484 ft (147.5 m) appears parallel to a possible inclined bedrock boundary.



Source: FHWA.

Figure 46. Illustration. Reflectogram migrated image of Abut1 superimposed on volumetric velocity model (Jalinoos 2015).

The seismic imaging and logging results were used by FHWA engineers to fill the construction voids using the jet grouting method prior to the bridge widening operation.

Jalinoos et al. (2017) describe a more rigorous application of the waveform tomography technique using the ultraseismic method for bounded medium.

CHAPTER 7. CONCLUSIONS

This report presents the wireline logging results from the Willow Valley Creek (Lake Mary Road) Bridge in Arizona. The following conclusions are drawn from the logging investigation:

1. The gamma logs on the density and ELOG tools were easily correlated through different absolute values due to detector size. Features could be correlated in the ABI and OBI images, and these logs could also be correlated to the one-arm caliper log. There were correlation depth offsets greater than 5 ft (1.5 m) in the individual logs. The magnetometer is offset 4 ft (1.2 m) higher than the OBI and ABI detector windows, which means that the raw image logs responded to steel interference at the top of the coreholes.
2. The mechanical one-arm caliper readily shows the deficits (voids, washouts, and enlargements) in the stone masonry pier construction on the original piers (coreholes B3–B6). The near-vertical joint-like deficit in B5 is enlarged to 15 in (38 cm) in an HQ corehole. These deficits were confirmed in the image logs of these coreholes and are obvious in the density log values, which average 160 lb/ft³ (2,563 kg/m³) in the good construction and go down to 70 lb/ft³ (1,121 kg/m³) in the major deficit in B5. These deficits likely occurred during the drilling of the coreholes due to friable mortar being eroded; however, the log data are insufficient to positively confirm this supposition.
3. The coreholes on the 1968 foundations (B1, B2, B7, and B8) showed the stone masonry construction to be in good condition without the deficits seen in the older foundation. Black clasts are apparent in the new construction that are not evident in the original construction. There were no cracks or fractures detected in the concrete pads in these coreholes.
4. The dip calculated on the image feature picks utilized a fixed corehole diameter of 3.78 in (9.6 cm). Planar image features were picked only in the bedrock. Determining whether the apparent features in the stone and masonry structure were edges of clasts or rubble or were actual fractures is not possible; therefore, they were not picked. The bedrock foundation was massive, with low-lying to flat bedding and foliation features. The apparent changes in the dip and dip direction of these features are probably related to soft bed deformation during deposition. The average dip for all the features is 3.45 degrees toward the N23.5E (MN). Due to the lack of good bedding planes, a more accurate bedrock dip should be calculated using the bed noted in B1 (28.7 ft or 8.7 m), B2 (26.6 ft or 8.1 m), B3 (26 ft or 7.9 m), B4 (28.4 ft or 8.7 m), B6 (26.2 ft or 8m), and B7 (26.9 ft or 8.2 m). Two vugs were noted at 20–21 ft (6.1–6.4 m) in B4.

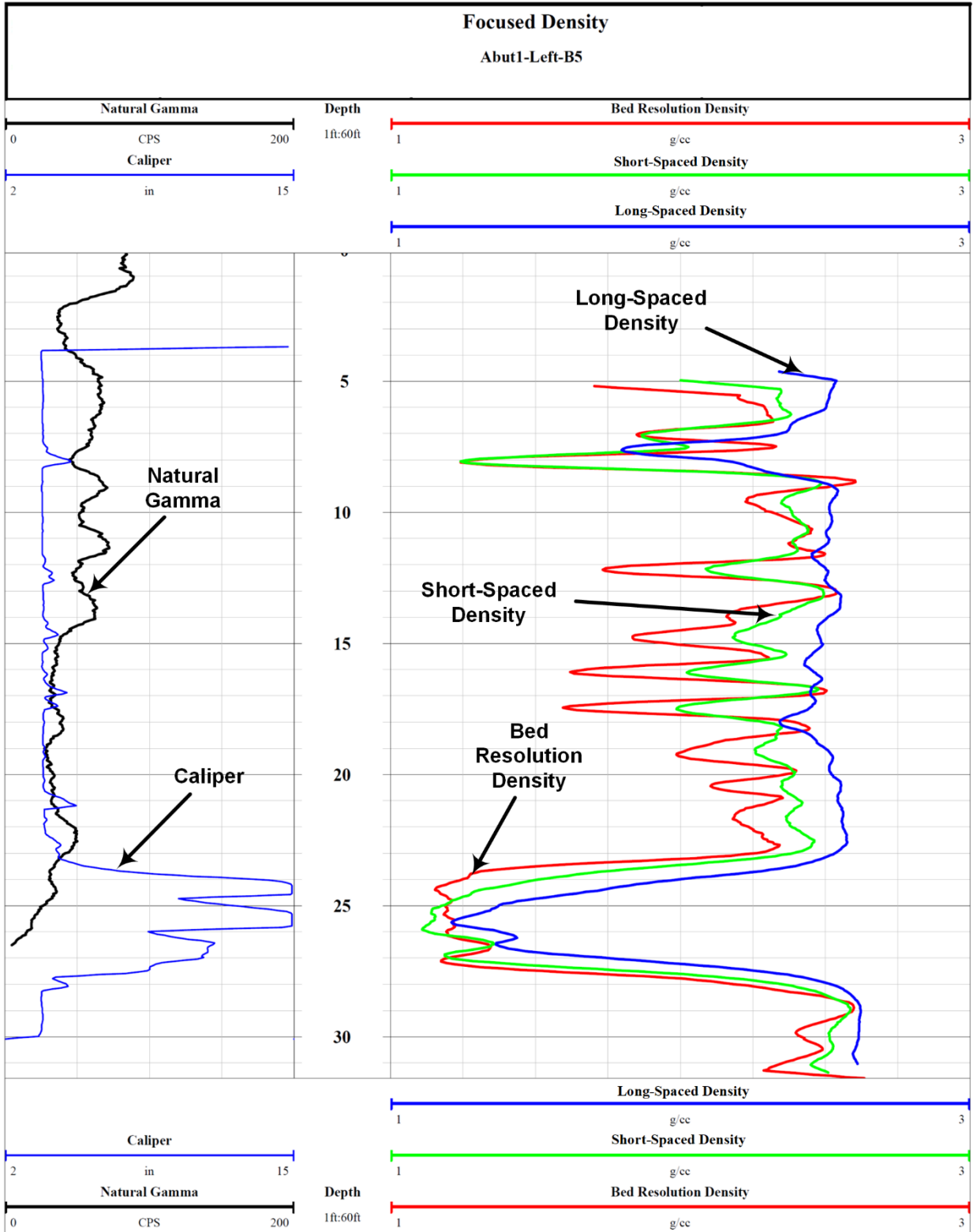
5. The average density in the stone masonry was 161.8 lb/ft³ (2,592 kg/m³) in the 1968 foundations and 160.1 lb/ft³ (2,565 kg/m³) in the original foundations. Note that the density did decrease markedly in the deficits. The density in the concrete pads was 160 lb/ft³ (2,563 kg/m³) in three of the four coreholes and 158.25 lb/ft³ (2,535 kg/m³) in B7. The density in the bedrock averaged 163.3 lb/ft³ (2,616 kg/m³). The bedrock was higher density than the human-made construction. The density of the stone masonry and concrete pad was similar when in good condition.
6. Velocity data could only be collected in two coreholes in the stone masonry due to a lack of fluid and saturation: B1 and B2 had compressional velocities of 11,290 ft/s (3,441 m/s) and 8,000 ft/s (2,438 m/s), respectively. The shear velocity was 7,762 ft/s (2,366 m/s) in B1. The compression velocity in the concrete pads ranged from 11,525 ft/s (3,513 m/s) to 12,000 ft/s (3,658 m/s) with 11,842 ft/s (3,609 m/s) average. Shear velocity averaged 66,992 ft/s (20,419 m/s).
7. Bedrock velocities were more variable but averaged 11,742 ft/s (3,579 m/s) for compressional velocity and 6,964 ft/s (2,123 m/s) for shear velocities. Therefore, the average values were very similar to the overlying concrete. The reflected tube waves were not observed on any of the sonic waveform data. However, this observation is not unexpected for sonic data collected above the permanent water table.
8. Downhole seismic surveys were also conducted in selective coreholes. The average velocity of the direct seismic waves in the masonry structure was around 4,900 ft/s (1,500 m/s) for abutment 1, 4,800 ft/s (1,463 m/s) for abutment 2, approximately 4,500 ft/s (1,372 m/s) for pier 1, and around 4,250 ft/s (1,295 m/s) for pier 2.
9. Wireline investigations in human-made structures require careful planning for drilling to ensure corehole verticality, core sample management, and means for retaining water in the coreholes in case voids are encountered in the structure or in the bedrock.

The project was part of broader geotechnical, geophysical, and nondestructive evaluation (NDE) investigations to determine the structural integrity and suitability of the bridge substructure for reuse (Agrawal et al. 2018). The logging and seismic imaging results were also used for identifying previously unknown voids in the foundation walls and subsequently filling them by jet grouting. Compared to full bridge replacement, the reuse option resulted in at least \$500,000 in cost savings and 3 mo in construction time (FHWA 2015). This saving is significantly higher than the cost of the field investigations for determining foundation capacity, integrity, and durability.

Although this project was performed to evaluate suitability for reuse of an existing bridge substructure, the methodology presented herein can be used for condition evaluation of concrete or stone masonry structures for other investigations such as posthazard assessment.

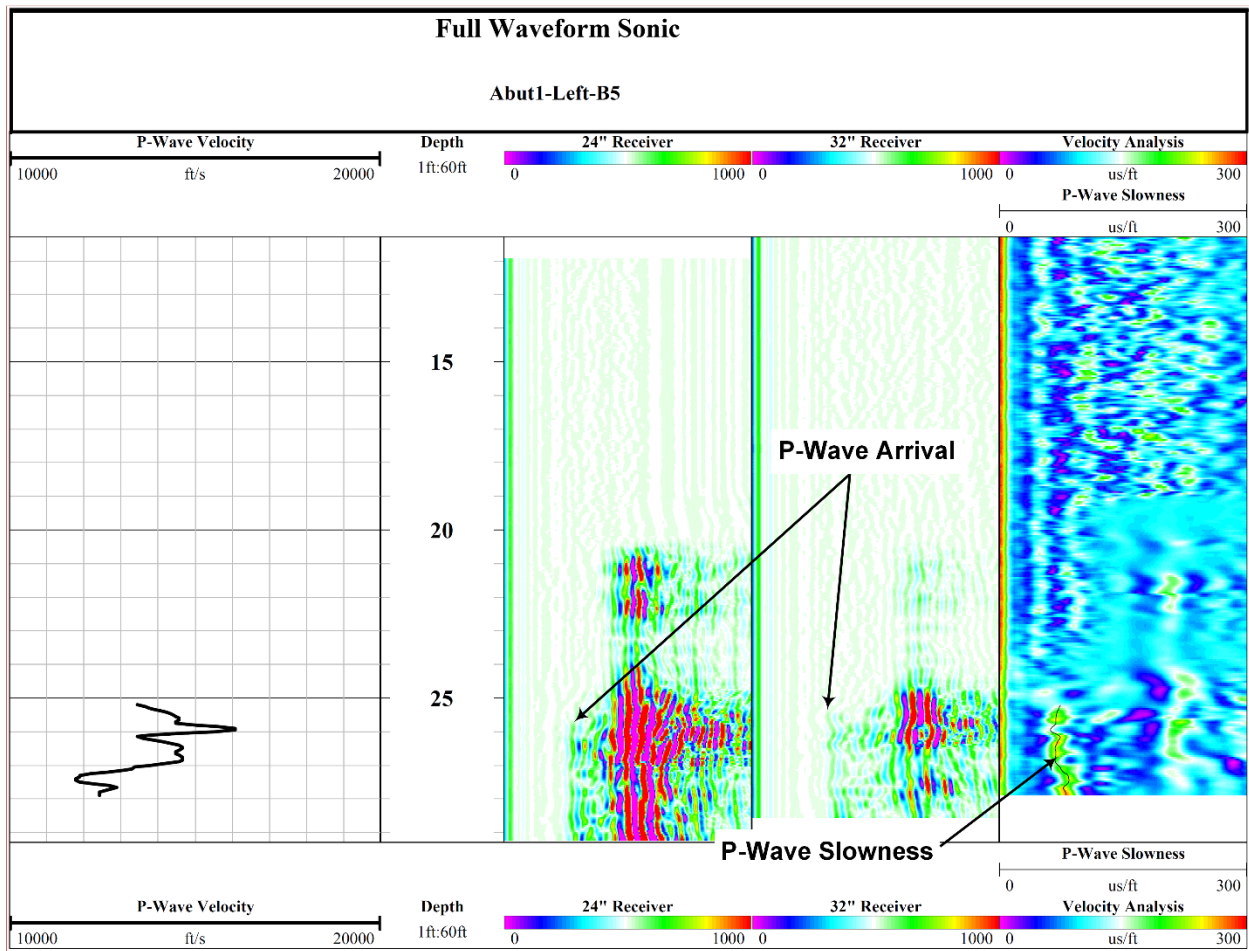
APPENDIX. GEOPHYSICS LOGGING RESULTS

Supplemental geophysical logging results from the Willow Valley Creek Bridge project are presented herein in figure 47 through figure 70.



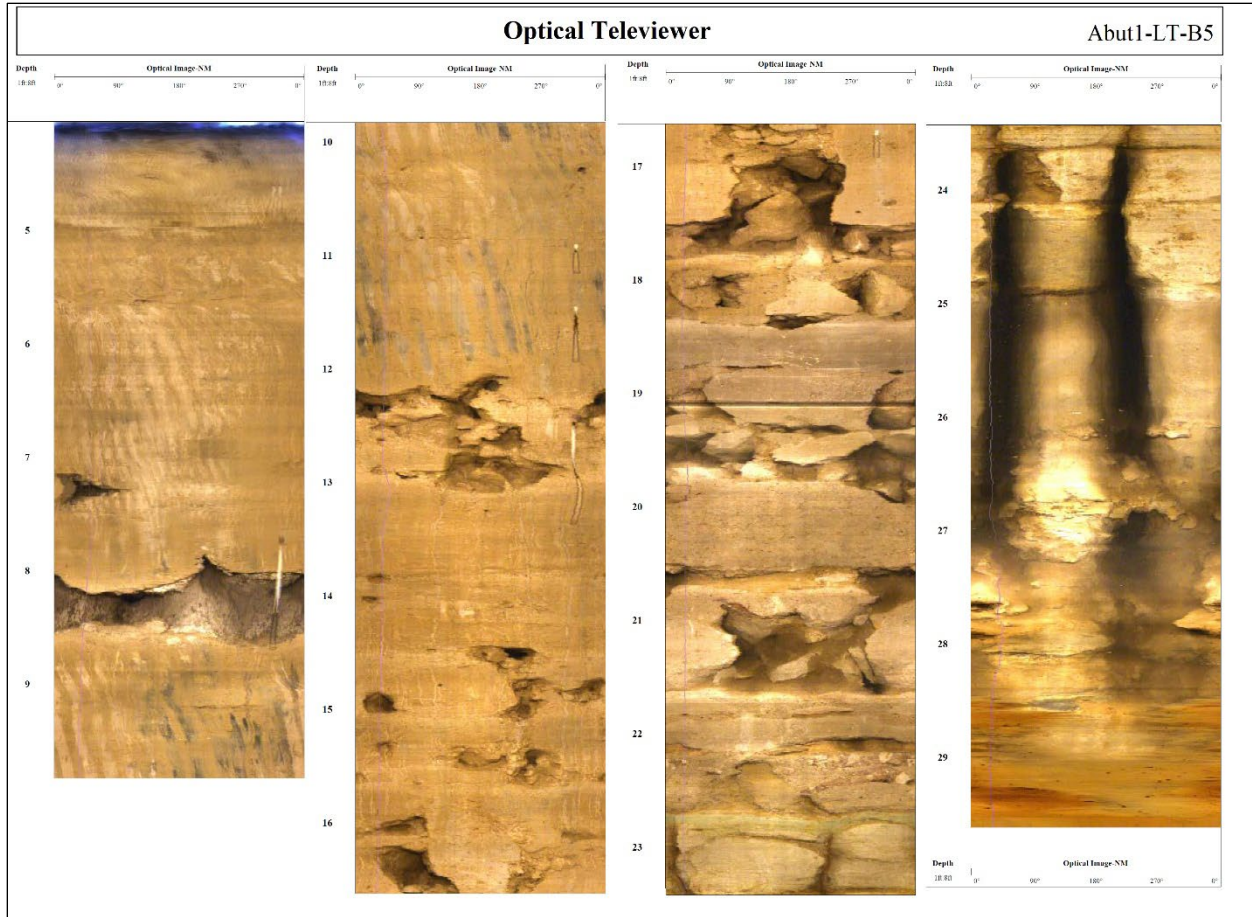
Source: FHWA.

Figure 47. Illustration. Density log of Abut1-LT-B5.



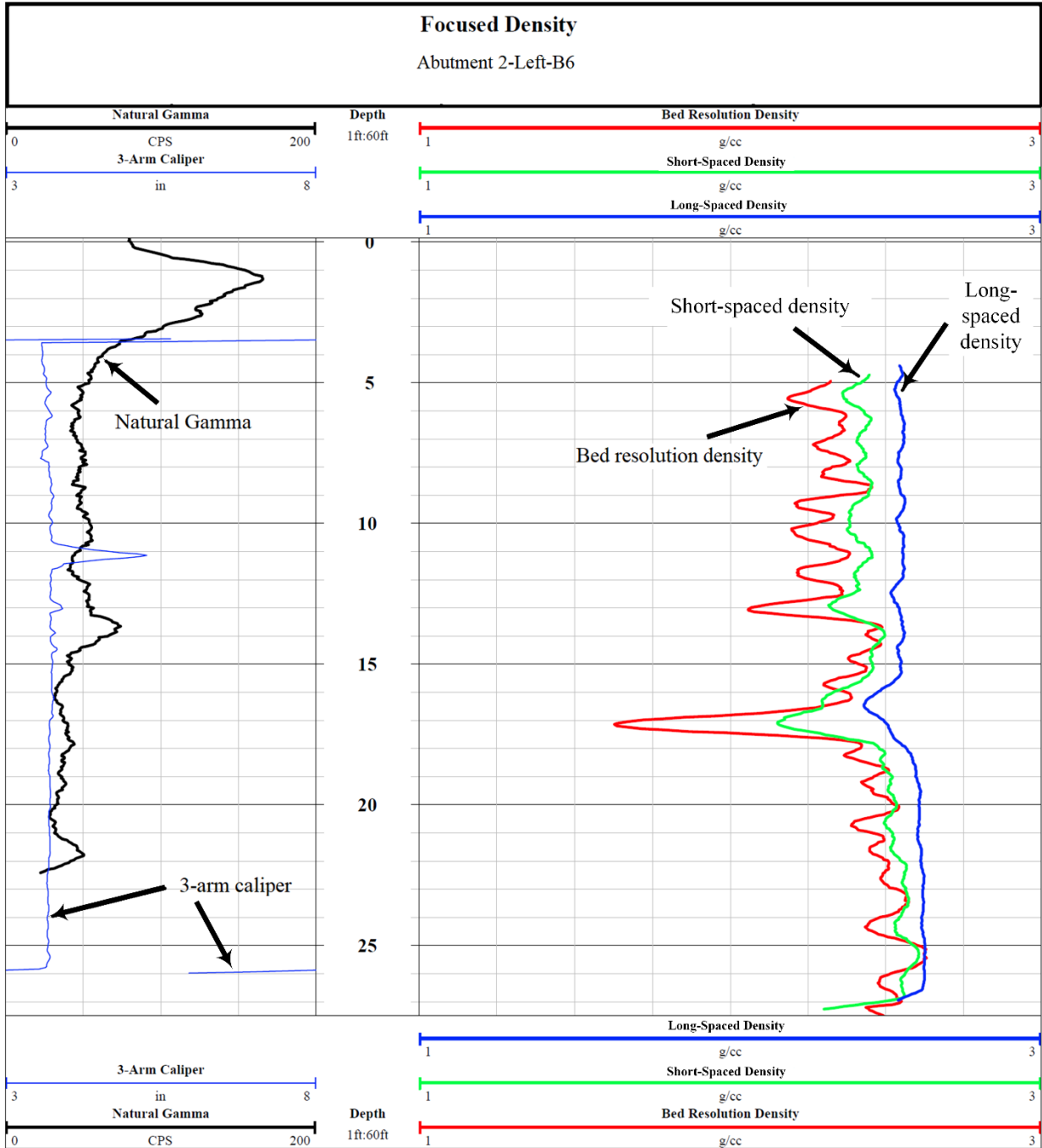
Source: FHWA.

Figure 48. Illustration. Sonic log of Abut1-LT-B5.



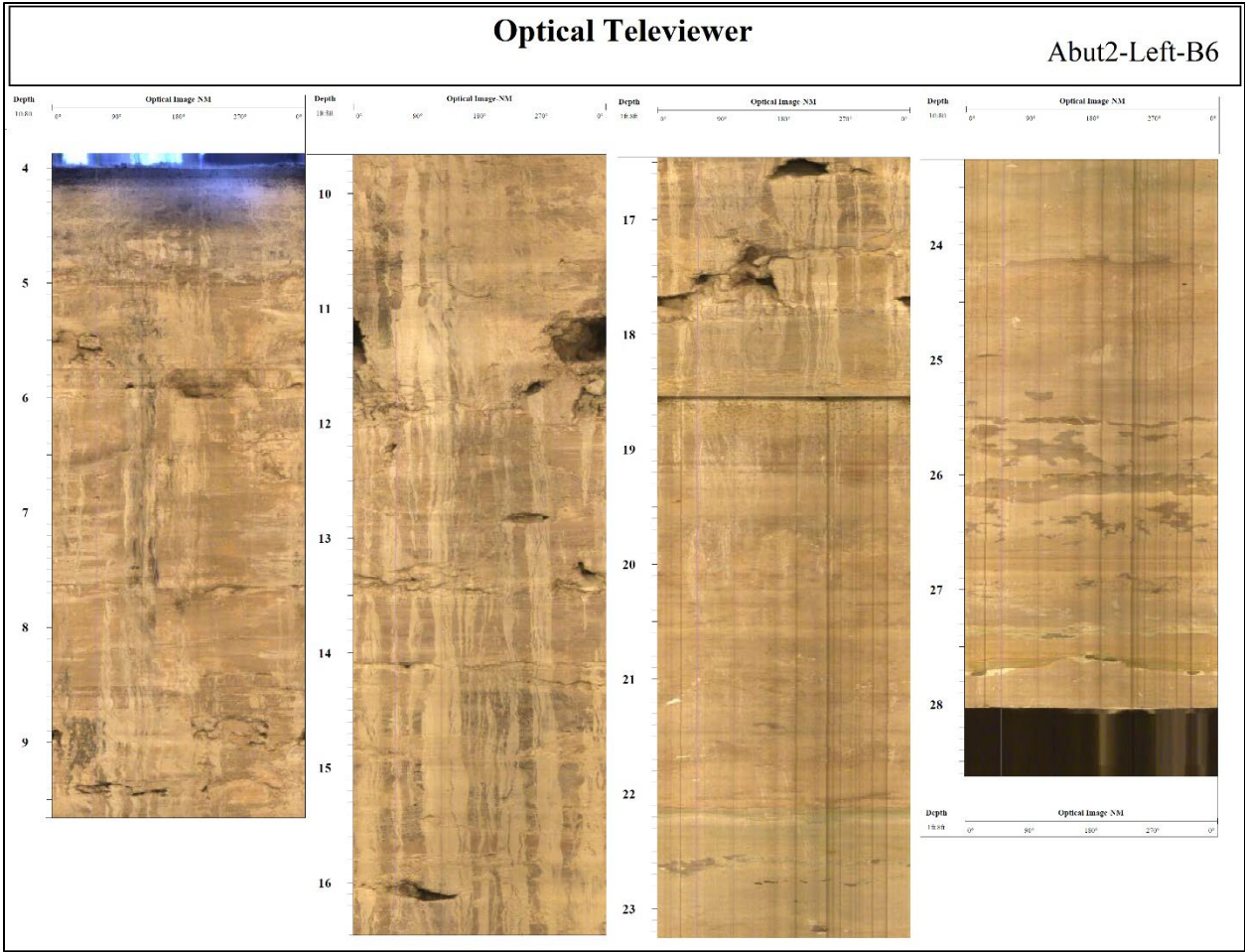
Source: FHWA.

Figure 49. Illustration. Optical images of Abut1-LT-B5.



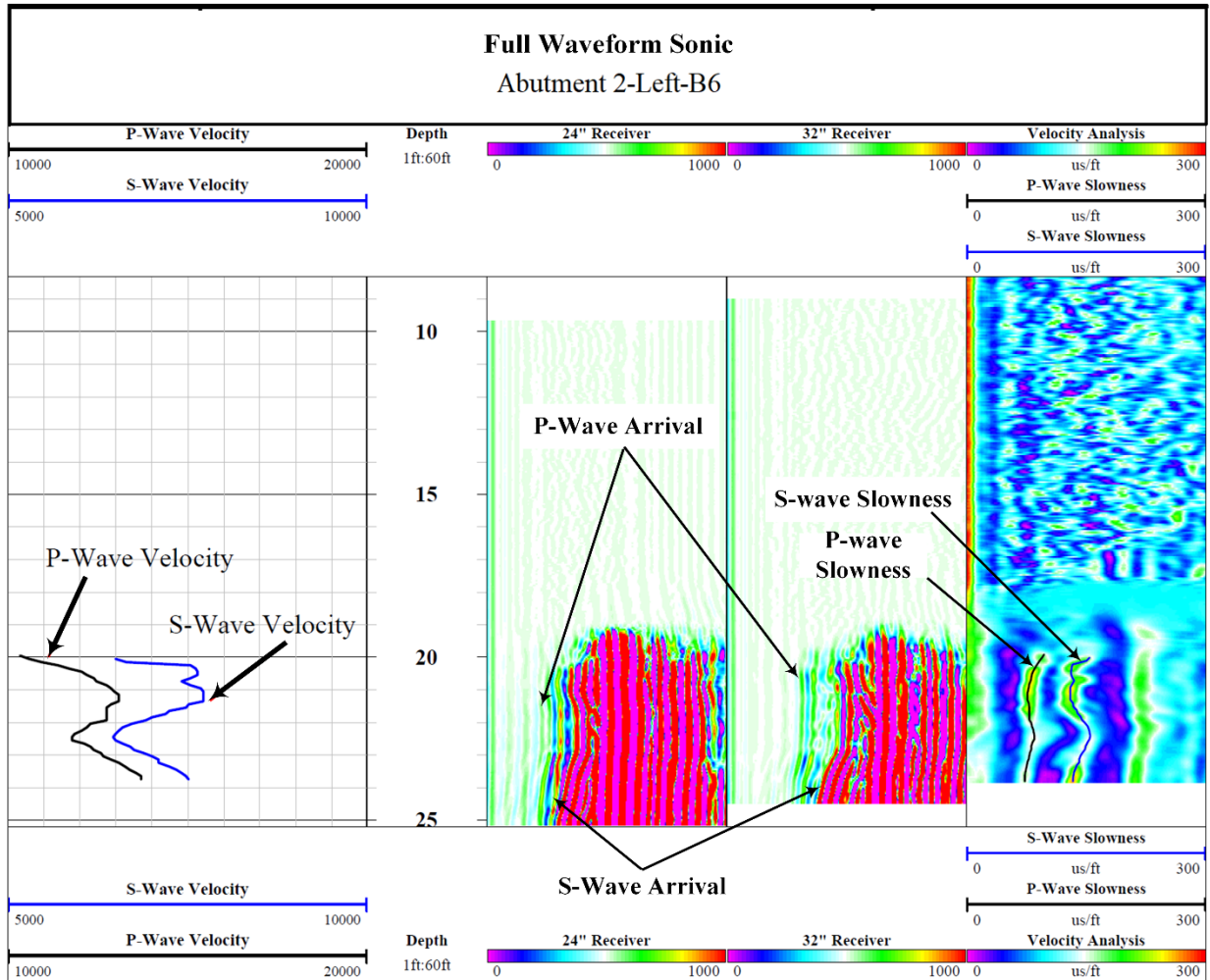
Source: FHWA.

Figure 50. Illustration. Density log of Abut2-LT-B6.



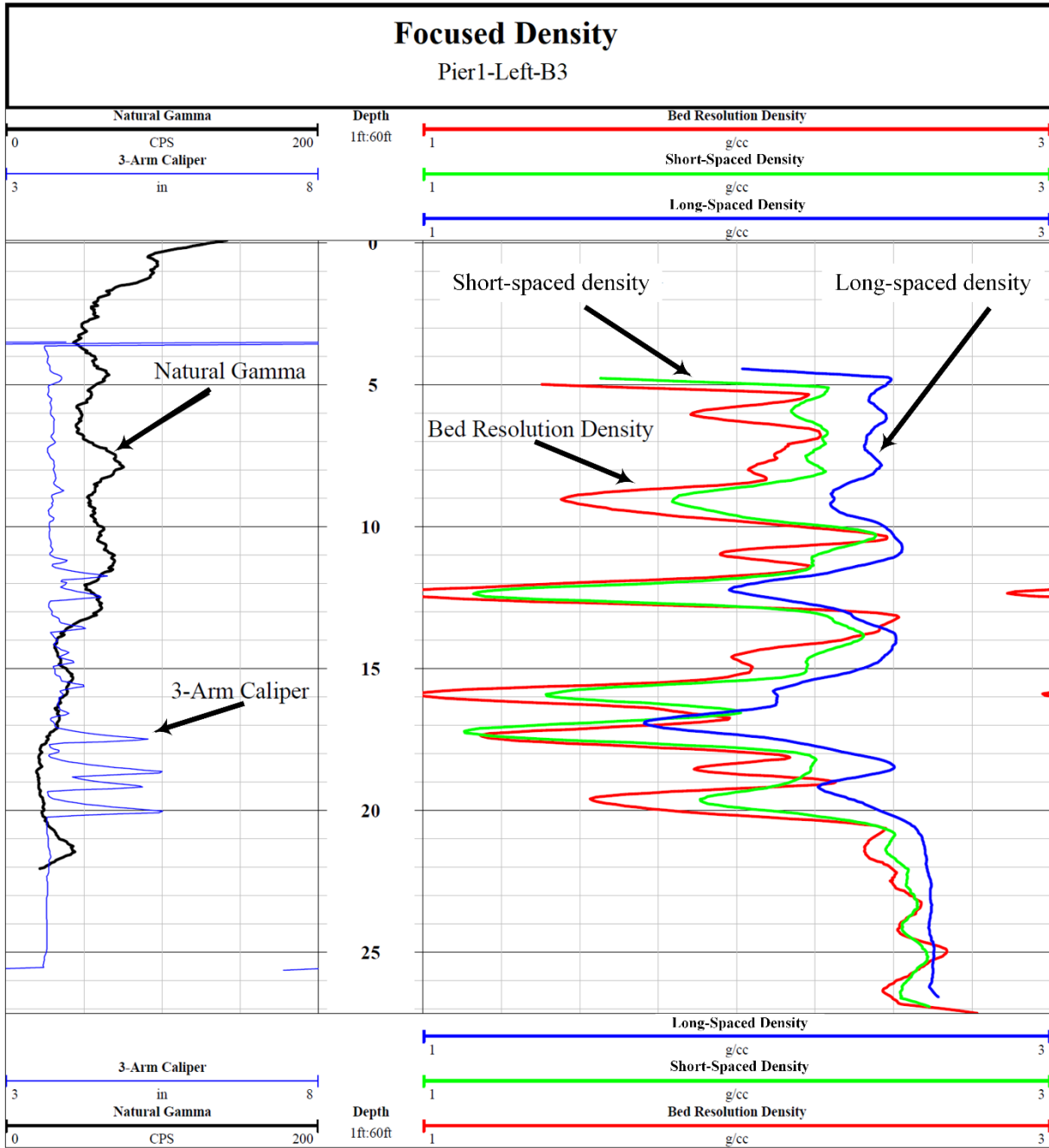
Source: FHWA.

Figure 51. Illustration. Optical images of Abut2-LT-B6.



Source: FHWA.

Figure 52. Illustration. Sonic log of Abut2-LT-B6.

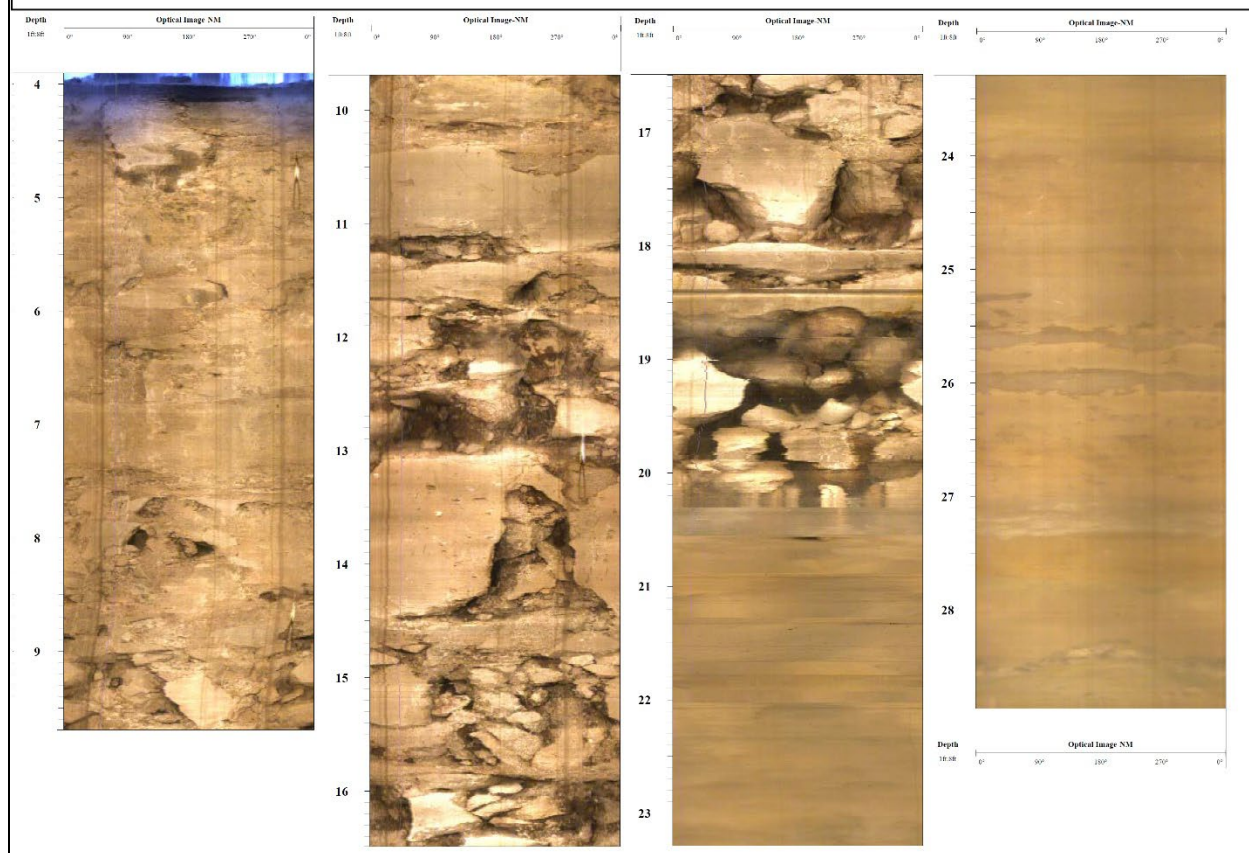


Source: FHWA.

Figure 53. Illustration. Density log of Pier1-LT-B3.

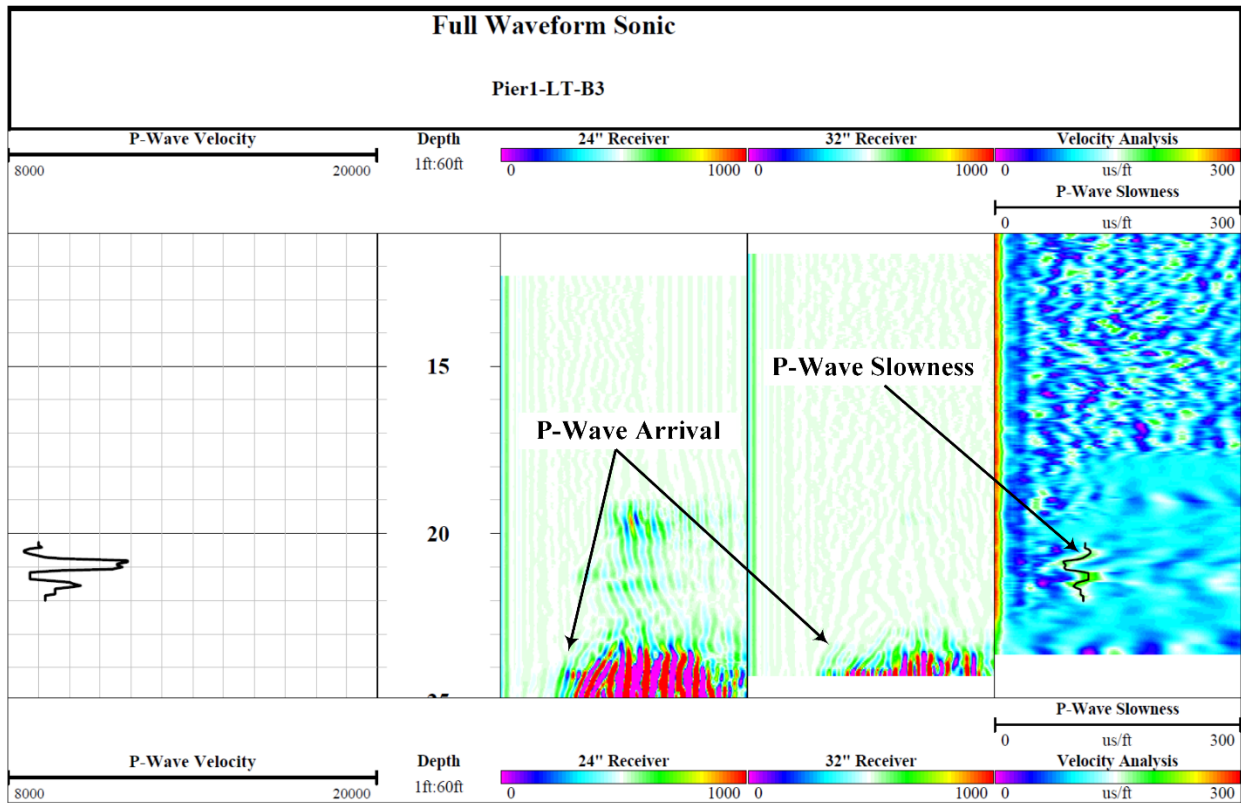
Optical Televiewer

Pier1-LT-B3



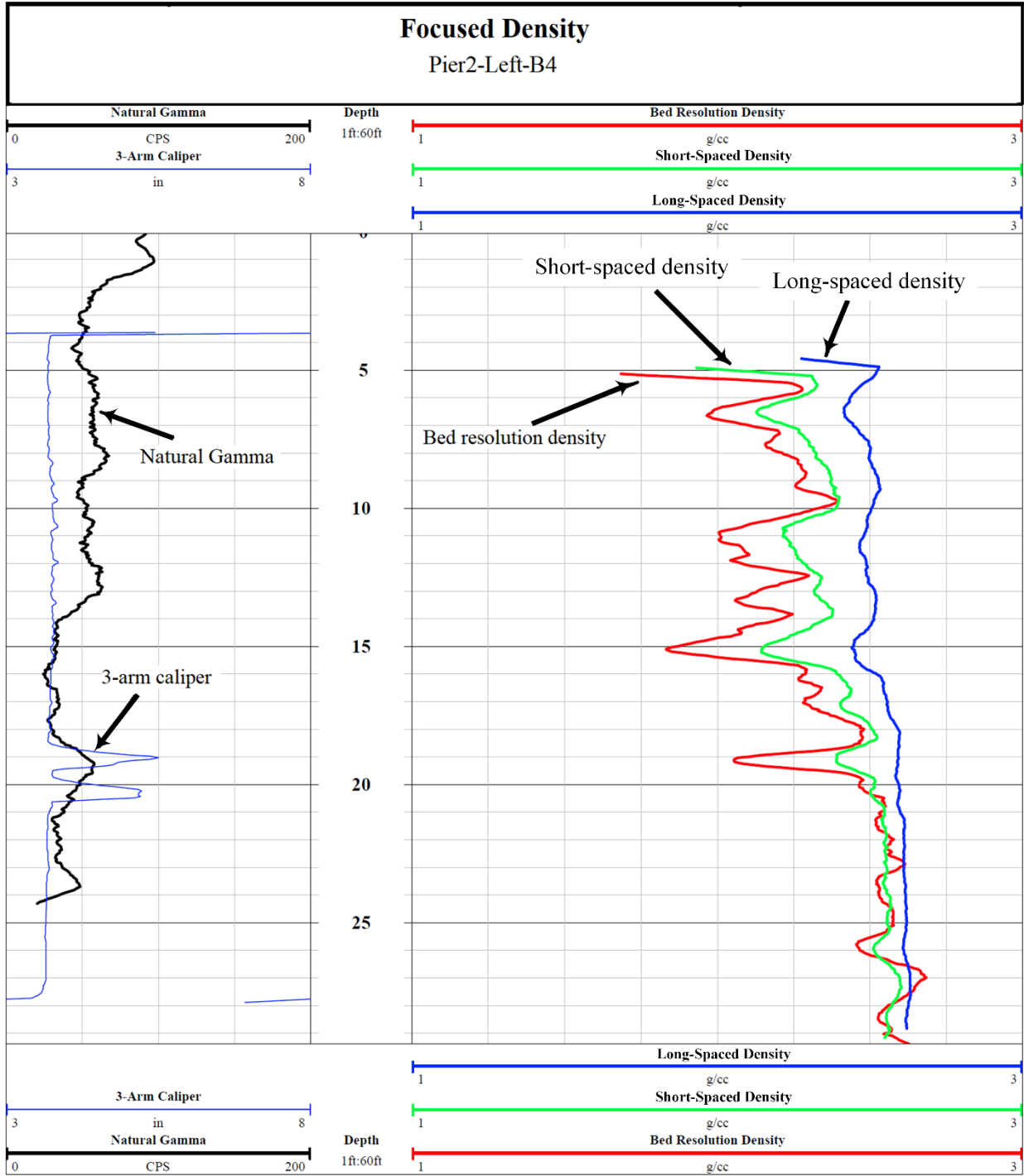
Source: FHWA.

Figure 54. Illustration. Optical images of Pier1-LT-B3.



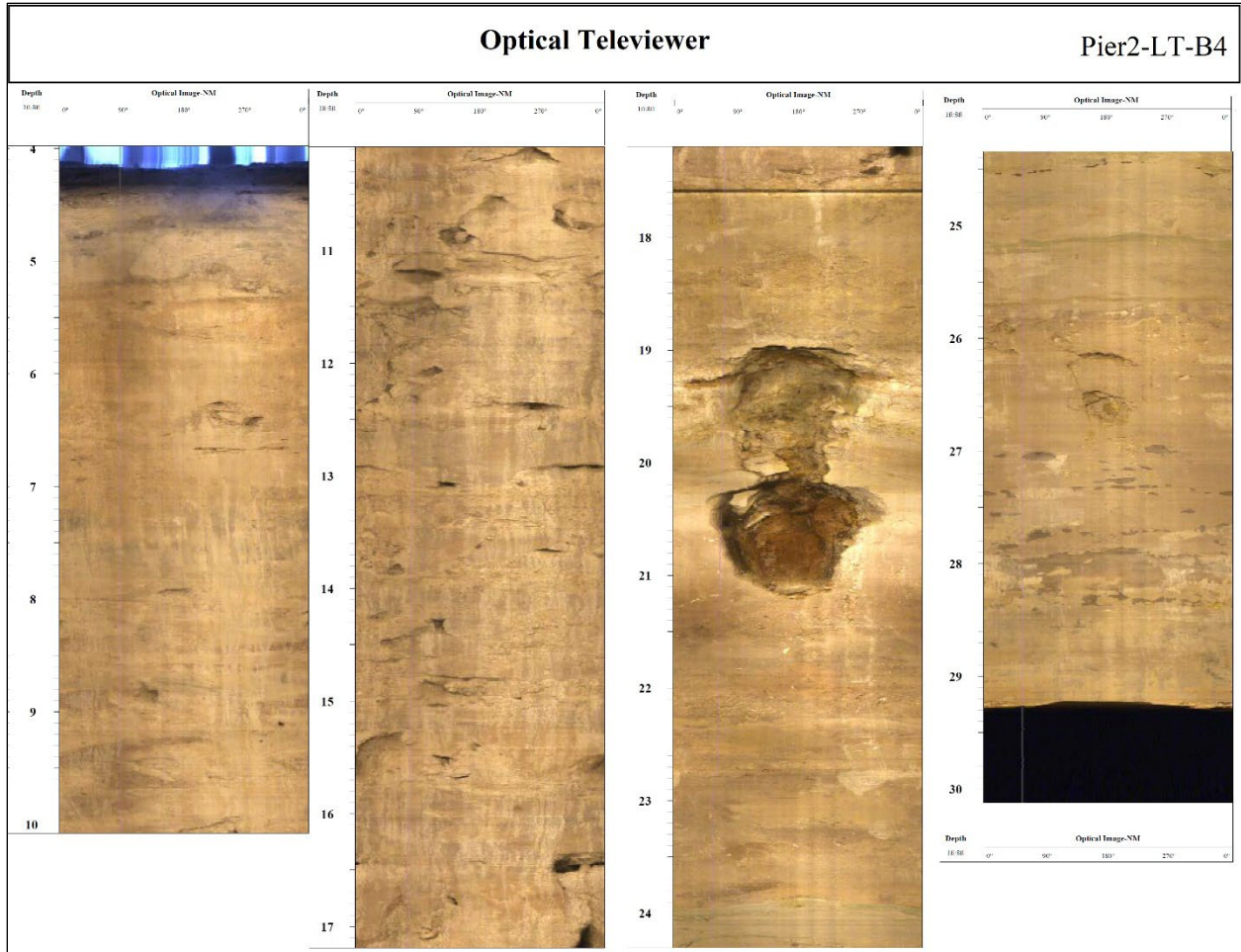
Source: FHWA.

Figure 55. Illustration. Sonic log of Pier1-LT-B3.



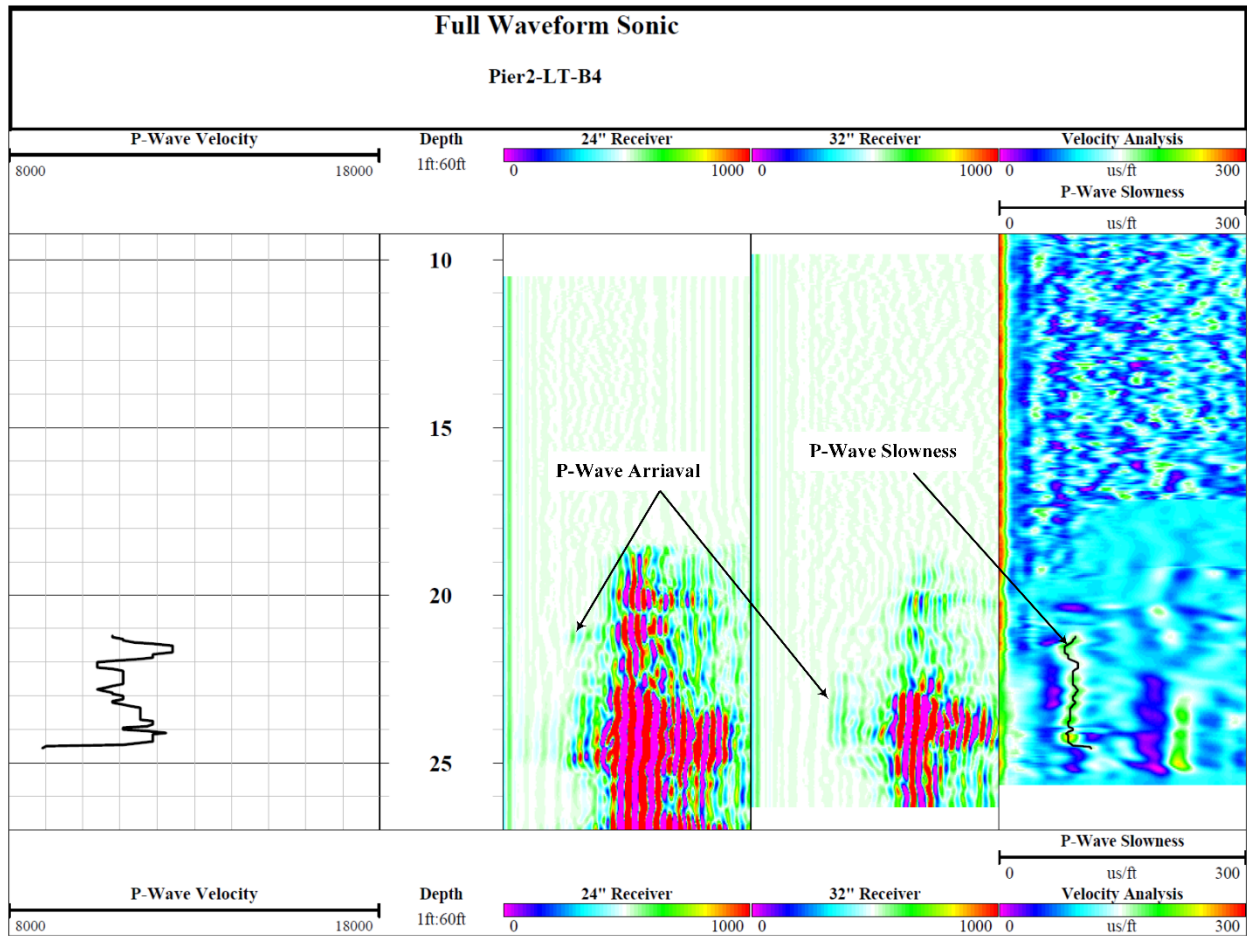
Source: FHWA.

Figure 56. Illustration. Density log of Pier2-LT-B4.



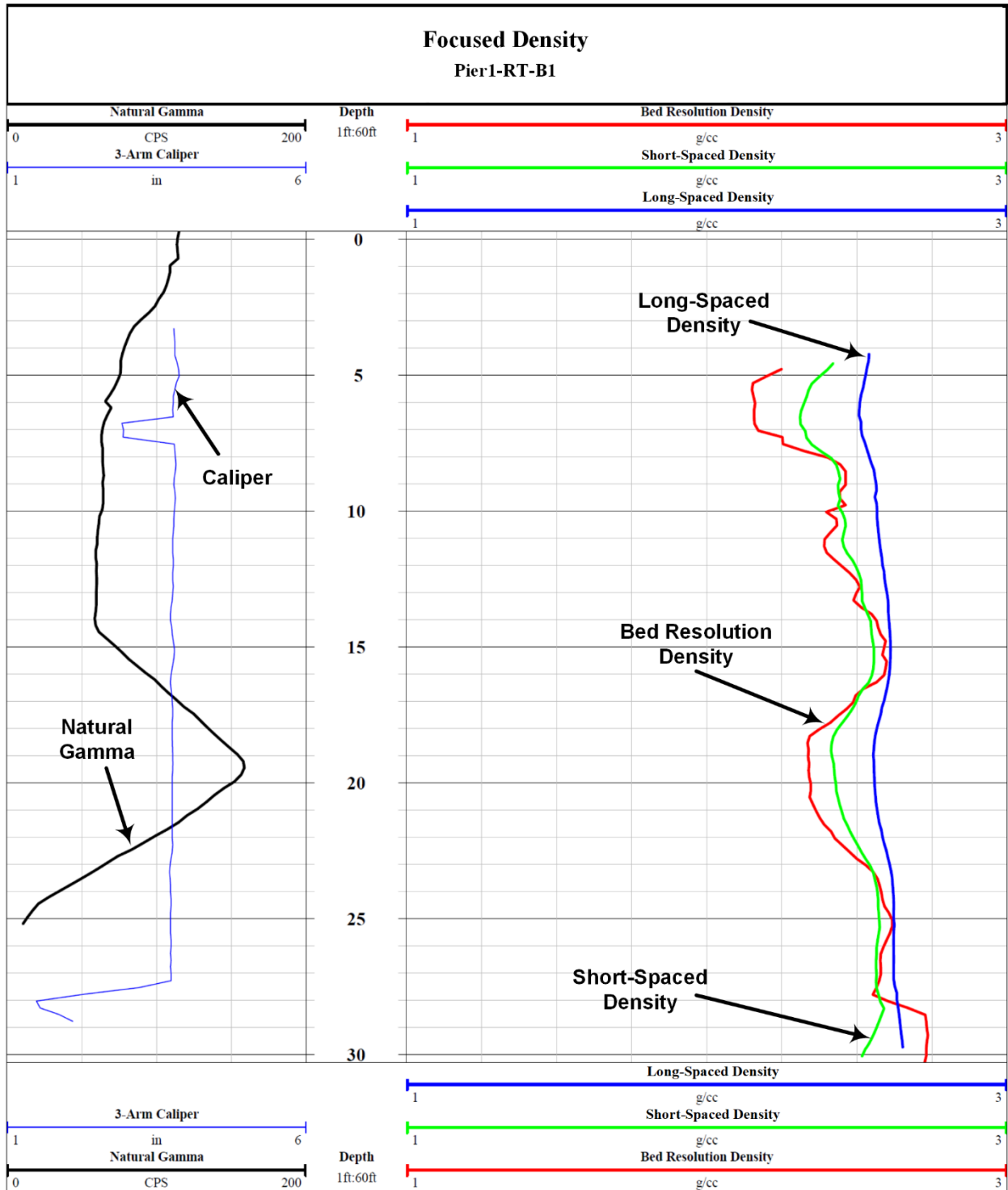
Source: FHWA.

Figure 57. Illustration. Optical images of Pier2-LT-B4.



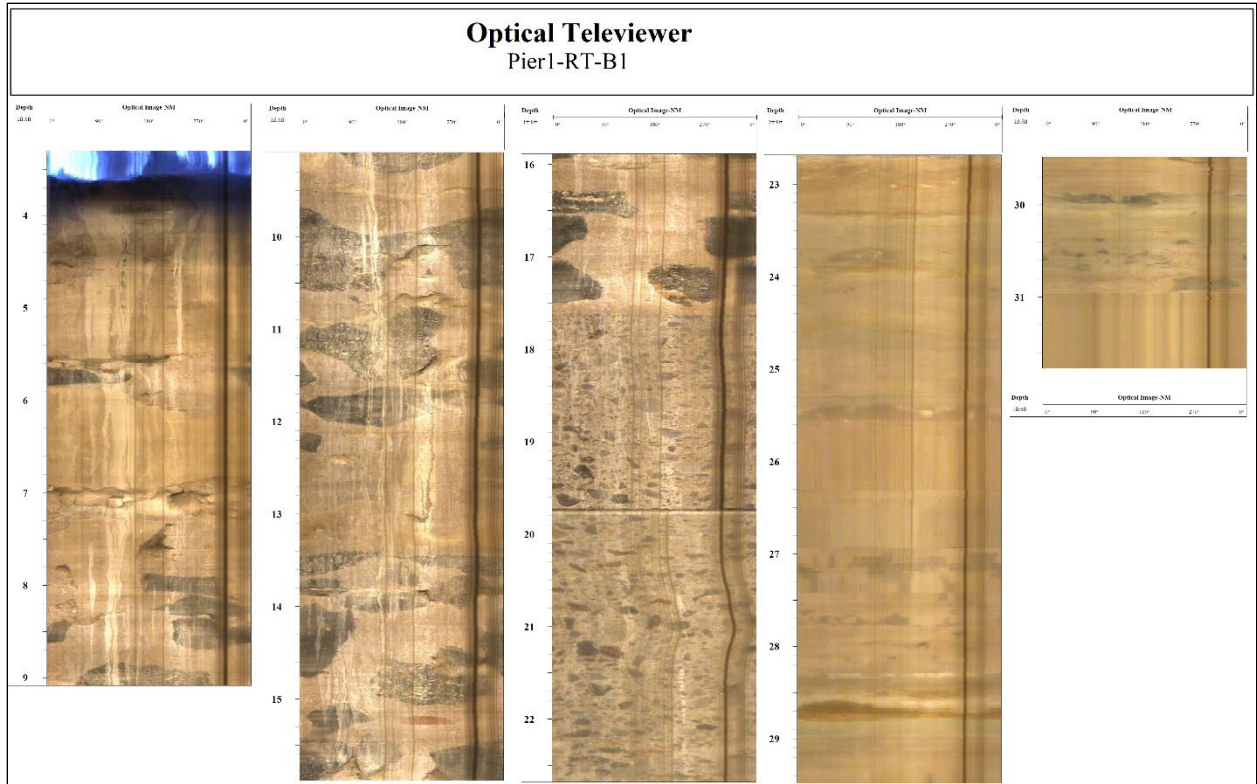
Source: FHWA.

Figure 58. Illustration. Sonic log of Pier2-LT-B4.



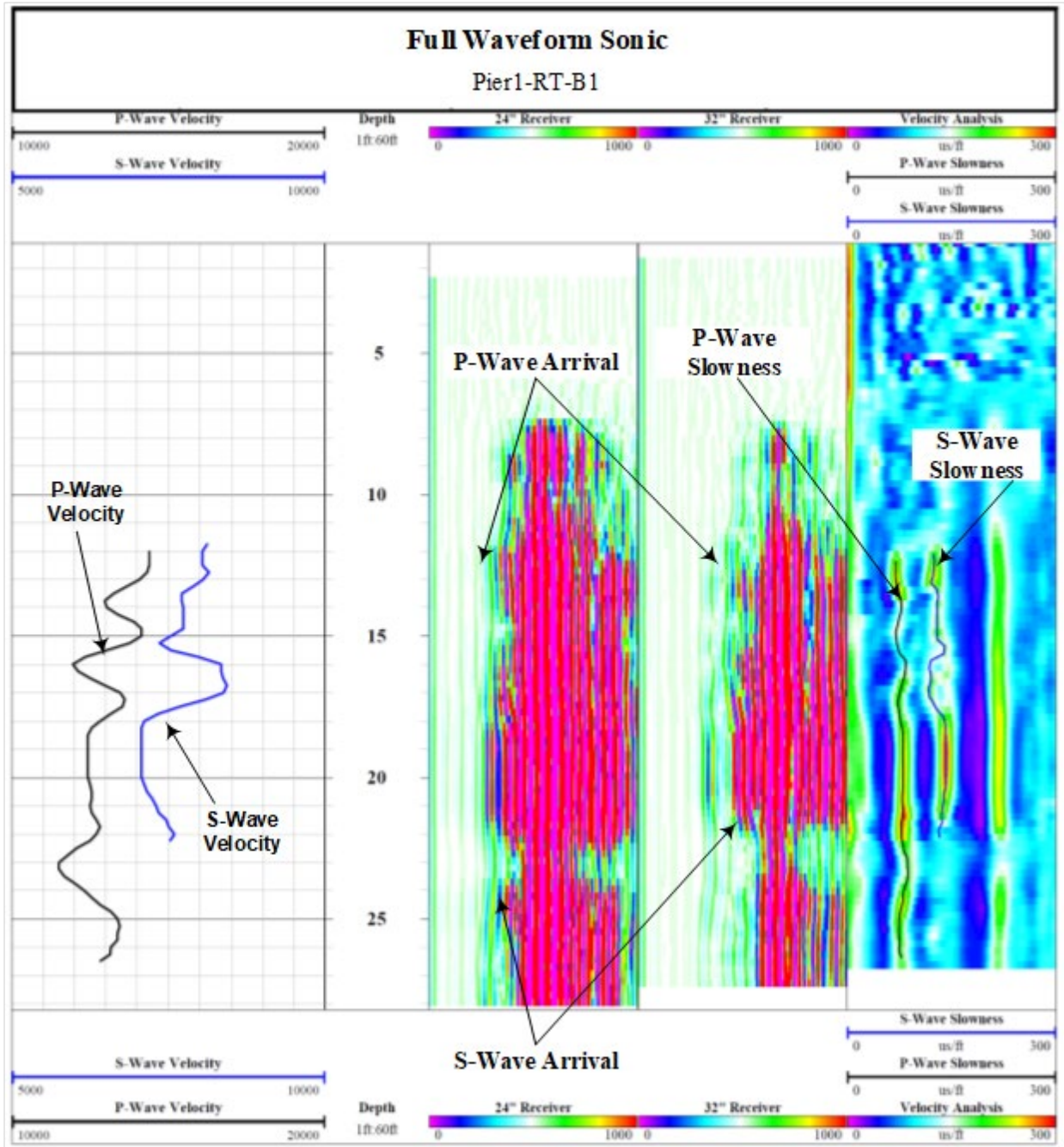
Source: FHWA.

Figure 59. Illustration. Density log of Pier1-RT-B1.



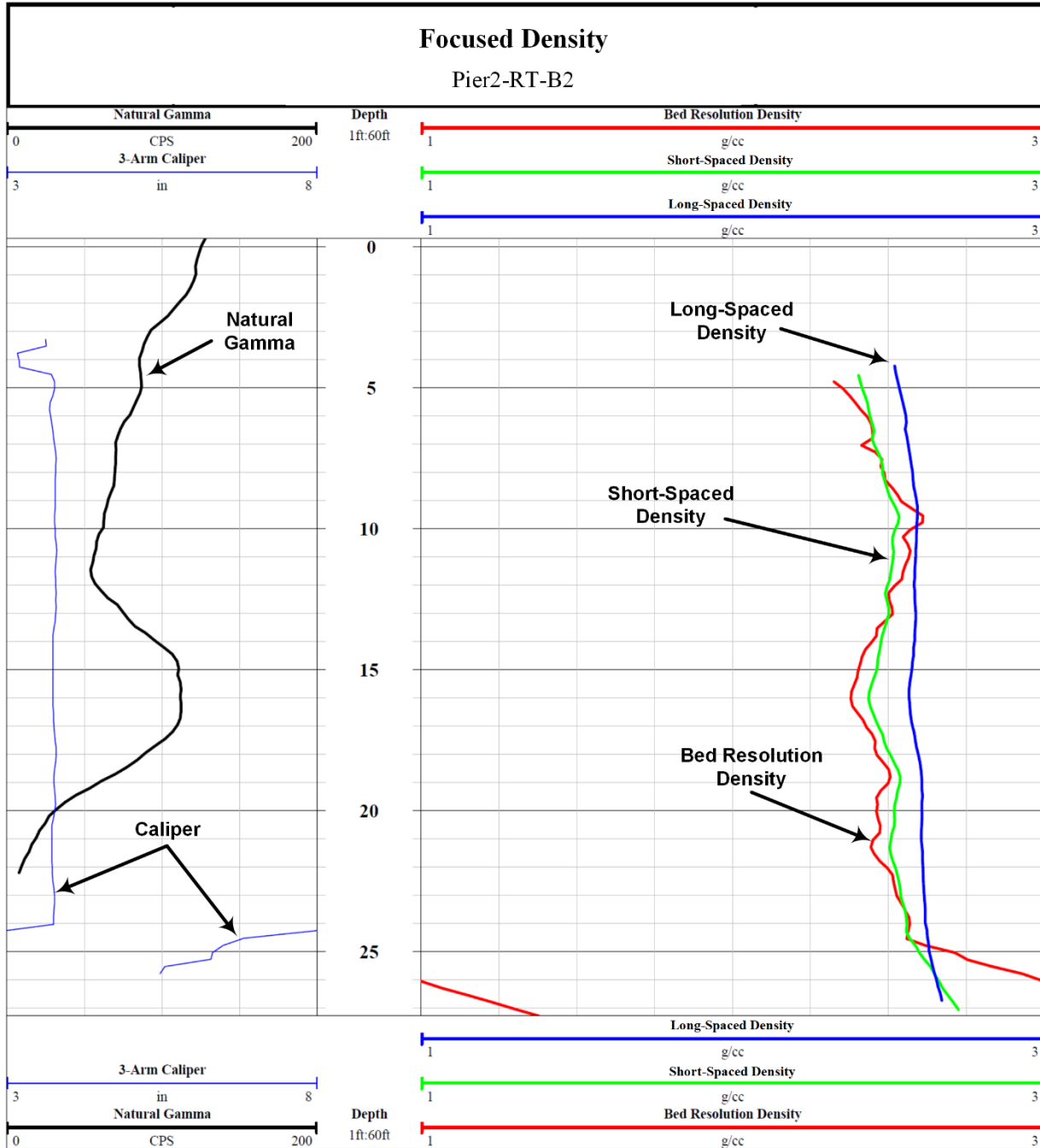
Source: FHWA.

Figure 60. Illustration. Optical images of Pier1-RT-B1.



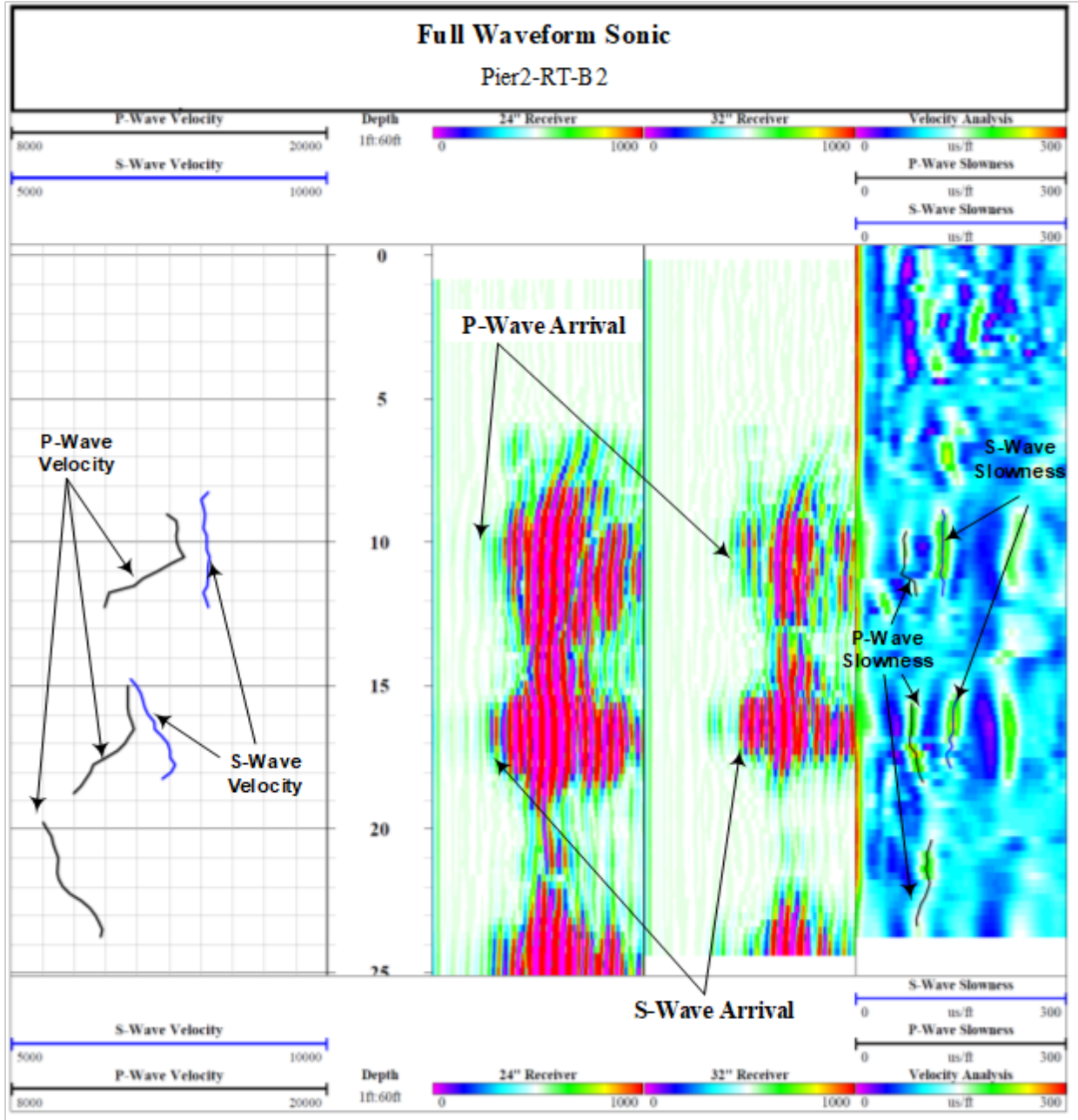
Source: FHWA.

Figure 61. Illustration. Sonic log of Pier1-RT-B1.



Source: FHWA.

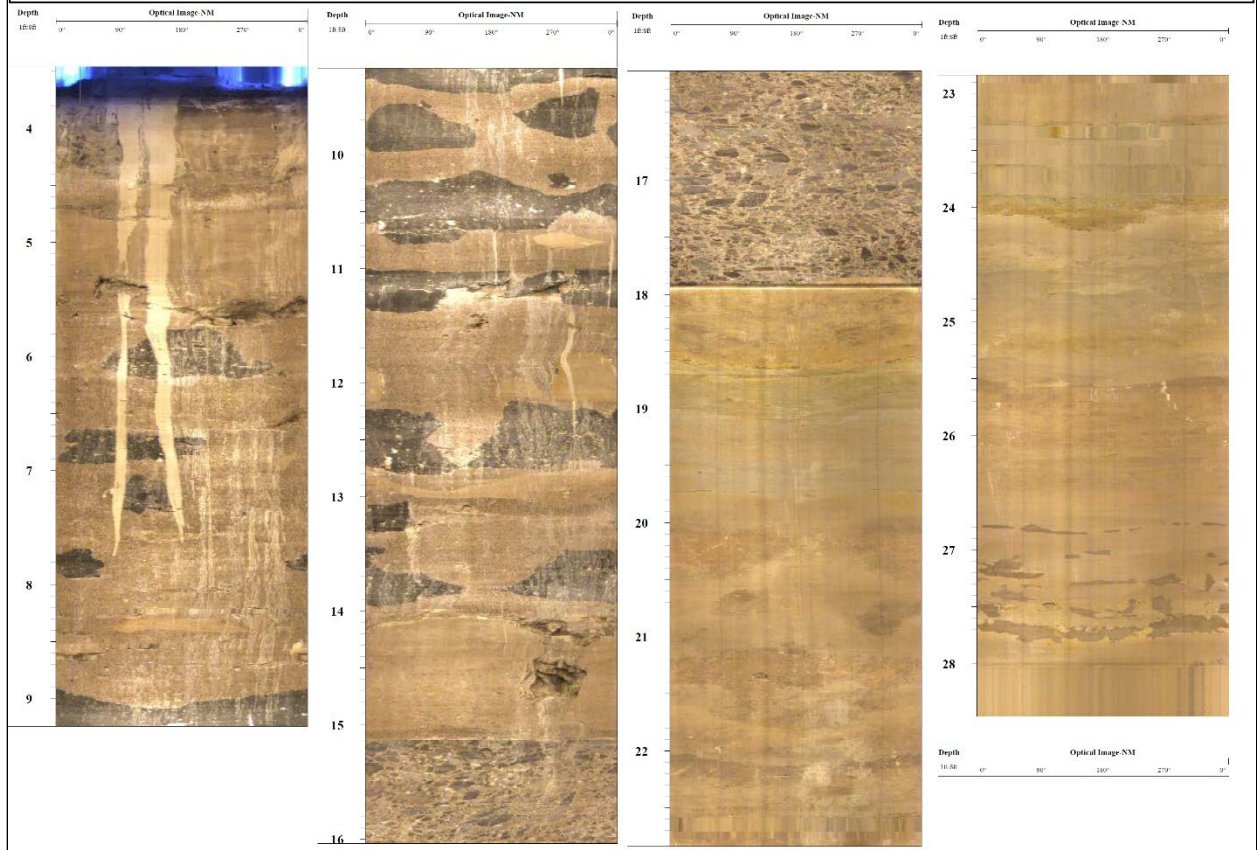
Figure 62. Illustration. Density log of Pier2-RT-B2.



Source: FHWA.

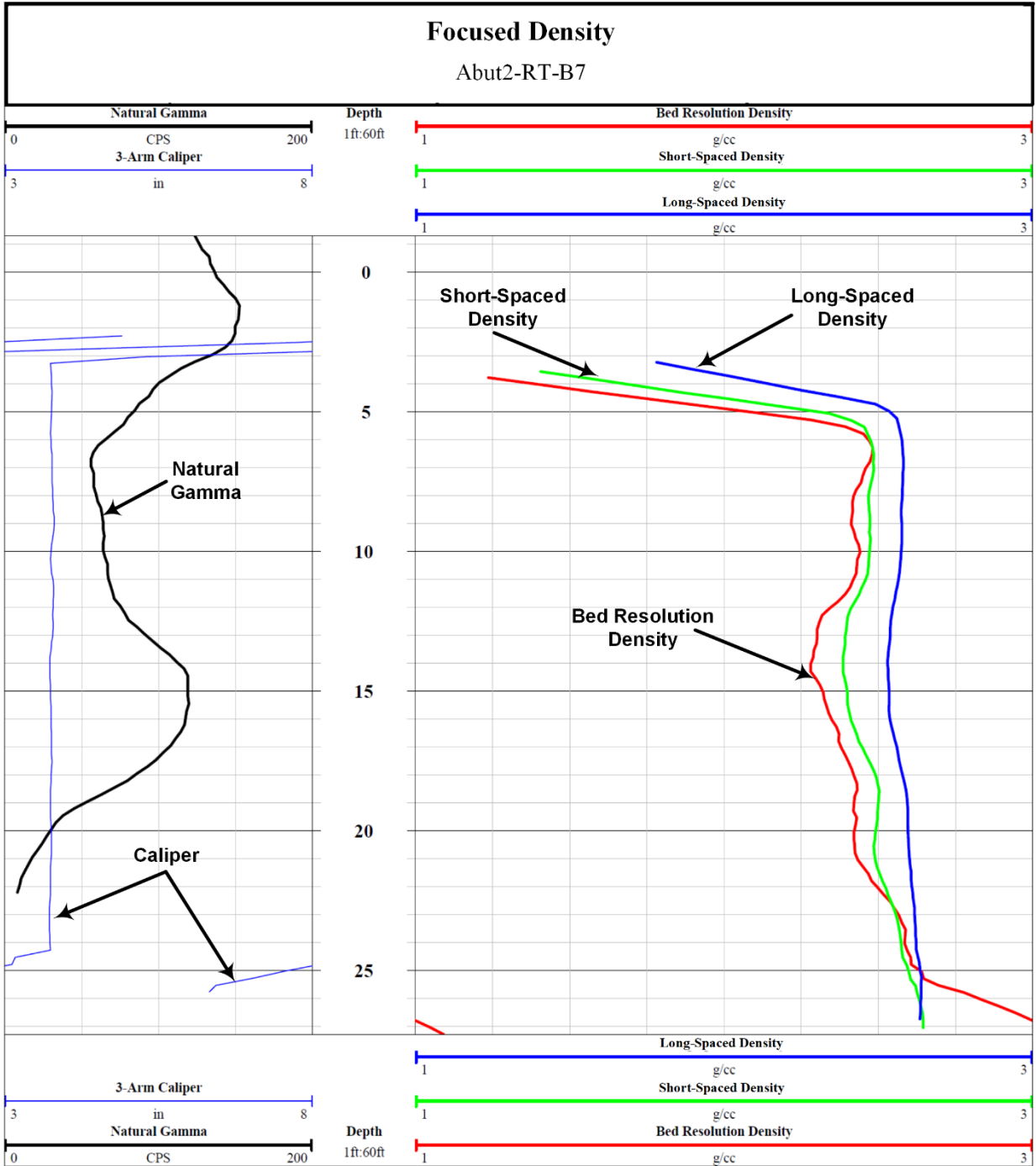
Figure 63. Illustration. Sonic log of Pier2-RT-B2.

Optical Televiewer Pier2-RT-B2



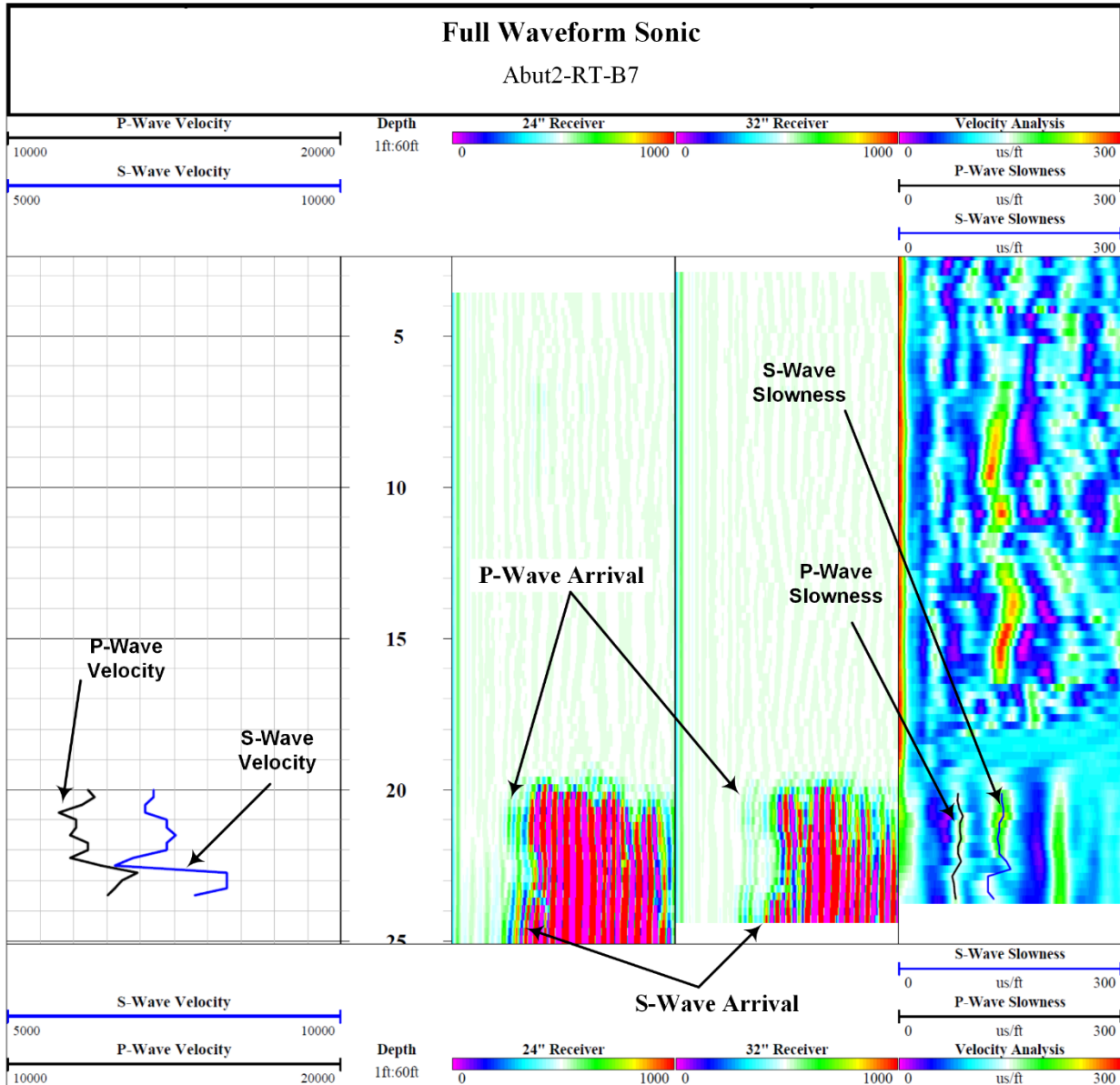
Source: FHWA.

Figure 64. Illustration. Optical images of Pier2-RT-B2.



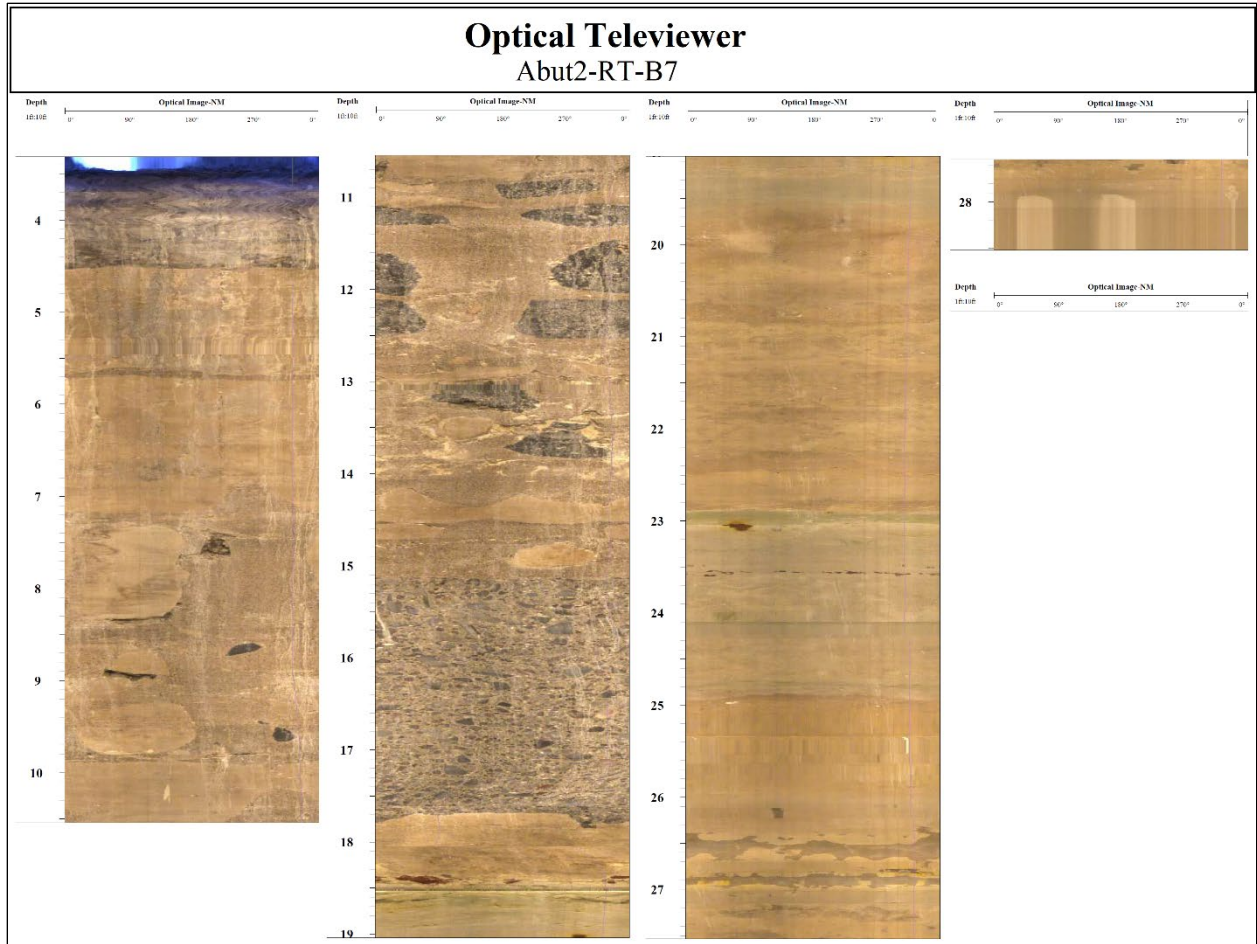
Source: FHWA.

Figure 65. Illustration. Density log of Abut2-RT-B7.



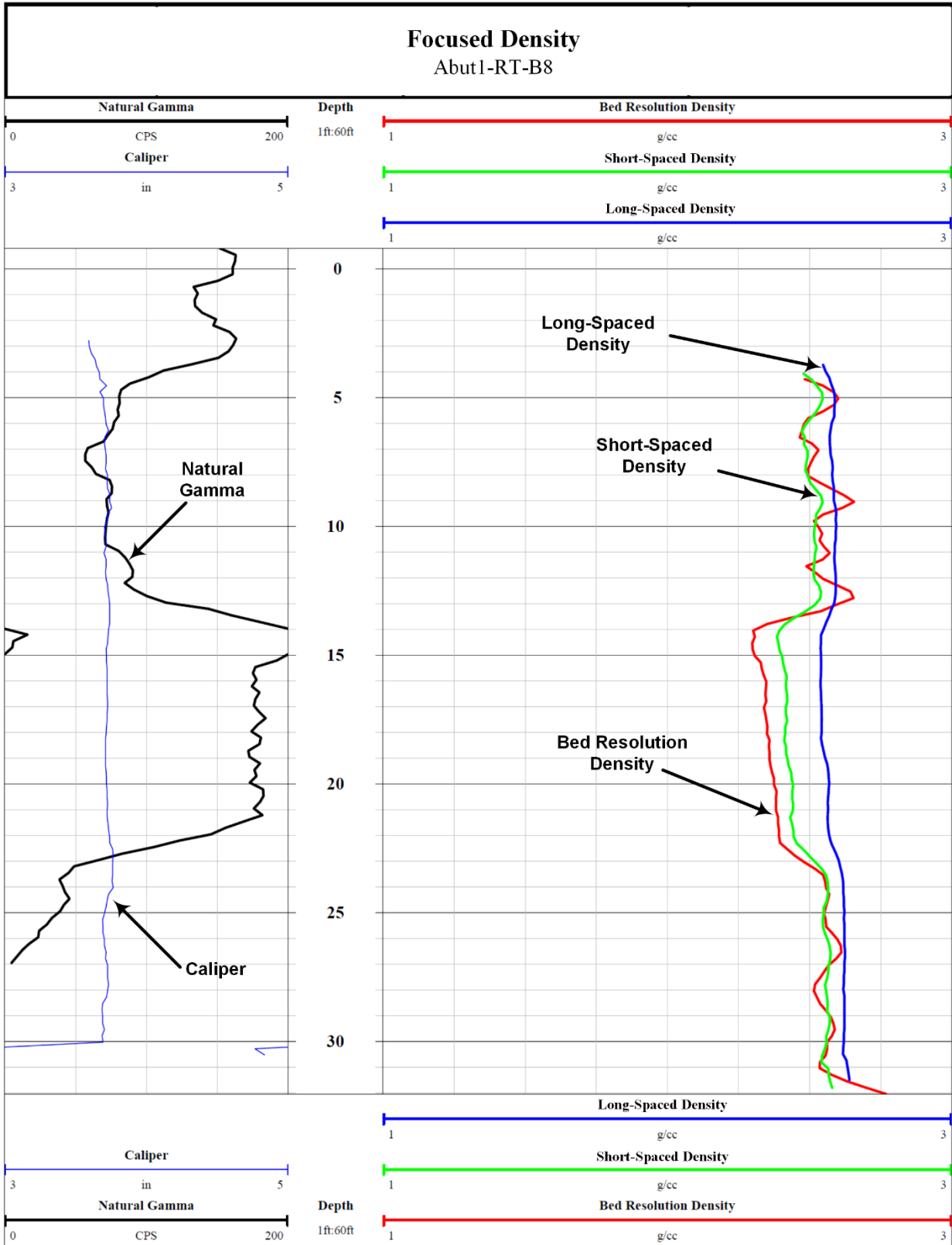
Source: FHWA.

Figure 66. Illustration. Sonic log of Abut2-RT-B7.



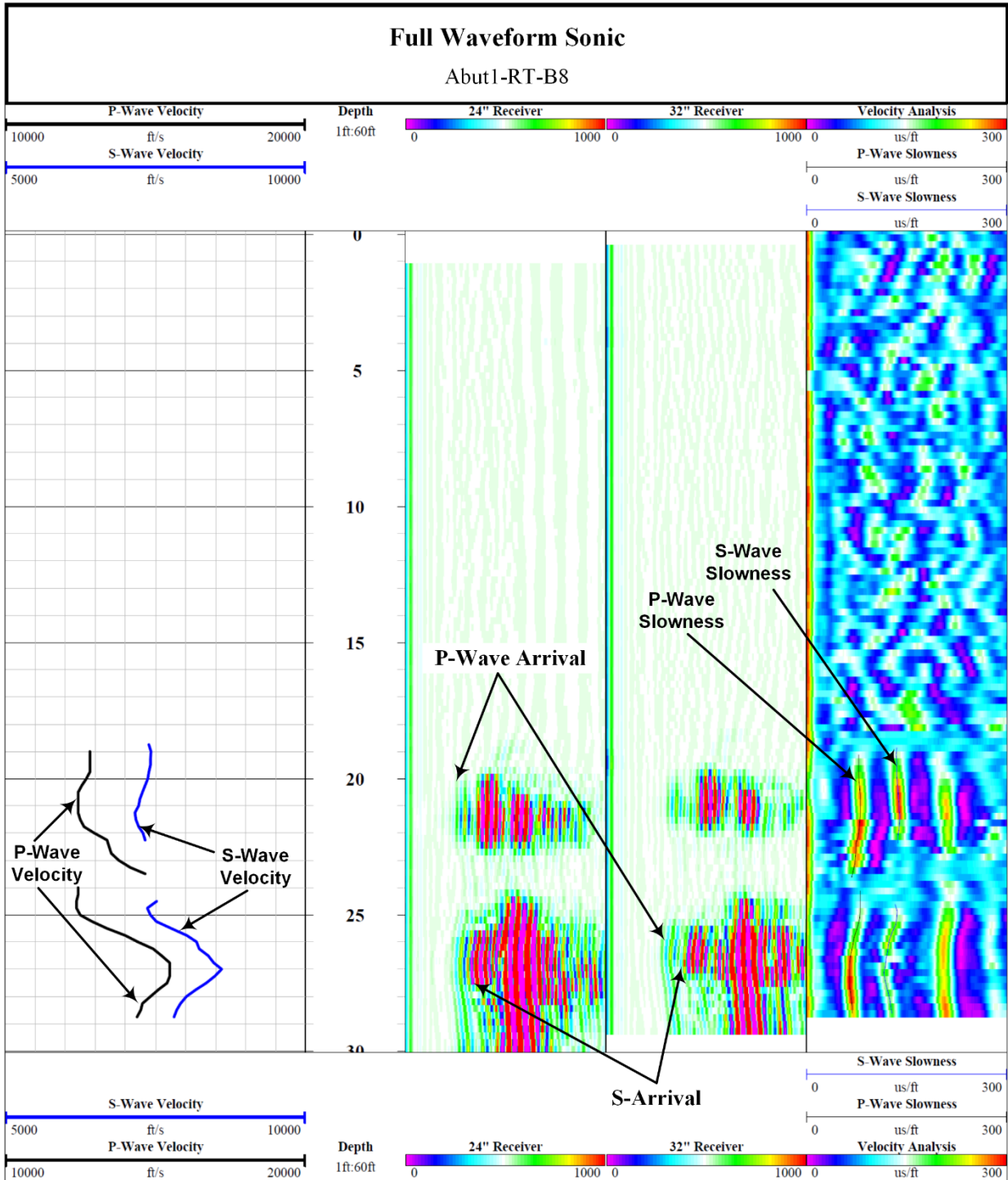
Source: FHWA.

Figure 67. Illustration. Optical images of Abut2-RT-B7.



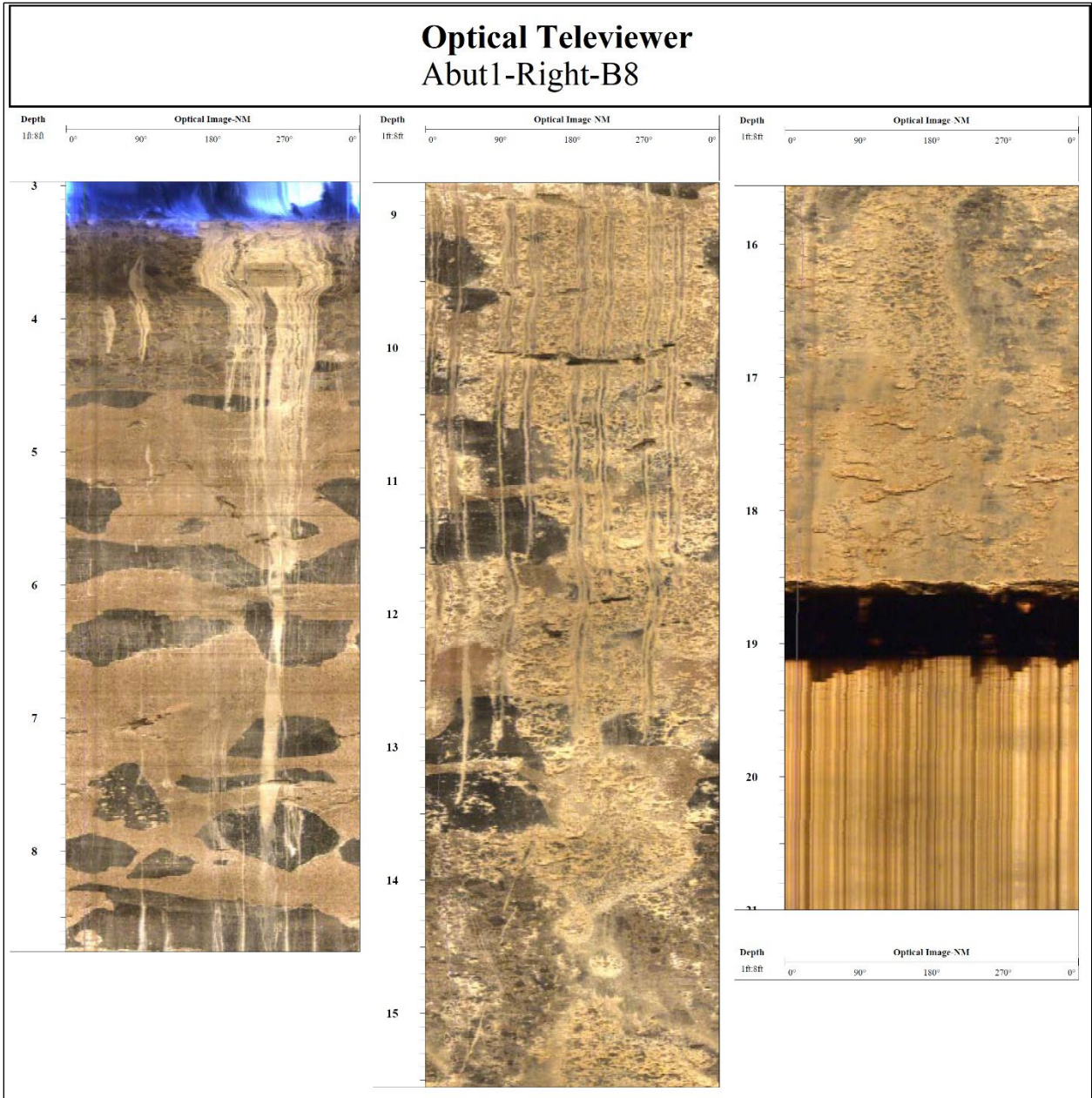
Source: FHWA.

Figure 68. Illustration. Density log of Abut1-RT-B8.



Source: FHWA.

Figure 69. Illustration. Sonic log of Abut1-RT-B8.



Source: FHWA.

Figure 70. Illustration. Optical images of Abut1-RT-B8.

ACKNOWLEDGEMENT

We acknowledge project assistance and advice from Khamis Haramy who was FHWA Central Federal Lands Highway Division's lead geotechnical engineer for the Willow Valley Creek Bridge project. His dedication, hard work, and visionary commitments were critical to the successful completion of this research project.

REFERENCES

- AASHTO. 2020. *LRFD Bridge Design Specifications*, 9th ed. Washington, DC: American Association of State Highway and Transportation Officials.
- Agrawal, A. K., F. Jalinoos, N. Davis, E. Hoomaan, and M. Sanayei. 2018. *Foundation Reuse for Highway Bridges*. Report No. FHWA-HIF-18-055. Washington, DC: Federal Highway Administration.
- Ashida Y., and K. Sassa. 1993. "Depth Transform of Seismic Data by use of Equi-Travel Time Planes." *Exploration Geophysics* 23: 341–346.
- FHWA. 2015. *Structure Selection Report: Lake Mary Road*. Willow Valley Creek Bridge AZ FLAP 234(3). Washington, DC: Central Federal Lands Highway Division, Federal Highway Administration.
- Jalinoos, F. 2015. "Reusing Bridge Foundations." Federal Highway Administration, *Public Roads*, November/December, Vol. 79, no. 3.
- Jalinoos, F., K. T. Tran, T. D. Nguyen, and A. K. Agrawal. 2017. "Evaluation of Bridge Abutments and Wall Type Structures with Ultraseismic Waveform Tomography." *Journal of Bridge Engineering* 22, no. 12.
- Keys, W. S. 1990. "Borehole Geophysics Applied to Ground-water Investigations," in *Techniques of Water-Resources Investigations of the United States Geological Survey*. Denver, CO: U.S. Geological Survey.
- Wightman, W., F. Jalinoos, P. Sirles, and K. Hanna. 2004. *Application of Geophysical Methods to Highway Related Problems*. Report No. FHWA-IF-04-021. Washington, DC: Federal Highway Administration.
- Williams, J. H., and J. W. Lane. 1998. "Advances in Borehole Geophysics for Ground-water Investigations." *U. S. Geological Survey Fact Sheet 002-98*. Denver, CO: U.S. Geological Survey.
- Zemanek, J., R. L. Caldwell, E. E. Glenn Jr., S. V. Holcomb, L. J. Norton, and A. J. D. Straus. 1969. "The Borehole Televiewer - A New Logging Concept for Fracture Location and Other Types of Borehole Inspection." *Journal of Petroleum Technology* 21, no. 6: 762–774.



Recommended citation: Federal Highway Administration,
Substructure Condition Evaluation of the Willow Valley Creek Bridge
Using Geophysical Logging Methods (Washington, DC: 2023)
<https://doi.org/10.21949/1521385>

HRDI-30/10-23(WEB)E